research report

WYLE LABORATORIES
TESTING DIVISION, HUNTSVILLE FACILITY

WYLE LABORATORIES - RESEARCH STAFF

REPORT WR 70-2

EXPERIMENTAL INVESTIGATION OF TURBULENT VELOCITIES IN A SUBSONIC CIRCULAR JET

By

B. J. Tu

Work Performed Under Contract NAS8-21060

February 1970

WYLE LABORATORIES

RESEARCH DIVISION, HUNTSVILLE FACILITY

COPY NO. 5

SUMMARY

Turbulent velocity components at four different azimuth angles in the meridian plane, u_{0°, u_{45°, u_{90° (or v), u_{135°, and the circumferential component w were measured to study the turbulence structure in a cold air jet. The air jet employed for these experiments had an exit diameter of 4 inches and the exit air speed was held constant at 300 ft/sec ($M_j = 0.273$). Measurements resulted in a specification of the mean velocity profiles, the intensity profiles of different turbulent velocity components, Reynolds stresses, power spectra, and the noise source intensity factor, $\overline{U^2} \cdot \overline{u^2}$. Hot-wire techniques were employed and the experimental setup was designed such that the mean velocity or intensity profiles could be measured continuously as a function of position within the jet.

Results showed that in the initial segment of the jet, where data were taken between 0.5 and 12 diameters from the jet exit, the relative magnitude of intensity of various turbulent velocity components on the center line of the jet mixing layer follows the following order:

$$\overline{u^2_{45^\circ}} > \overline{u^2_{0^\circ}} > \overline{w^2} > \overline{u^2_{90^\circ}} > \overline{u^2_{135^\circ}}$$

Accurate data taken at a distance of four diameters from the exit showed that $\overline{u^2}_{45^\circ}$ is 2.9 times larger than $\overline{u^2}_{135^\circ}$. Furthermore, at the same location, principal directions of turbulent stresses have been computed to be 29.2° and 119.2°, and in these directions $\overline{u^2}_{29.2^\circ}$ has been found to be 3.25 times larger than $\overline{u^2}_{119.2^\circ}$. It is believed that the latter result may partially explain the directivity pattern of far field jet noise intensities.

The fluctuating flow field inside the potential core of the jet was also observed and analyzed. Results showed that such fluctuating flow inside the core is rotational.

Two hundred and twenty sets of covariant velocity fluctuation measurements for turbulent velocity components at azimuth angles of 0-, 45-, and 90-degrees were made and recorded on magnetic tapes. Each set of measurement consisted of signals or the square of the signals from one fixed probe and one moving probe. Probe spacings were varied over a three-directional network for each turbulent velocity component. The work is continuing to reduce these data in order to obtain the wave number-frequency spectra for further analysis.

TABLE OF CONTENTS

TABLE OF CONTENTS (Continued)

LIST OF FIGURES

LIST OF FIGURES (Continued)

LIST OF FIGURES (Continued)

LIST OF FIGURES (Continued)

LIST OF SYMBOLS

D	-	diameter of the jet exit
i,j	-	tensor indices, i, j = 1, 2, 3 corresponding to x_1-, x_2-, and x_3-direction, respectively.
M_j	-	Mach number at the jet exit
p	-	pressure
r	-	radius of the jet exit
t	-	time
U_j	-	jet exit velocity
$\overline{U}$, $\overline{V}$	-	mean velocity in x_1 and x_2 directions
u, v, w	-	fluctuating velocity components in x_1, x_2, and x_3 directions
u_θ ($\theta = 0^\circ, 45^\circ, 90^\circ, 135^\circ$)	-	fluctuating velocity component at angle θ with the jet central axis
x_1, x_2, x_3 (or x, y, z)	-	orthogonal coordinates: x_1 axial, x_2 radial (origin on axis at nozzle exit)
θ	-	azimuth angle
μ	-	coefficient of viscosity
ν	-	kinematic viscosity
ξ_i	-	spacing or separation between two points
ρ	-	density
σ	-	normal stress
τ	-	shear stress

LIST OF SYMBOLS (Continued)

$\Phi_{u_\theta u_\theta}$	-	one third octave band level of $\overline{u_\theta^2}$, dB re: Overall PSL (Overall PSL = $\overline{u_\theta^2}$)
ω_i	-	fluctuating vorticity components
Ω_i	-	vorticity components
$\rightarrow$ (or ~)	-	symbol for vectors
— (overbar)	-	average

1.0 INTRODUCTION

The theory of aerodynamic noise was initiated by Lighthill (Reference 1) and since this original work, extensions or further developments of the theory have been pursued by different researchers (e.g., References 2, 3, 4). In the last decade, emphasis has been focused particularly on the topic of jet noise because of its applications to the noise problems of modern rocketry and jet airplanes. Recently, under the same topic, Pao and Lowson at Wyle Laboratories (Reference 5) proposed a spectral theory of jet noise which can be applied to jet noise prediction. This theory has the following advantages: (1) detailed noise generation mechanisms in the turbulence structure can be examined in terms of narrow band analysis, (2) the retarded time effect which is essential in the analysis of noise radiation can be handled more conveniently, and (3) the difficulty in computations of higher derivatives which was encountered using the correlation method (e.g., Reference 3) can be avoided. In this theory the sources terms of "shear noise" and "self noise", which are related to the four-dimensional cross spectra of $\overline{v\,v'}\ (\vec{\xi}, t)$ and $\overline{u^2_\theta\, u'^2_\theta}\ (\vec{\xi}, t)$, respectively, have to be defined experimentally. The present experimental program was designed for the measurement of some of the turbulent flow parameters mentioned above, as part of an integrated effort to arrive at accurate and reliable methods of jet noise prediction. A region centered at $x_1 = 4$ D, $x_2 = 0.5$ D and $x_3 = 0$ was chosen for the study of turbulence structure since, in this location, the turbulence in the mixing layer is normally spread in directions normal to the jet axis. This region also corresponds to the region of most intense noise generation (Reference 3). Such a region was considered to be the most representative of the overall turbulence structure of subsonic jets from the standpoint of noise generation.

Extensive measurements of mean velocity profiles, turbulent velocity intensity profiles, turbulence velocity spectra, and the noise intensity factor, $\overline{U^2} \cdot \overline{u^2}$ have been obtained. The experimental results should provide vital information which can be employed directly in theoretical computations to predict noise, and also furnish some insight into the detailed structures of the turbulent flow in a circular jet. It is also anticipated that these data will be of importance in revealing the noise generating mechanism and for correcting computations using current theories which were formulated with basic assumptions. For example, in the theory by Pao and Lowson (Reference 5), a constant mean velocity gradient and a homogeneous turbulent flow were assumed so that the problem could be simplified to the point that noise predictions could be made. A better understanding of the real structure of both the mean flow and the turbulence will be helpful in making more accurate noise predictions by means of this theory.

Some early experimental work on turbulent jets was reported by Kuethe (Reference 6) and by Corrsin and Uberoi (Reference 7). Recently Davies, et al. (Reference 8) measured the axial turbulent velocity component in the mixing region of a one inch diameter cold air jet at Mach numbers ranging from 0.2 to 0.55. One of their more interesting results was that the local intensity of the turbulence was equal to 0.2 times the shear velocity. This velocity is defined as the product of the local integral length-scale of the turbulence with the local shear. The local intensity is defined as the root-mean-square (rms) value of the local fluctuations of the axial velocity component. However, it was found that the length-scale was proportional to the distance from the jet orifice, while the maximum shear was also related to this distance as well as to the jet exit velocity. And according to Davies, et al., these two similarity relations break down near the jet exit and also at locations beyond the first six diameters downstream.

In a 2 in. diameter, cold air jet, Bradshaw, et al. (Reference 9) measured the three orthogonal turbulent velocity components at a Mach number of 0.3. They were able to show that about a quarter of the Reynolds shear stress is produced by large eddies within a narrow range of wavelengths. These eddies are of the form of mixing jets, inclined to the radial direction in any sectional plane across the jet flow. It was believed that these eddies dominate the near-field pressure fluctuations. All these results were mainly deduced from the study of the nine orthogonal spatial correlations. A similar method was used by Grant (Reference 10) in a wake flow. It is the belief of the present author that the inclination to the radial direction of these large eddies is closely related to the principal directions of turbulent stresses, which will be discussed in Section 5.1. A close relation among the turbulent eddies, the turbulent vorticity, and the turbulent stresses in a shear flow can be seen as follows: When turbulent vorticity lines are stretched in the flow by the shear and normal stresses the direction of stretching defines the direction of eddies. Concurrently, the vorticity intensity increases to cause a maximum normal stress normal to the direction of stretching and a minimum normal stress in the direction of stretching.

It is also of interest here to point out that the flow in the potential core of a circular jet has been considered in the past as being irrotational (e.g., Reference 9). Present observations indicate that the fluctuating flow inside the core is rotational A brief discussion of this is given in Section 5.2.

Laurence (Reference 11) made extensive measurements in a 3.5 in. diameter free jet with Mach numbers ranging from 0.2 to 0.7, mainly to study the intensities and the spatial integral scales of the axial turbulent velocity component. He found that (1) the lateral and longitudinal scales of turbulence were nearly independent of Mach number, and in the initial mixing zone that it varies in proportion to the distance from the jet exit, (2) further downstream of the jet the longitudinal scale reached a maximum and then decreased approximately linearly with distance, and (3) near the jet exit the lateral scale was much smaller than the longitudinal one. Laurence also reported some spectrum measurements of the velocity component in the radial direction. As discussed by Pao and Lowson (Reference 5), the overall noise intensity per unit volume of jet is inversely proportional to the spatial scale of turbulence. Thus, the findings of Laurence are of special interest in the estimation of noise intensity.

Chu (Reference 3) also made an experimental study in a round jet of 4 in. diameter and a jet exit speed of 142 fps. He measured space-time correlations of the velocity components, u_{0°, u_{45°, and u_{60° quite extensively. However, the two hot-wire probes in these measurements were moved simultaneously in order to reach different spacings, and, therefore, it is difficult to evaluate the correlation so obtained in a non-homogeneous shear flow. It is the belief of the present author that one of the two hot wires should have been fixed at one point to avoid extraneous errors due to large non-homogeneous regions within the jet.

It is felt that the existing experimental data provides some significant insight into the jet turbulence structure; however, more detailed analyses are required to define in more detail the structure of a turbulent jet flow for the purpose of jet noise prediction. Thus, reduction and analysis of the present experimental measurements are continuing.

2.0 TEST APPARATUS AND INSTRUMENTATION

The test apparatus and instrumentation showing all supporting equipment as well as defining the co-ordinate system for the measurements are presented in Figures 1 - 7. Various components of the test apparatus and instrumentation will be discussed separately in the following sections.

2.1 Test Apparatus

2.1.1 Model Jet Facility

The model jet facility is shown in Figure 1. An air jet flow with a speed of 300 fps at the sonic nozzle exit was supplied by the main air compressor system of Wyle Laboratories. The compressor system includes a heat-exchanger with a water cooling tower. The temperature of the supplied air can be maintained close to the temperature of the ambient atmosphere. The air jet facility, which is mounted inside a room, includes a settling chamber of 10 in. diameter and 5 ft. in length and a sonic nozzle of 4 in. diameter at the exit. Seven screens with a mesh size of 50 holes per inch were fixed in the settling chamber so as to produce a smooth flow of low turbulence level. The contraction of the 4 in. sonic nozzle (Figure 2) was designed such that a uniform air flow without separation can be reached. The turbulence level at the jet exit and along the jet centerline within the potential core was measured to be in the range of 0.3 to 0.5 percent for either $\sqrt{\overline{u^2}}/U_j$ or $\sqrt{\overline{v^2}}/U_j$, with the noise level from the measuring electronics included.

2.1.2 Traversing Mechanism

A traversing mechanism (Figure 1) which was constructed during an earlier phase of this project was used to position the probes accurately in a horizontal plane. Minor components were added so that the probe could be positioned at various vertical and circumferential locations. The traversing mechanism was mounted on isolation pads and leveled prior to commencing the tests. The massive size of the structure provided a very stable platform for the hot wire probes.

2.2 Instrumentation for Data Acquisition

2.2.1 Hot-Wire Anemometer

Constant temperature anemometers with linearizers were employed to monitor the signals of hot wires in the flow. These anemometers are the recently developed Model 1054A, (Figure 4) manufactured by Thermo-Systems, Inc. These anemometers give a linear voltage response within the speed range of air flow from 0 to 300 fps. The linear zero and the linear span control devices of the anemometer made it possible to match the sensitivity of one wire with that of another wire in case their electrical resistances are slightly different. This improves the accuracy of an X-wire probe when the two wire resistances of the probe have not been matched. Manufacturer specifications indicate that the frequency response of the model 1054A anemometer is flat from d.c. to 200 K Hz.

2.2.2 Hot-Wire Probes

The hot-wire probes (e.g., Figure 3) were single-wire and X-wire probes. A single straight wire was placed normal to the stream to measure the streamwise velocity component, while a pair of wires in the form of an X was employed for the cross-stream components. In the present study, X-wire probes were also employed for measuring the u_{45^o} and u_{135^o} components when only one of the two wires of the probe was connected to the hot-wire anemometer. The probes were constructed at Wyle Laboratories, and made of tungsten wires of 0.00015 in. diameter and 0.04 in. effective length. The wire was electro-plated with copper before it was mounted on the probe with soft solder.

2.2.3 Pitot-Static Tube and Water Manometer

A pitot-static tube having an inside diameter of 1/8 inch was used in combination with a water manometer to determine the exit velocity of the model air jet. These data were used to establish the calibration sensitivity factors for the hot-wire probes.

2.2.4 D. C. Differential Amplifier and Multiplier/Divider

Subtraction, multiplication, squaring, and taking the square-root of hot-wire signals during measurements were performed using a Burr-Brown Model 3088/16 d.c. differential amplifier and Burr-Brown Model 1671/16 multiplier/divider (Figure 4). Manufacturer specifications of frequency response give a flat response within ± one percent up to 15 K Hz for Model 3088/16 and up to 40 K Hz for Model 1671/16.

2.2.5 Tape Recorder/Reproducer

In order to study wave number-frequency power spectra, hot-wire signals of turbulent velocity and their squares were recorded using a Consolidated Electrodynamics Corporation model GR-2800 magnetic tape recorder/reproducer system (Figure 5). This recording system has a capacity of 14 channels and its frequency response is from d.c. up to 10 K Hz at the tape speed of 30 in./sec. using an FM recording mode.

2.3 <u>Instrumentation for Data Reduction</u>

2.3.1 Root-Mean-Square Voltmeter

A Ballantine Model 320 true rms voltmeter was employed for measuring turbulent intensities. Frequency response range of the Model 320 voltmeter is from 5 Hz to 4 M Hz.

2.3.2 X-Y Plotter

All profiles of mean velocity and turbulent velocity components in the jet flow were recorded by using a F.L. Mosely Model 135C X-Y plotter.

2.3.3 Audio-Frequency Spectrometer and Level Recorder

The audio-frequency spectrometer was a Brüel and Kjaer Type 2112 and level recorder Type 2305 (Figure 5). These instruments were employed to obtain the power spectral density of different turbulent velocity components. The spectrometer provides for one-third octave band analyses with a 22 - 45,000 Hz selective frequency coverage.

3.0 TEST DESCRIPTION

3.1 Test Procedure

3.1.1 Determination of the Jet Aerodynamic Centerline

Initial studies consisted of defining the mean velocity profiles of the jet flow to determine the true aerodynamic centerline of the jet. The hot-wire probe was mounted on the traversing mechanism with its axis located at the geometrical centerline of the jet nozzle and the settling chamber. Mean velocity profiles were then taken with the hot-wire probe by surveying across the jet flow in both horizontal and vertical directions. Profiles were measured at three longitudinal stations, 2, 4 and 7 diameters aft of the nozzle exit. The deviation between the aerodynamic jet centerline and the geometric jet centerline was small; however, the true aerodynamic centerline was used as a reference for subsequent surveys.

3.1.2 Measurements of Mean and Turbulent Velocity Profiles

Since the temperature of the jet flow was maintained close to that of the ambient air in the laboratory (maximum difference of temperature not more than 3° F) and since a well designed linearizer was employed with the constant temperature hot-wire anemometer, the electrical voltage response from the hot wires was directly proportional to the true value of the velocity component at any point inside the jet flow. On this basis the mean velocity and the turbulent velocity intensity profiles were measured continuously by surveying the jet flow with the hot-wire probe and recording the output using an X-Y recorder. Position readout was obtained by using a linear potentiometer. Chromell wires of 0.0159 in. diameter and of uniform sections were mounted in directions normal and parallel to the jet axis and were excited with small but constant electric current. A sliding contact was connected between the Chromell wire and the hot-wire probe holder. The distance of the hot wire location from a reference point was then measurable because the electrical voltage-drop along the Chromell wire was proportional to its length.

Calibrations of the hot wires were performed with a pitot-static tube mounted at the jet centerline and one inch downstream of the jet exit. The pitot-static tube read total and static pressures simultaneously which were converted to jet exit speed.

In the measurement of the mean velocity in a turbulent flow, a small error is involved even if the measuring hot wire anemometer is equipped with a linearizer. Davies, et al., (Reference 8) gave an estimation of the error to be 2 percent when the three turbulent velocity components have intensities equal to 20 percent of the jet exit velocity. No correction for such an error was attempted in the present measurements.

3.1.3 Measurement of Turbulent Velocity Components

Two separate hot-wire probes were used in the measurement of turbulent velocity components. Each probe consisted of either straight wire or X-wire elements as discussed in Section 2.2.2. One of these probes was fixed at a distance of four diameters aft of the jet exit and one-half of a diameter from the jet centerline; whereas, the second probe was movable to any position in the jet. The reason for selecting the position $x_1 = 4D$, $x_2 = 0.5D$, $x_3 = 0$ for the fixed probe was that at this location the turbulent mixing layer of the jet is well developed and previous experiments indicate that jet noise generation is at its highest level. It is probably the best location for a representative study of the turbulence structure for application to jet noise prediction techniques.

Hot-wire signals from the two probes were recorded simultaneously on two channels of magnetic tape using the tape recorder. Also, the hot-wire signals were conditioned through squaring circuits and these outputs were recorded on two other channels of the tape recorder simultaneously with the unconditioned signals.

3.2 Test Conditions

Experiments which have been conducted during the present study are summarized in the following paragraphs. Figure numbers of results corresponding to the various test conditions are also given.

1. The Measurement of Mean Velocity Profiles

   a) Transverse to the jet flow (Figures 8, 9)
      Eight profiles with $x_1/D = 0.5, 1.25, 2.5, 4, 5.5, 7, 9$ and 12 with $x_3/D = 0$.

   b) Parallel to the jet centerline (Figure 10)
      Two profiles with $x_2/D = 0$ and 0.5 with $x_3/D = 0$.

2. The Measurement of Profiles of Turbulent Velocity Intensities

   a) Transverse to the jet flow (Figures 11 through 44)

Turbulent Velocity Components	$x_3 / D = 0$								Number of Profiles Taken
	$x_1 / D = 0.5$	1.25	2.5	4	5.5	7.0	9.0	12	
u	1	1	1	1	1	1	1	1	8
v		1	1	1		1		1	5
w		1	1	1		1		1	5
$u_{45°}$		1	1	1		1		1	5
$u_{135°}$		1	1	1		1		1	5
						Total			28

b) Parallel to the jet centerline (Figures 45, 46).

Turbulent Velocity Components	$x_3 / D = 0$		Number of Profiles Taken
	$x_2 / D = 0$	$x_2 / D = 0.5$	
u	1	1	2
v	1	1	2
w	1	1	2
$u_{45°}$		1	1
$u_{135°}$		1	1
		Total	8

3. The Measurement of Profiles of Jet Noise Intensity Factor, $\overline{U}^2 \cdot \overline{u^2}$

Transverse to the jet flow (Figure 47)

Eight profiles with $x_1 / D = 1.0, 1.5, 2, 4, 5.5, 7, 9$ and 12 with $x_3 / D = 0$.

4. In addition to surveys taken in the turbulence regions of the jet, additional surveys were taken in the potential core where observations of growing instabilities were made (Figure 48). The primary purpose of these tests were to define inherent instabilities in the potential core of the jet. It was discovered that these instabilities were extremely small. However, a growth of disturbances resulting from jet flow was observed.

A total of 220 runs were recorded on magnetic tape using a recording time of 2.5 to 3.0 minutes for each run with a tape speed of 30 inches per second. A more detailed index of runs with a specification of the spacings between probes (ξ_1 , ξ_2, ξ_3) is given in the Appendix.

3.3 Data Reduction

Test results presented in this report were reduced using analog instrumentation. Reduction of the measurements to more complex statistical parameters will be performed in the near future using digital computational equipment; however, these data are not available for the present report. Thus, the present data reduction consisted of only a preliminary evaluation of the measurements.

The analog data reduction instrumentation was discussed in Section 2.3. These instruments were used to define:

- The mean velocity profiles of the jet flow.
- The turbulent velocity intensity profiles in the jet flow.
- The turbulent velocity components u, v, u_{45° , for various locations in the jet flow. Simultaneous measurements will be reduced using digital equipment to determine their correlation properties and will be reported in a later publication.
- The profiles of jet noise intensity factor $\overline{U^2} \cdot \overline{u^2}$.
- The profiles of Reynolds stress $-\overline{uv}$ were determined from the relation $-\overline{uv} = (\overline{u^2}_{135^\circ} - \overline{u^2}_{45^\circ})/2$ (See Section 4.3) for both the transverse direction at $x_1/D = 4.0$, $x_3/D = 0$ and parallel to the jet flow at $x_2/D = 0.5$, $x_3/D = 0$ (Figures 49, 50). Also, one profile of $(-\overline{u_{45^\circ} u_{135^\circ}})$ was obtained at $x_2/D = 0.5$, $x_3/D = 0$ (Figure 51).
- The one-third octave power spectra of the turbulent velocity components u, v, and u_{45° for different points in the jet

flow. These data were recorded on a logarithmic scale using the B and K audio-frequency spectrometer and graphic level recorder with a 50 dB potentiometer. These records were made for the purpose of constructing wave number frequency spectra. The frequency range of the data was limited to 10 K Hz which was the upper frequency limit of the tape recorder. However, the upper frequency limit was considered to be sufficiently high for the purpose of defining the critical range of turbulent frequencies for application to jet noise prediction of the present low speed subsonic jet.

4.0 THE RESULTS OF MEASUREMENTS

4.1 Mean Velocity Profiles

Mean velocity profiles across the jet flow at different sections ranging from 0.5 D to 12 D are shown in Figure 9. Since .iginal measurements showed that the jet flow was axisymmetric relative to the jet aerodynamic centerline, the profiles plotted in Figure 9 cover only half of the jet cross section. Comparison of the profile at $x_1 / D = 4$ was made with those measured by Laurence (Reference 11) and Bradshaw (Reference 9). Excellent agreement was found as shown in Figure 8.

Figure 10 shows the profile taken at the jet axis and the profile taken at a distance of $x_2 / D = 0.5$ (i.e., the centerline of the mixing layer) parallel to the jet axis. Along the jet axis the mean velocity maintained its magnitude at the nozzle exit up to about 4.5 D and then started to decrease. The decrease of velocity between 7 D and 12 D was found to be linear. The normalized rate of change is $(D/U_j) \cdot d\bar{U}/dx_1 \approx -0.0715$. Comparing the velocities at $x_1 / D = 4$ and $x_1 / D = 12$, a velocity drop was measured to be 45 percent. However, the mean velocity profile along the centerline of the mixing layer attenuated rather slowly in the downstream direction. Between $x_1 / D = 4$ and $x_1 / D = 12$ a velocity drop of only 21.6 percent was measured.

4.2 Turbulent Velocity Intensity Profiles

Turbulent velocity intensity profiles are shown in Figure 11 through Figure 46. These include the profiles of u, v, w, u_{45° and u_{135° across the jet flow at different cross sections, along the jet axis and along the centerline of the mixing layer. At the centerline of the mixing layer, the turbulence intensity profiles of different velocity components decreased slowly in the direction of the jet flow as shown by Figure 46. A decrease of 15 percent of the streamwise turbulent velocity intensity was measured between $x_1/D = 4$ and 12. The turbulence intensity profiles of u, v, w and u_{45° measured at the section $x_1 / D = 4$ were compared with those measured by Laurence (Reference 11), Chu (Reference 3), Davies, et al. (Reference 8), and Bradshaw, et al. (Reference 9). They are in good agreement as shown by Figure 11 except for the profiles of w and u_{45° for which a slight difference was found when compared to the results by Bradshaw, et al. (w-measurement) and by Chu (u_{45°-measurement). The lack of agreement with Chu's data is possibly due to the effect of the jet exit speed since in Chu's report a jet exit speed of 142 fps was employed which is less than one-half of the speed employed in the present measurements. However, the reason which may explain the small difference of w-measurements between the present work and the work by Bradshaw, et al. has not been determined so far.

In present measurements, the turbulent velocity intensity profiles at the centerline of the mixing layer (Figure 46) showed that they maintain quite flat levels at least in a range covering $x_1 = 1\,D$ to $x_1 = 9\,D$, and also showed that

$$\sqrt{\overline{u^2}_{45^\circ}} > \sqrt{\overline{u^2}} > \sqrt{\overline{w^2}} > \sqrt{\overline{v^2}} > \sqrt{\overline{u^2}_{135^\circ}}$$

At $x_1 = 4\,D$, their normalized values were observed to be

$$\sqrt{\overline{u^2}_{45^\circ}} / U_j = 0.17$$

$$\sqrt{\overline{u^2}} / U_j = 0.16$$

$$\sqrt{\overline{w^2}} / U_j = 0.13$$

$$\sqrt{\overline{v^2}} / U_j = 0.12$$

$$\sqrt{\overline{u^2}_{135^\circ}} / U_j = 0.102$$

and one can see that the magnitude of $\sqrt{\overline{u^2}_{45^\circ}}$ is 1.7 times larger than the magnitude of $\sqrt{\overline{u^2}_{135^\circ}}$. The measurement $\sqrt{\overline{u^2}_{45^\circ}}$ by Chu (Reference 3) also showed that $\sqrt{\overline{u^2}_{45^\circ}} > \sqrt{\overline{u^2}}$. However, the result of $\sqrt{\overline{u^2}_{135^\circ}}$ has not been found in the existing literature, and therefore no comparison can be made at the present time.

The turbulent velocity intensity profiles along the jet axis (Figure 45) showed that $\sqrt{\overline{u^2}}$ is greater than $\sqrt{\overline{u^2}_{45^\circ}}$ (or $\sqrt{\overline{u^2}_{135^\circ}}$) and that $\sqrt{\overline{u^2}_{45^\circ}}$ (or $\sqrt{\overline{u^2}_{135^\circ}}$) is greater than $\sqrt{\overline{v^2}}$ (or $\sqrt{\overline{w^2}}$) and this possibly means that even along the jet axis, where mean shear does not exist, the turbulence structure of velocity fluctuations cannot be considered as isotropic.

4.3 Profiles of Reynolds Stress

Reynolds stresses have not been measured directly in the present work; however, since the following relation holds between the velocity components u, v, and u_{45^o}, u_{135^o}:

$$u = \frac{u_{45^o}}{\sqrt{2}} - \frac{u_{135^o}}{\sqrt{2}}$$

$$v = \frac{u_{45^o}}{\sqrt{2}} + \frac{u_{135^o}}{\sqrt{2}}$$

thus,

$$-\overline{uv} = \frac{1}{2}\left(\overline{u^2}_{135^o} - \overline{u^2}_{45^o}\right)$$

such that the Reynolds stress can be computed from the measurements of $\overline{u^2}_{45^o}$ and $\overline{u^2}_{135^o}$. Computed profiles of $-\overline{uv}$ and $-\overline{u_{45^o} u_{135^o}}$ (also using the above relation) along the centerline of the mixing layer and the profile of $-\overline{uv}$ across the jet at $x_1 = 4D$ are as shown by Figures 49 to 51. They were found in good agreement with the direct measurements of $-\overline{uv}$ by Bradshaw, et al. (Reference 9). However, the profile of $-\overline{u_{45^o} u_{135^o}}$ computed with the measurement of $\sqrt{\overline{u^2}}$ and $\sqrt{\overline{v^2}}$ by Bradshaw, et al. (Reference 9, Figures 31-32) showed some difference with the present work (Figure 51). A close examination showed that Figures 9, 31, 32, 36, and 37 of the report by Bradshaw, et al. may be inconsistent to one another. In their report, if Figures 36-37 are used instead of Figures 31-32, good agreement can be obtained with the present measurements and computation. However, this only covers two points, i.e., $x_1 = 4D$ and $x_1 = 7D$.

4.4 Profiles of the Noise Source Intensity Factor

Profiles of the noise source intensity factor $\overline{U^2} \cdot \overline{u^2}$, were measured directly at different sections of the jet flow and are presented in Figure 47. The maximum value of $\overline{U^2} \cdot \overline{u^2}$ was found to be located at about two diameters downstream of the jet exit. It can also be seen in Figure 47 that the peak value of $\overline{U^2} \cdot \overline{u^2}$ in a cross sectional profile in the initial region of the jet is only slightly at the inner side of the centerline of the mixing layer. Further downstream, the peak moves rapidly towards the jet central axis. A comprehensive study of the noise source factor, $\overline{U^2} \cdot \overline{u^2}$, which is related to the sound source distribution in a jet flow can be found in Reference 12.

4.5 Power Spectra of Turbulent Velocity Components

The power spectra of u, v, and u_{45° at different points in the jet flow measured in one-third octave bands were plotted as shown by Figures 52-59. The power spectra of the u-component as measured by Laurence (Reference 11) at $x_1 = 4D$, $x_2 = 0.5D$ and $x_3 = 0$ were replotted and compared with the present measurement. They are in good agreement as shown in Figure 52.

In Figures 53-54, a (0) slope and a (-7/10) slope line has been drawn for comparison with one-third octave measurements. The slopes correspond to a (-1) slope and a (-5/3) slope lines, respectively, for power spectral density where a constant narrow band filter is employed. The same slope lines were used for comparison with wall turbulence spectra by Klebanoff (Reference 13) and Laufer (Reference 14). Similarly, in the present measurement, the part of the u-spectrum which follows the (0) slope is related to the turbulence produced during its interaction with the main shear while the part of u-spectrum which follows the (-7/10) slope corresponds to the inertial subrange. In the inertial subrange, energy transfer occurs only among different wave numbers of the same turbulent velocity component. However, the applicability of the above comparison of slope depends on how close the actual turbulent flow is to the isotropic turbulence. In Figure 59 there is a comparatively lower energy level in the lower wave number range for the v-spectrum which is also similar to the result in a pipe flow which was studied by Laufer (Reference 14). This has been explained (Reference 15) by the fact that, in the lower wave number range of the energy containing eddies, more energy related to the u-component is produced. A portion of this energy, then, is transferred through the pressure-velocity-gradient correlation to the v-component in addition to its transfer of energy to the higher-wave number range of the same velocity component. Since this correlation contains the velocity gradient it is reasonable to expect that the energy transfer to the v-component will occur at a higher rate in the higher-wave number range.

5.0 DISCUSSIONS

5.1 Principal Directions of the Mean Stresses in the Mixing Layer

The principal axes of mean stress and mean strain-rate were previously studied by Townsend (Reference 16), Corrsin (Reference 17), and Grant (Reference 10). In a turbulent shear flow if the mean profile is not too steep, the turbulent shear stress is usually much greater than the mean shear stress. Then, the principal axes along which all mean shear stresses vanish are practically the same axes at which only the turbulent shear stress vanishes. For example, in a circular jet like the one used in the present study, if one takes x_1-axis along the jet axis and x_2-axis normal to it, the normal stresses σ_{x_1} and σ_{x_2}, and the shear stress $\tau_{x_1 x_2}$ (or $\tau_{x_2 x_1}$), may be expressed as:

$$\sigma_{x_1} = -\overline{p} + 2\mu \frac{\partial \overline{U}}{\partial x_1} - \rho \overline{u^2} \qquad (1)$$

$$\sigma_{x_2} = -\overline{p} + 2\mu \frac{\partial \overline{V}}{\partial x_2} - \rho \overline{v^2} \qquad (2)$$

$$\tau_{x_1 x_2} = \tau_{x_2 x_1} = \mu \left(\frac{\partial \overline{U}}{\partial x_2} + \frac{\partial \overline{V}}{\partial x_1} \right) - \rho \overline{uv} \qquad (3)$$

where $\overline{p}$ is the mean static pressure which can be dropped out since it holds the same magnitude in all directions. Also, as already pointed out in the above and verified by measurements (present work and References 8, 9, 11), the stresses which are induced by mean velocity gradients are much smaller than the turbulent stresses. Therefore, Equations (1) to (3) become

$$\sigma_{x_1} \doteq - \rho \overline{u^2} \qquad (4)$$

$$\sigma_{x_2} \doteq - \rho \overline{v^2} \qquad (5)$$

$$\tau_{x_1 x_2} \doteq - \rho \overline{uv} \qquad (6)$$

For the principal direction of mean stresses (Figure 60), α may be computed by following the well-known formula,

$$\alpha = \frac{1}{2} \tan^{-1} \left(\frac{2\,\tau_{x_1 x_2}}{\sigma_{x_1} - \sigma_{x_2}} \right)$$

$$= \frac{1}{2} \tan^{-1} \left(\frac{2\,\overline{u v}}{\overline{u^2} - \overline{v^2}} \right) \qquad (7)$$

The magnitudes of principal stresses are given by

$$\sigma_{max.\ (or\ min.)} = \sigma_{x_1} \cos^2 \alpha + \sigma_{x_2} \sin^2 \alpha + \tau_{x_1 x_2} \sin 2\alpha$$

or $$-\rho\, \overline{u_\alpha^2} = -\rho\, \overline{u^2} \cos^2 \alpha - \rho\, \overline{v^2} \sin^2 \alpha - \rho\, \overline{u v} \sin 2\alpha \qquad (8)$$

where α refers to principal direction.

At the point $x_1 = 4D$ and $x_2 = 0.5D$, present measurements showed that

$$\left.\begin{array}{l} \sqrt{\overline{u^2}}/U_j = 0.16 \\ \sqrt{\overline{v^2}}/U_j = 0.12 \end{array}\right\} \quad \text{(Figure 46)}$$

$$\frac{\overline{u v}}{U_j^2} = 0.009 \qquad \text{(Figure 50)}$$

with U_j = 300 (fps)

Then, from Equation (7), the azimuth angle of the principal directions are

$$\alpha = \frac{1}{2} \tan^{-1} 2 \left[\frac{(0.009) \times 300^2}{(0.16 \times 300)^2 - (0.12 \times 300)^2} \right] = 29.2^\circ \text{ or } 119.2^\circ;$$

and from Equation (8) with $\alpha = 29.2°$

$$\frac{\overline{u^2_\alpha}}{U_j^2} = \frac{\overline{u^2}}{U_j^2} \cos^2\alpha + \frac{\overline{v^2}}{U_j^2} \sin^2\alpha + \frac{\overline{uv}}{U_j^2} \sin 2\alpha$$

$$= (0.16)^2 \cos^2 29.2° + (0.12)^2 \sin^2 29.2° + (0.009) \sin 58.4°$$

$$= 0.0306$$

and therefore the value of the maximum turbulent intensity is

$$\frac{\sqrt{\overline{u^2}_{29.2°}}}{U_j} = 0.175$$

Similarly, with = 119.2°, the minimum turbulent intensity takes the value of

$$\frac{\sqrt{\overline{u^2}_{119.2°}}}{U_j} = .097$$

From these results one can see that the maximum turbulence intensity is 1.8 times larger than the minimum turbulence intensity. In other words, the maximum turbulent normal stress is 3.25 times larger than the minimum turbulent normal stress.

Turbulent velocity compounds at directions 29.2° or 119.2° have not been measured at the present time such that the above computed result cannot be verified, although trends in the data suggest that these values are correct. For example, the present measurements do include turbulent velocity components at the direction of 45° and of 135°, which showed (Figure 46):

$$\frac{\sqrt{\overline{u^2}_{45°}}}{U_j} = 0.17 \qquad \text{and} \qquad \frac{\sqrt{\overline{u^2}_{135°}}}{U_j} = 0.102$$

Again from Equation (8), with $\alpha = 45^\circ$, one finds

$$\frac{\sqrt{\overline{u^2}_{45^\circ}}}{U_j} = \left[\frac{\overline{u^2}}{U_j} \cos^2 45^\circ + \frac{\overline{v^2}}{U_j^2} \sin^2 45^\circ + \frac{\overline{uv}}{U_j^2} \sin 90^\circ \right]^{\frac{1}{2}}$$

$$= \left[(0.16)^2 \cdot \frac{1}{2} + (0.12)^2 \cdot \frac{1}{2} + 0.009 \right]^{\frac{1}{2}}$$

$$= 0.17 \text{ (Computed)}$$

and similarly, with $\alpha = 135^\circ$

$$\frac{\sqrt{\overline{u^2}_{135^\circ}}}{U_j} = \left[(0.16)^2 \cdot \frac{1}{2} + (0.12)^2 \cdot \frac{1}{2} - 0.009 \right]^{\frac{1}{2}}$$

$$= 0.105 \text{ (Computed)}$$

Their agreement with direct measurements is excellent.

5.2 Flow Fluctuations Inside the Potential Core

Hot-wire signals of velocity fluctuations at different points along the jet central axis of the potential core were observed on an oscilloscope. As shown by Figure 48, small oscillations started at about $x_1 = 1.0D$ and built up gradually downstream, regardless of the constancy of the mean flow velocity inside the potential core (Figure 10). Observations showed also that

1) Oscillations (or fluctuations) were irregular but confined to a much narrower frequency band (Figure 55) as compared with the fully developed turbulence in the mixing layer (Figure 54).

2) The fluctuating level is quite steady.

3) Starting at five diameters downstream of the jet exit, high frequency spikes started to appear intermittently on top of the "smooth" oscillations.

Similar fluctuations in the potential core were also observed by Kuethe (Reference 6) and Bradshaw, et al. (Reference 9). Since a uniform mean velocity field holds inside the potential core it is plausible that the growing instabilities are induced by the vortex motion which exists between a moving jet and the ambient air. The next logical question is whether this fluctuating motion is rotational or irrotational. Irrotational fluctuations at the boundary between turbulence and an irrotational free stream were discussed by Phillips (Reference 18), Stewart (Reference 19), and Bradshaw, et al. (Reference 9). Obviously, the irrotational fluctuations which they found at the intermittent turbulent front in a free stream are not the same kind of fluctuations which, according to the present observation, appeared inside the potential core and grew steadly in the downstream direction. The fluctuating flow inside the core is rotational, which can be shown by the following analysis:

In an imcompressible flow, the equation of motion can be written as

$$\frac{\partial \vec{q}}{\partial t} - \vec{q} \times \vec{\Omega} = -\,\mathrm{grad}\left(\frac{p}{\rho} + \frac{q^2}{2}\right) + \nu \nabla^2 \vec{q} \qquad (9)$$

where $\overrightarrow{-q \times \Omega}$ is the vorticity term and no external force is involved. When Equation (9) is applied at the jet central axis inside the potential core, the following velocity, vorticity, and pressure components can be introduced:

$$\vec{q} \; : \quad q_1 = \overline{U} + u(t), \quad q_2 = v(t), \quad q_3 = w(t)$$

$$\vec{\Omega} \; : \quad \left.\begin{aligned} \Omega_1 &= \omega_1(t) \\ \Omega_2 &= \omega_2(t) \\ \Omega_3 &= \omega_3(t) \end{aligned}\right\} \text{ if it exists}$$

$$p \; : \quad p = \overline{p} + p'(t)$$

again, since,

$$\mathrm{grad}\left(\frac{\overline{p}}{\rho} + \frac{\overline{U}^2}{2}\right) = 0$$

$$\frac{\partial \overline{U}}{\partial t} = \nabla^2 \overline{U} = 0$$

and $\overline{u} = \overline{v} = \overline{w} = \overline{p'} = 0$

and Equation (9) becomes

$$\overline{v\,\omega_3} - \overline{w\,\omega_2} = \frac{\partial}{\partial x_1}\left(\frac{\overline{u_i\,u_i}}{2}\right) \qquad (10)$$

$$\overline{w\,\omega_1} - \overline{u\,\omega_3} = \frac{\partial}{\partial x_2}\left(\frac{\overline{u_i\,u_i}}{2}\right) \qquad (11)$$

and

$$\overline{u\,\omega_2} - \overline{v\,\omega_1} = \frac{\partial}{\partial x_3}\left(\frac{\overline{u_i\,u_i}}{2}\right) \qquad (12)$$

where

$$\overline{u_i\,u_i} = \overline{u^2} + \overline{v^2} + \overline{w^2}$$

At the jet central axis, measurements (Figures 45 and 40-42; or Reference 6 and 9) showed

$$\frac{\partial}{\partial x_1}\left(\frac{\overline{u_i\,u_i}}{2}\right) > 0$$

$$\frac{\partial}{\partial x_2}\left(\frac{\overline{u_i\,u_i}}{2}\right) = \frac{\partial}{\partial x_3}\left(\frac{\overline{u_i\,u_i}}{2}\right) = 0$$

also, in view of the axial symmetry of a circular jet, the following relation holds at the jet central axis,

$$\overline{v\,\omega_3} = -\,\overline{w\,\omega_2}$$

and finally Equation (10) can be written as

$$\overline{v\,\omega_3} = \frac{1}{4}\,\frac{\partial}{\partial x_1}\left(\overline{u_i\,u_i}\right) > 0 \qquad (13)$$

Equation (13) shows that ω_3 can not vanish at all times, or in other words:

$$\overline{\omega_3^{\,2}} > 0$$

Thus, the fluctuating flow inside the potential core is rotational.

6.0 WORK TO BE CONTINUED

6.1 Wave Number-Frequency Spectra

As described in Section 3.0, a total of 220 sets of covariance data for $\overline{v v'}$ and $\overline{u_\theta^2 u_\theta'^2}$ at $\theta = 0^\circ$, 45°, and 90° have been recorded. These data are expected to provide detailed wave number-frequency spectra of the turbulence structure in the most intense noise producing region of the jet. As discussed in References 5 and 12, the prediction of directivity and spectra of the noise requires knowledge of the four-dimensional wave number-frequency spectra of the turbulence structure in the mixing region of the jet.

In the continuing effort, the turbulence covariance data will be reduced through an analog/digital scheme. An outline of the preliminary plan to do this is as described in Wyle Laboratories Technical Proposal Number 570/7430/DE, January 1970.

6.2 The Measurement of Turbulence Intensity of Velocity Components at Principal Directions

In Section 5.1, computations using the present experimental result showed that at $x_1 = 4D$ and $x_2 = 0.5D$, principal directions of the mean turbulent stress are possibly oriented at azimuth angles of 29.2° and 119.2° to the jet axis. It should be of significant interest to verify this computation with measurements at different sections along the axis of the jet. Present computations showed that the ratio of maximum to minimum mean square velocity fluctuations at principal directions is as high as 3.25 (or 5 dB) which may partially explain the directivity of noise patterns produced by a turbulent jet.

7.0 CONCLUSIONS

Principal conclusions from the present study are as follows:

1. Measurements of the mean velocity profile along the jet central axis show that the constant mean velocity of the potential core starts to decrease at about 4.5 diameters aft of the jet exit. Between 7 diameters and 12 diameters downstream of the exit, the mean velocity drops more rapidly following a constant rate $(D/U_j)\, d\overline{U}/dx_1 \approx -0.0715$.

2. Measurements of profiles of the turbulent intensity of different velocity components show that along the centerline of the mixing layer their intensities maintain a constant level for about 9 diameters. Beyond this distance, the intensity levels slowly decline. Among different velocity components, measurements also showed that $\overline{u^2}_{45^\circ} > \overline{u^2} > \overline{w^2} > \overline{v^2} > \overline{u^2}_{135^\circ}$. At $x_1 = 4D$, $x_2 = 0.5D$ the ratio of $\sqrt{\overline{u^2}_{45^\circ}}$ to $\sqrt{\overline{u^2}_{135^\circ}}$ was observed to be 1.7.

3. Reynolds stress per unit mass $-\overline{uv}$ can be computed from the measurement of $\overline{u^2}_{45^\circ}$ and $\overline{u^2}_{135^\circ}$. Results are in good agreement with direct measurements by previous investigators.

4. A jet noise source factor, $\overline{U}^2 \cdot \overline{u^2}$, as defined by Pao and Lowson (Reference 5) was measured directly. Results show that the peak values of $\overline{U}^2 \cdot \overline{u^2}$ are located at about two diameters downstream of the jet exit. The peak of the noise intensity factor in a cross sectional profile in the initial region of the jet is only slightly inside the center of the mixing layer. Further downstream, the peak moves rapidly towards the jet axis.

5. One-dimensional power spectra of the v-component of jet turbulence in the mixing layer have less energy distributed in the range of lower wave number than the spectra of the u-component at the same location, which can be explained by energy transfer between u- and v-components through the pressure-velocity gradient correlations.

6. Principal directions of mean stress at the point $x_1 = 4D$, $x_2 = 0.5D$ and $x_3 = 0$ were computed by using measurements of $\overline{u^2}$, $\overline{v^2}$, and $-\overline{uv}$ at the same location. It was found that the maximum normal stress occurs at an angle of 29.2° and the minimum normal stress at an angle of 119.2° from the jet axis. The ratio of maximum stress to minimum stress $\overline{u^2}_{29.2^\circ}/\overline{u^2}_{119.2^\circ}$ was computed to be 3.25.

7. Fluctuation of velocity components was observed in the potential core along the jet axis, which steadily increased in the downstream direction. A simple analysis was given using the equation of motion, which showed that such a fluctuating flow field is rotational.

REFERENCES

1. Lighthill, M.J., "On Sound Generated Aerodynamically, I and II," Proceedings of Royal Society, Series A, Vol. 211, 564-578 (1952); Vol. 222, 1-32, (1954).

2. Ribner, H.S., "The Generation of Sound by Turbulent Jets," Advances in Applied Mechanics, Vol. 8, Academic Press, New York, 103-182, (1964).

3. Chu, W.T., "Turbulence Measurements Relevant to Jet Noise," University of Toronto, Institute for Space Studies, UTTAS Report No. 119, (1966).

4. Ffowcs Williams, J.E., "The Noise from Turbulence Convected at High Speed," Phil. Trans. Roy. Soc., London, Vol. A 255, 469-503, (1963).

5. Pao, S.P., and Lowson, M.V., "Spectral Techniques in Jet Noise Theory," Wyle Laboratories Research Report WR 68-21, (1969).

6. Kuethe, A.M., "Investigations of the Turbulent Mixing Regions Formed by Jets," Jour. Appl. Mech. 2, No. 3, (1935).

7. Corrsin, S., and Uberoi, M.S., "Spectra and Diffusion in a Round Turbulent Jet," NACA Report 1040, (1951).

8. Davies, P.O.A.L., et al., "The Characteristics of the Turbulence in the Mixing Region of a Round Jet," The Fluid Mech., Vol. 15, (1963) - also, NATO, AGARD Report 451, (1963).

9. Bradshaw, P., Ferriss, D.H., and Johnson, R.F., "Turbulence in the Noise-Producing Region of a Circular Jet," NATO, AGARD Report 450, (1963).

10. Grant, H.L., "The Large Eddies of Turbulent Motion," J. Fluid Mech., Vol. 4, (1958).

11. Laurence, James C., "Intensity, Scale, and Spectra of Turbulence in Mixing Region of Free Subsonic Jet," NACA Report 1292, (1956).

12. Lowson, M.V., and Pao, S.P., "Some Applications of Jet Noise Theory," Wyle Laboratories Research Report WR 70-4, (1969).

13. Klebanoff, P.S., and Diehl, Z.W., "Some Features of Artificially Thickened Fully Developed Turbulent Boundary Layers with Zero Pressure Gradient," NACA Report 1110, (1952).

14. Laufer, J., "The Structure of Turbulence in Fully Developed Pipe Flow," NACA TN 2954, (1953).

15. Hinze, J.O., "Turbulence," McGraw-Hill, New York, (1959).

16. Townsend, A.A., "The Structure of Turbulent Shear Flow," Cambridge University Press, (1956).

17. Corrsin, S., "Some Current Problems in Turbulent Shear Flows," Sect XV, Symposium on Naval Hydrodynamics, National Academy of Sciences - National Research Council, Publication No. 515, Washington, D.C., (1957).

18. Phillips, O.M., "The Irrotational Motion Outside a Free Turbulent Boundary," Proc. Camb. Phil. Soc., Vol. 51, 220, (1955).

19. Stewart, R.W., "Irrotational Motion Associated with Free Turbulent Flows," J. Fluid Mech., Vol. 1, 6, 593, (1956).

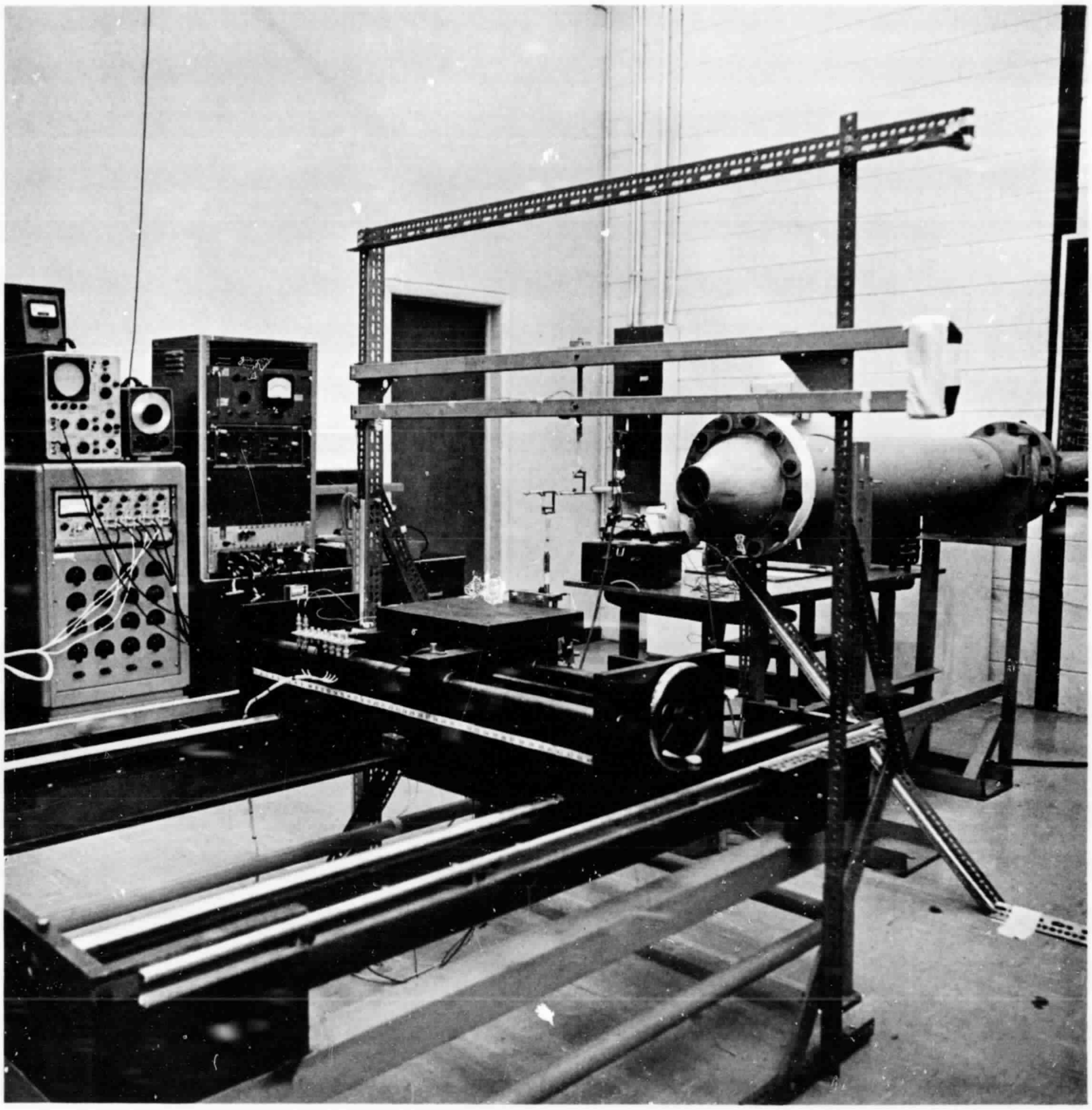

Figure 1. Test Apparatus for the Study of the Turbulence Structure in a Circular Jet

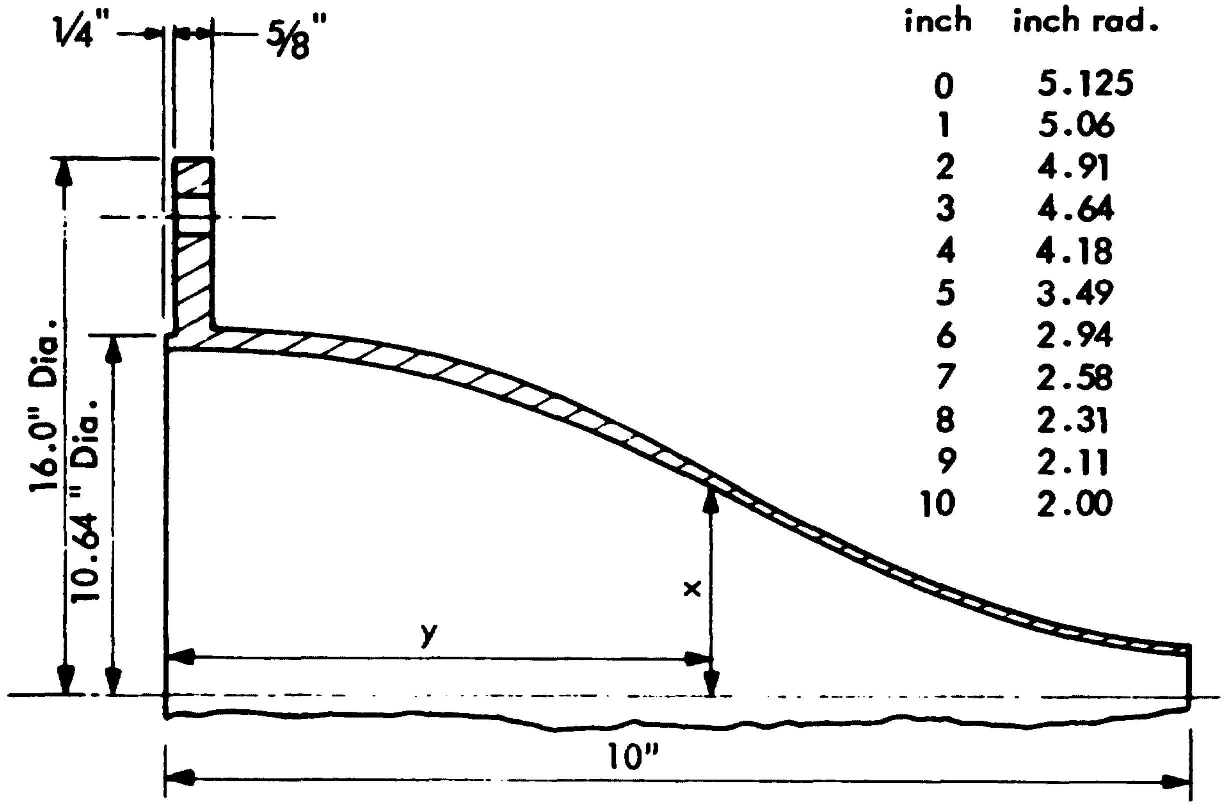

4" Exit Diameter Nozzle

DIMENSIONS

y inch	x inch rad.
0	5.125
1	5.06
2	4.91
3	4.64
4	4.18
5	3.49
6	2.94
7	2.58
8	2.31
9	2.11
10	2.00

Figure 2. Dimensions of 4" Exit Diameter Nozzle

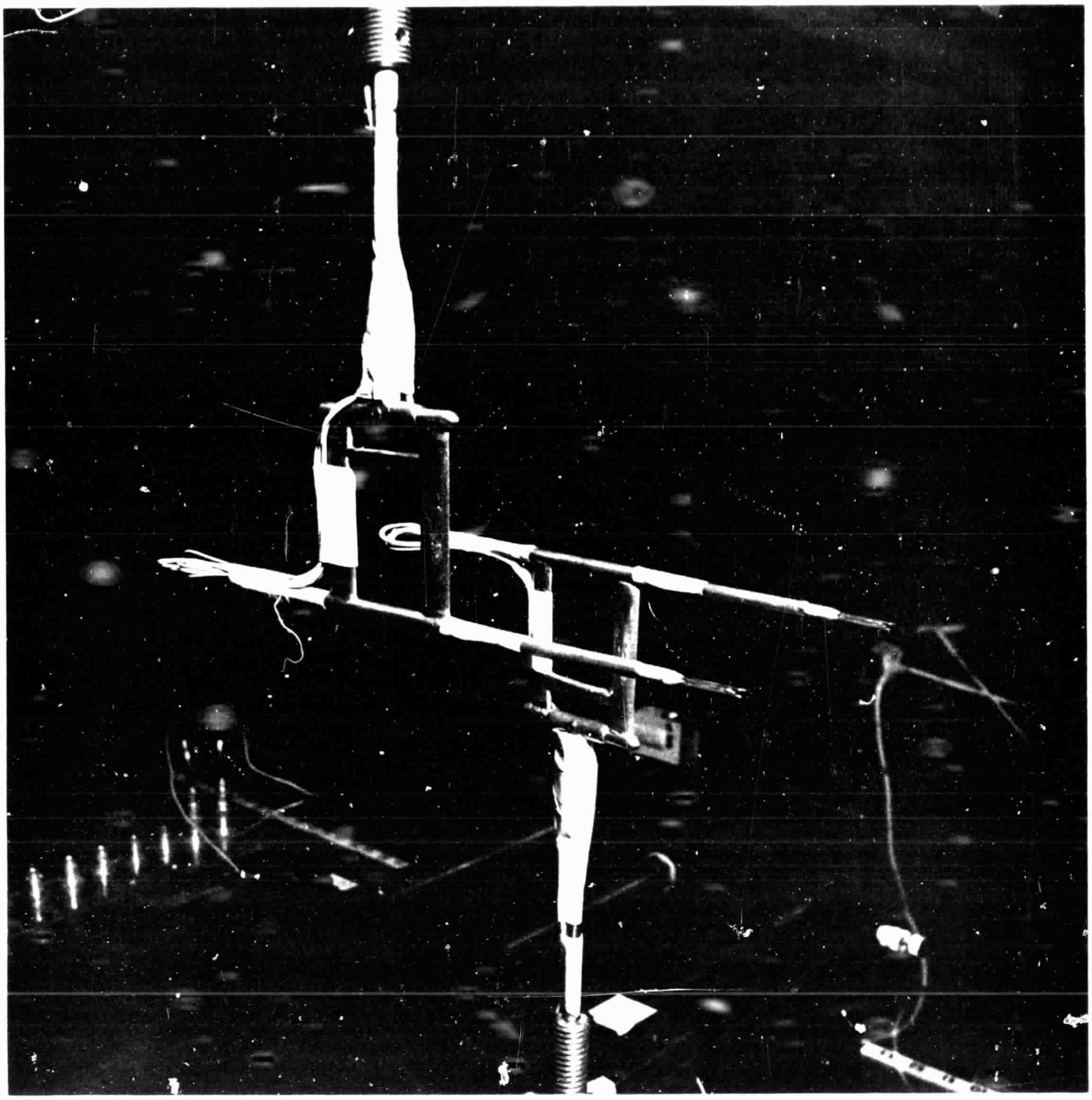

Figure 3. Hot-Wire Probes Mounted in Their Holders

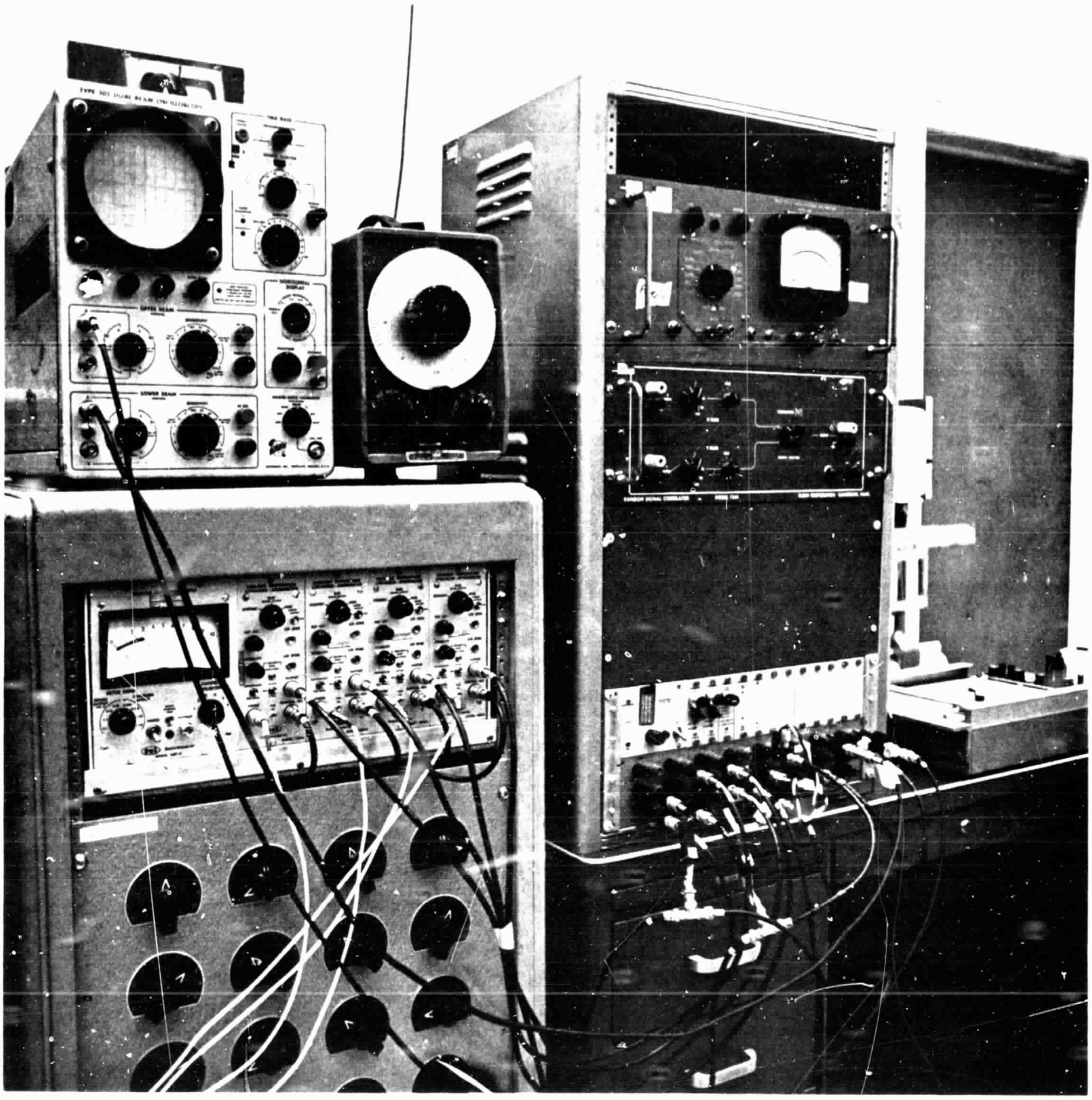

Figure 4. Supporting Electronics and the Constant Temperature Anemometers with Linearizers

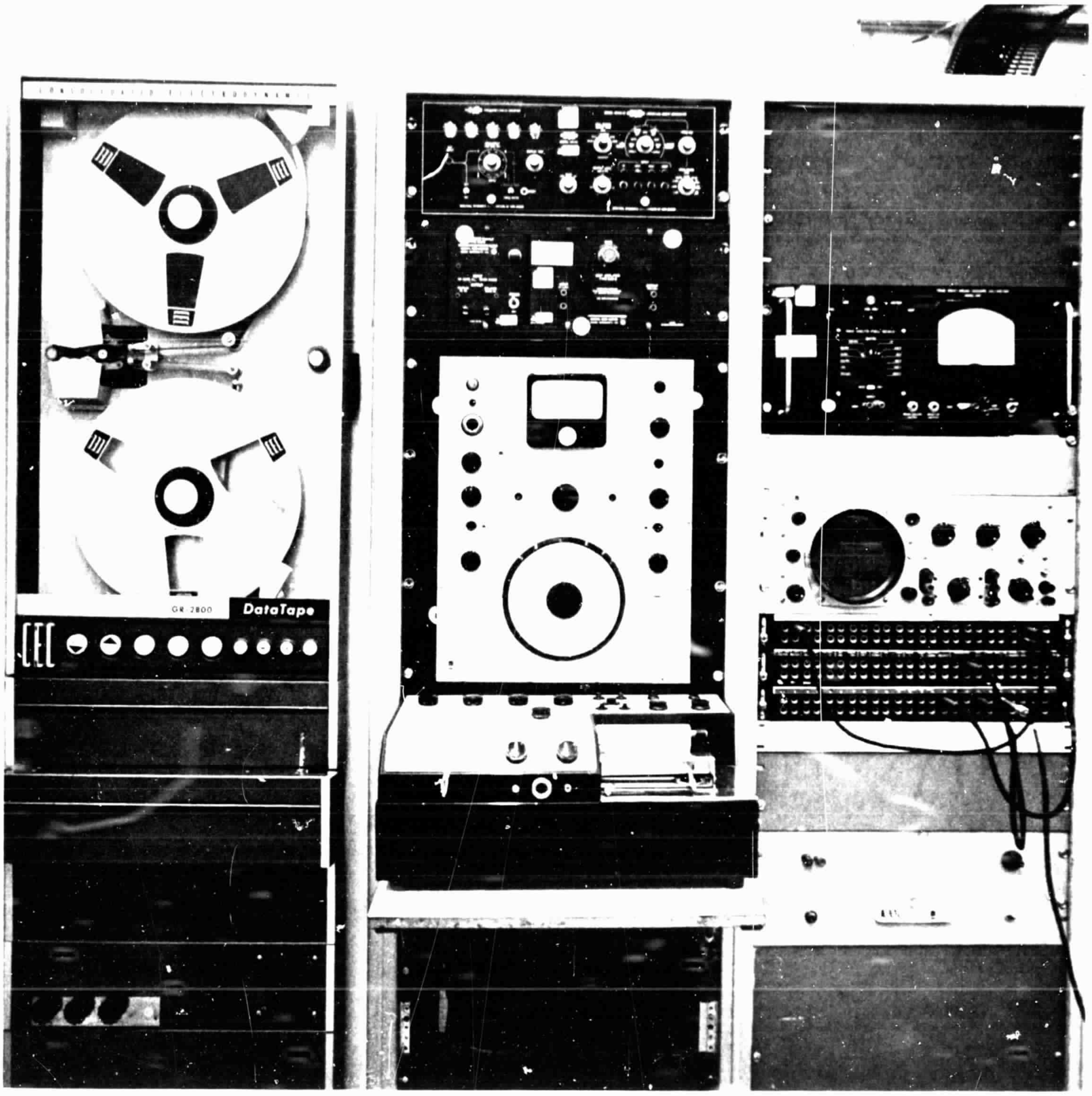

Figure 5. Tape Recorder and the Analog Wave Analyzer Assembly

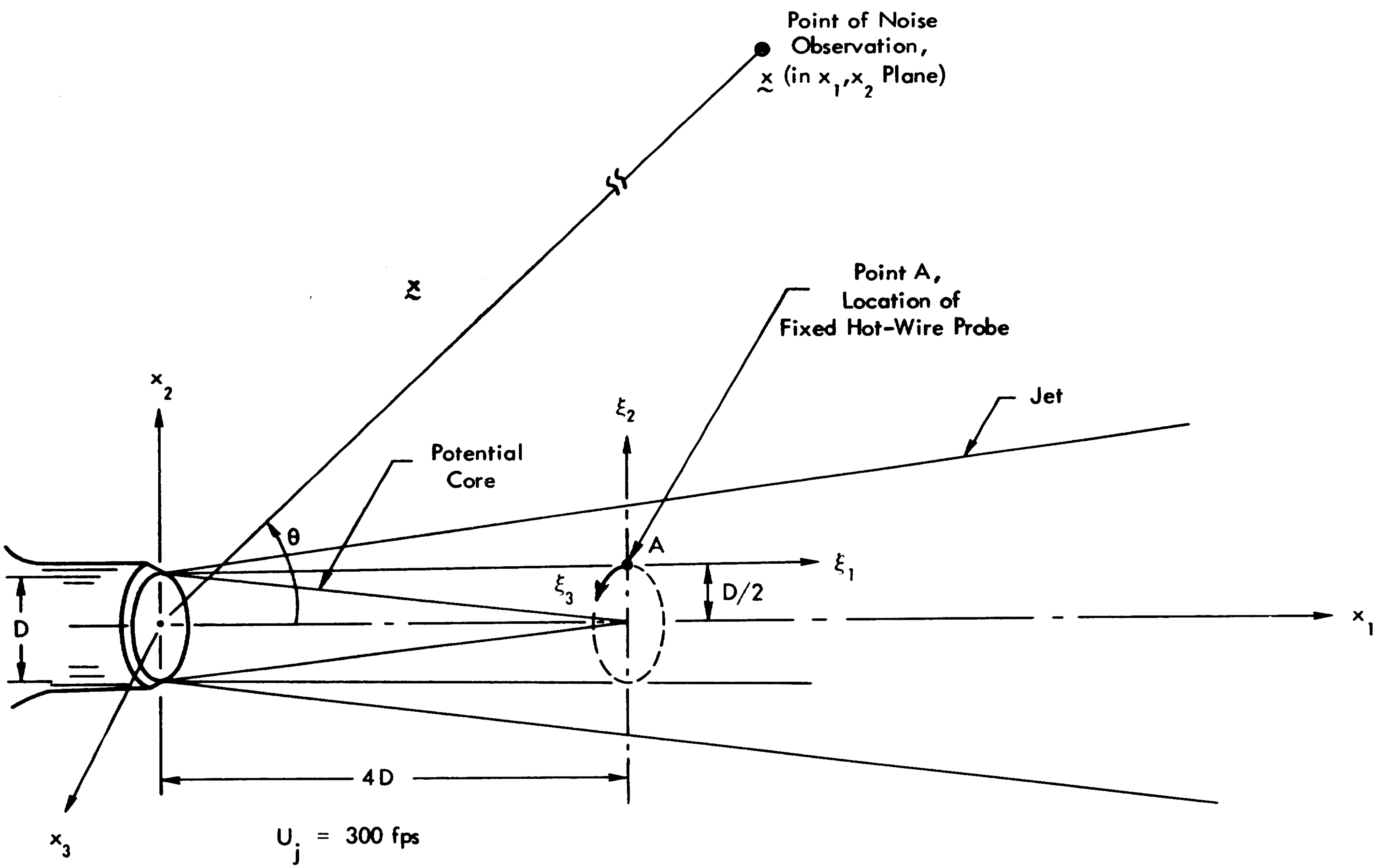

U_j = 300 fps

D = 4 in.

Figure 6. Coordinate System of the Jet

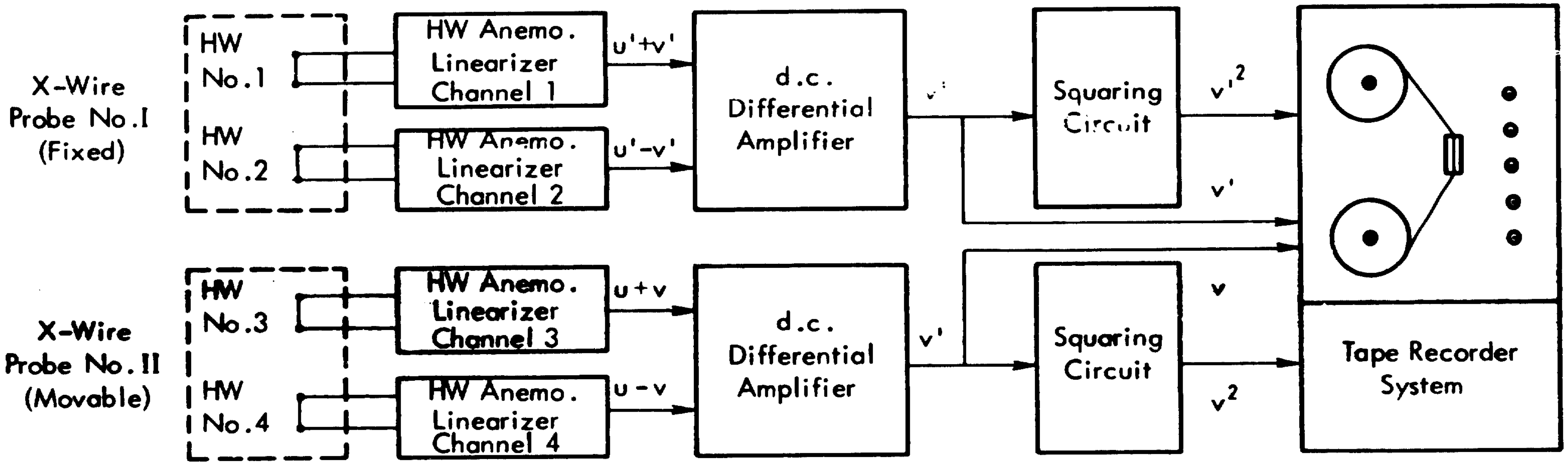

(a) Experimental Setup for the Recording of Turbulent Velocity Components

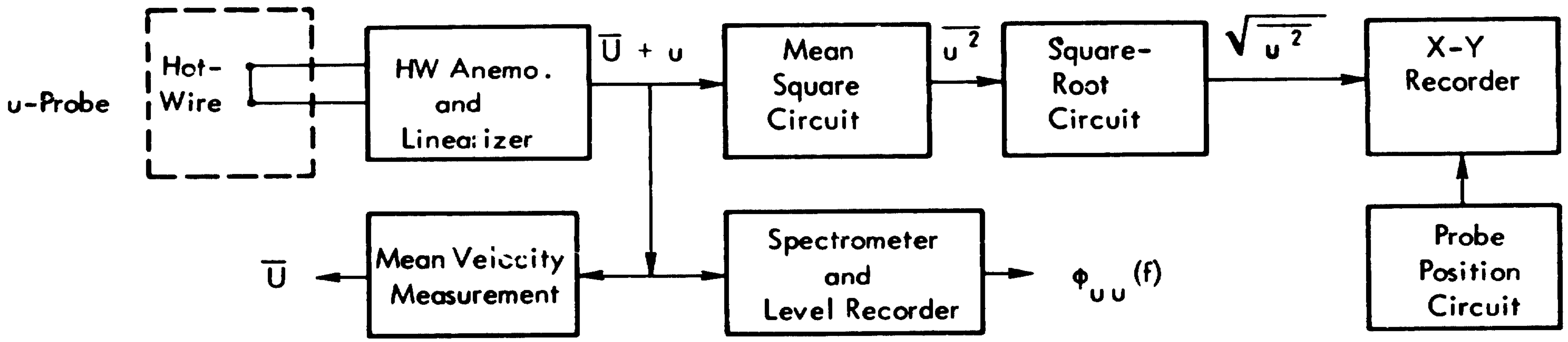

(b) Experimental Setup for Measuring $\overline{U}, \sqrt{\overline{u^2}}, \phi_{uu}$, etc.

Figure 7. Analog Data Acquisition, Reduction, and Monitoring Systems

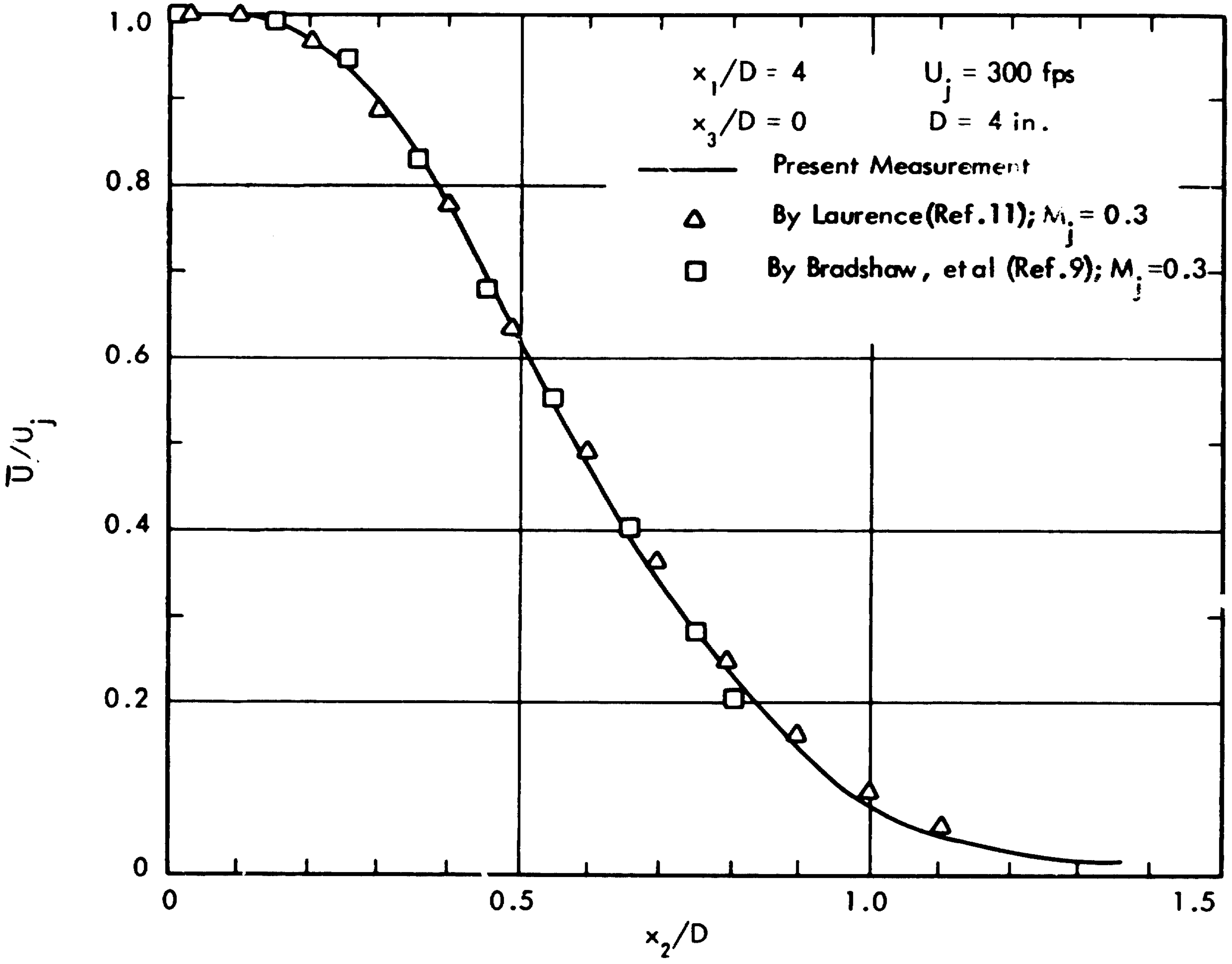

Figure 8. Comparison of the Mean Velocity Profile with Previous Results

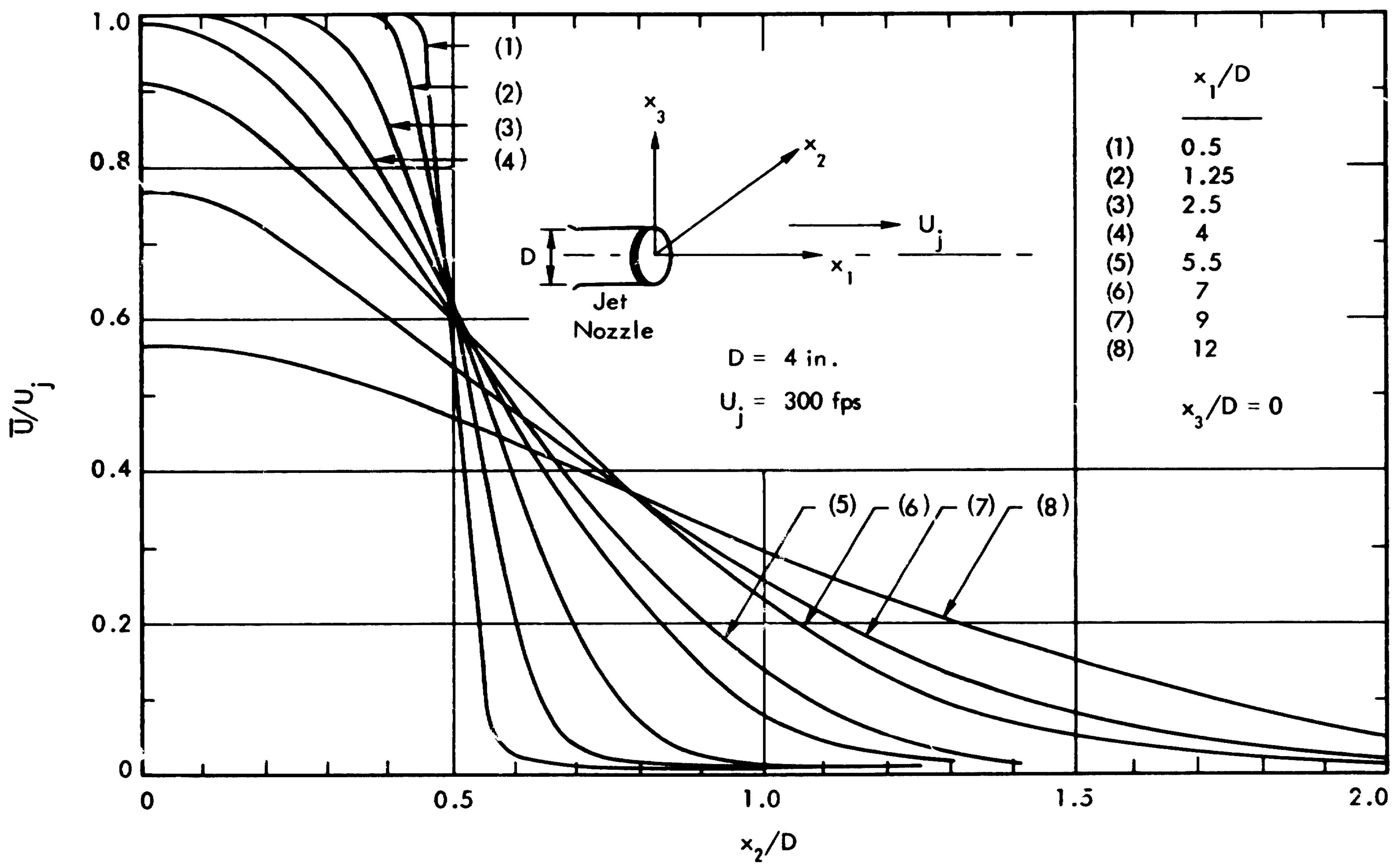

Figure 9. Mean Velocity Profiles Measured Across the Jet Flow

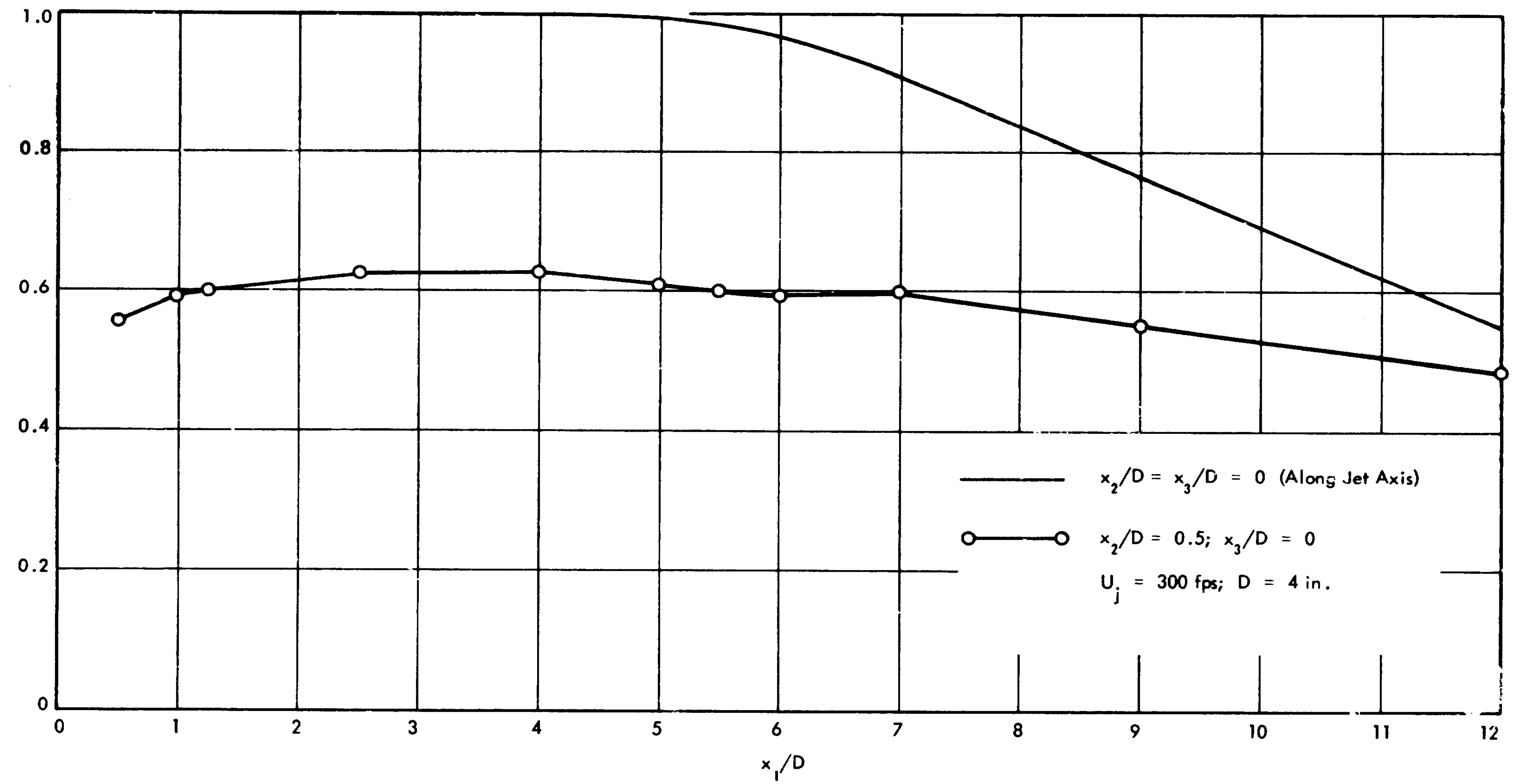

Figure 10. Mean Velocity Profiles Measured Along the Jet Flow

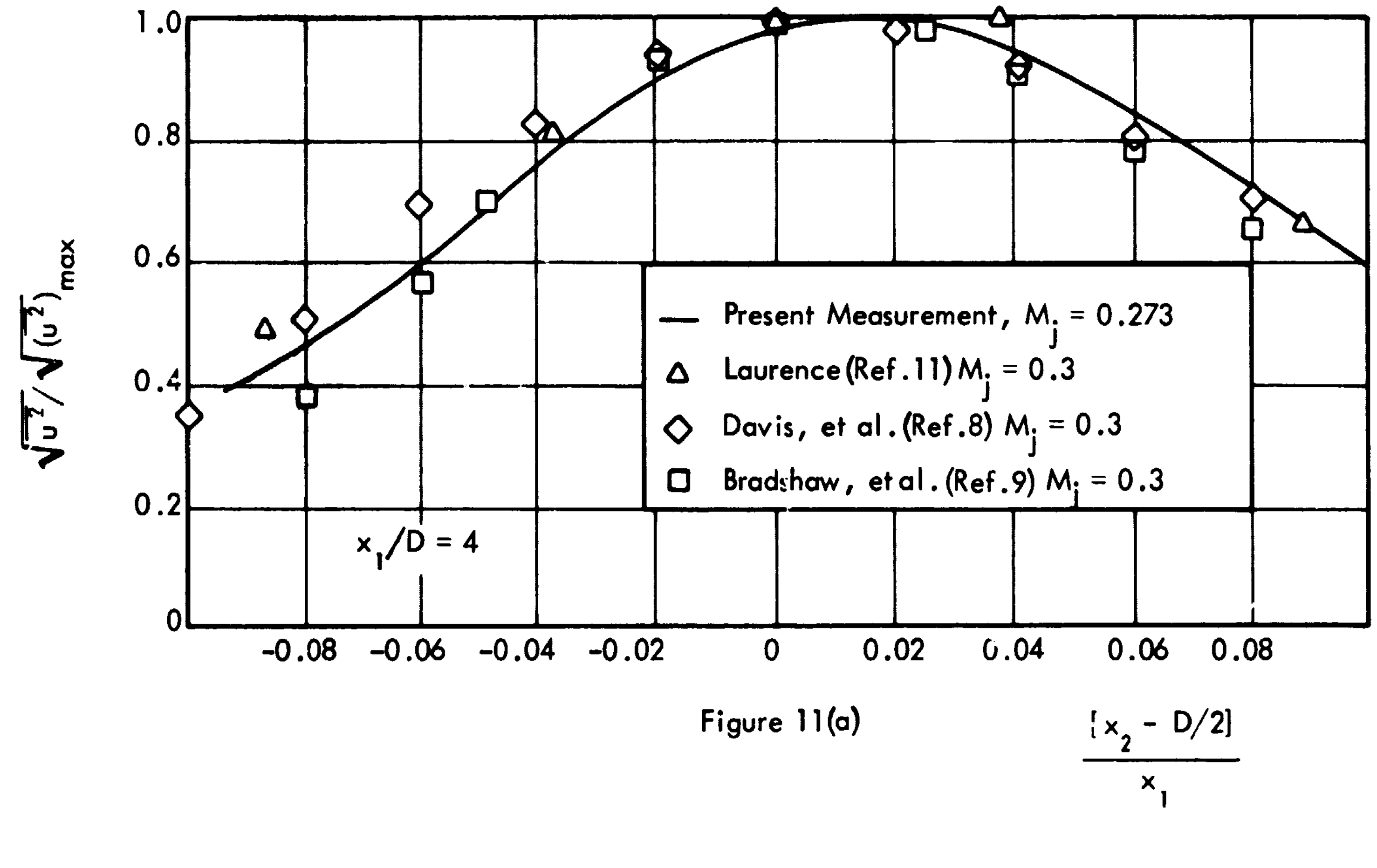

Figure 11(a)

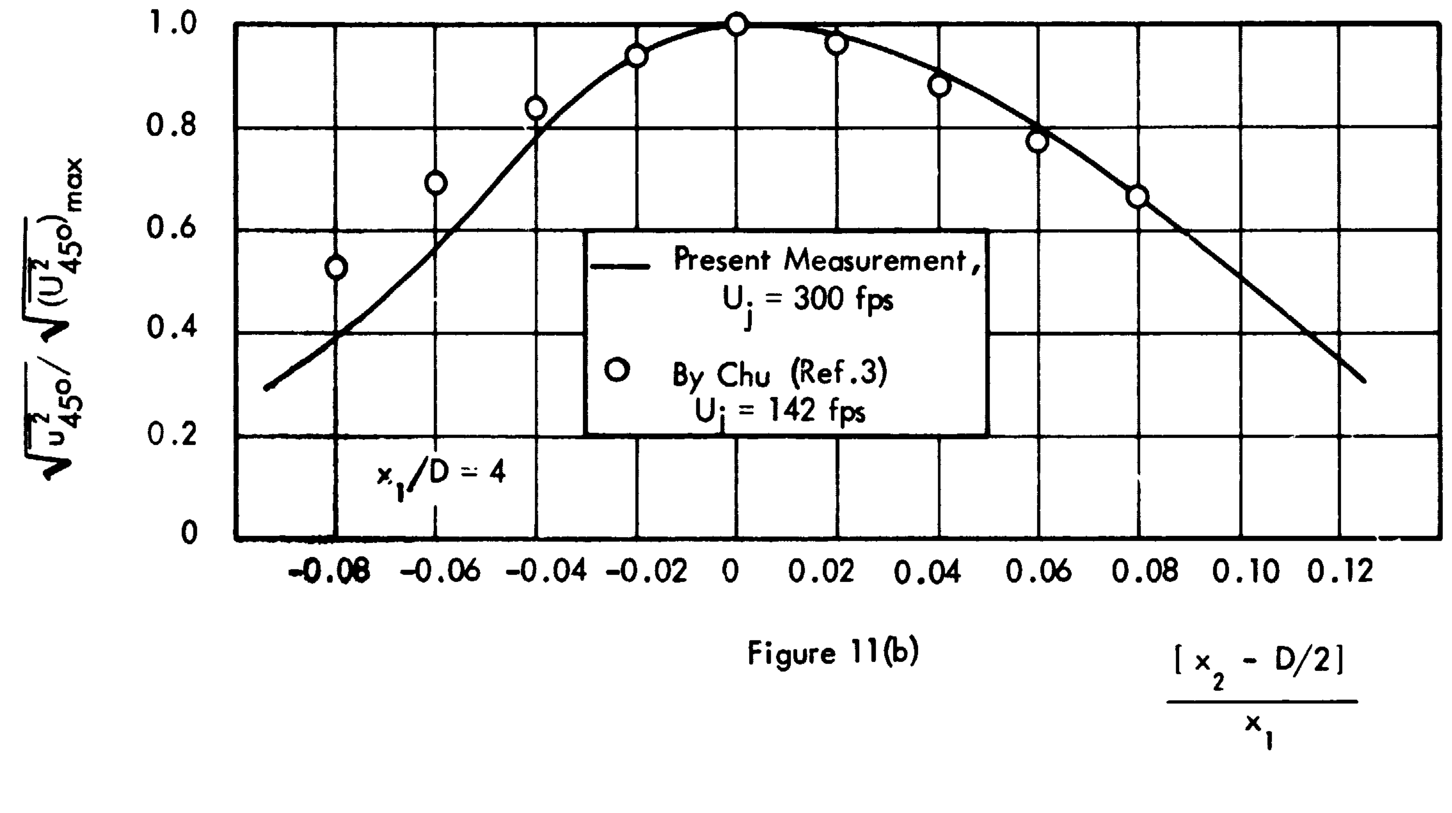

Figure 11(b)

Figure 11. Comparison of the Turbulence Intensity Profiles with Previous Results

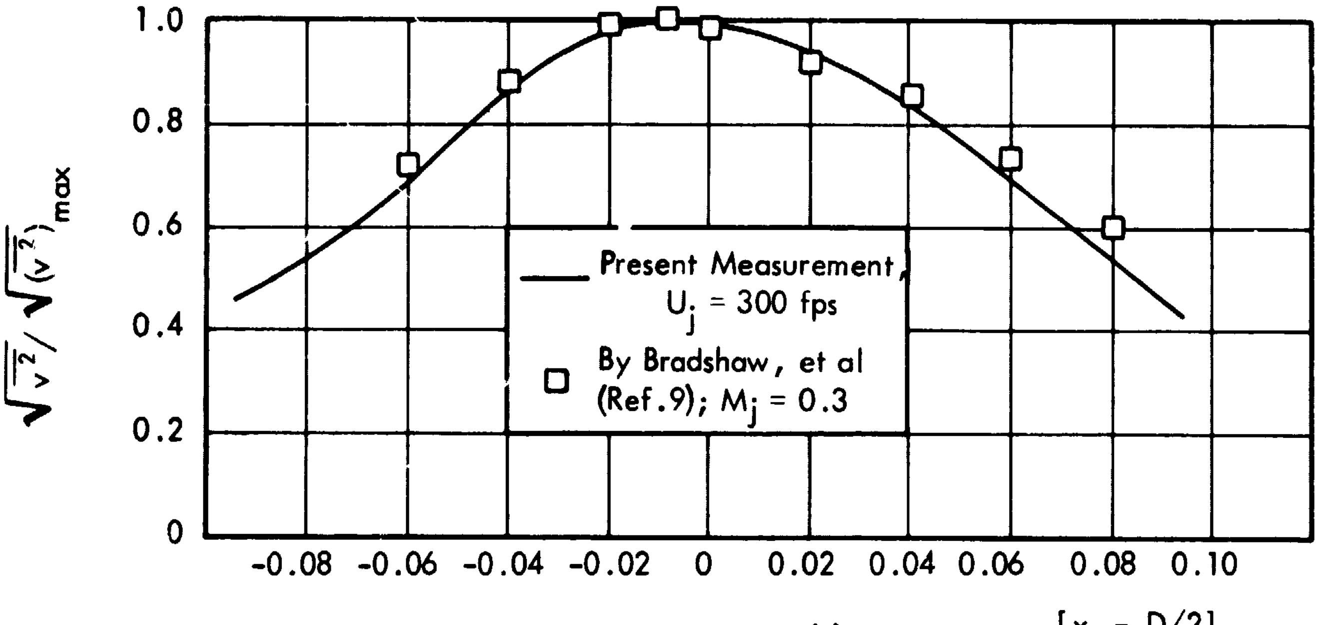

Figure 11(c)

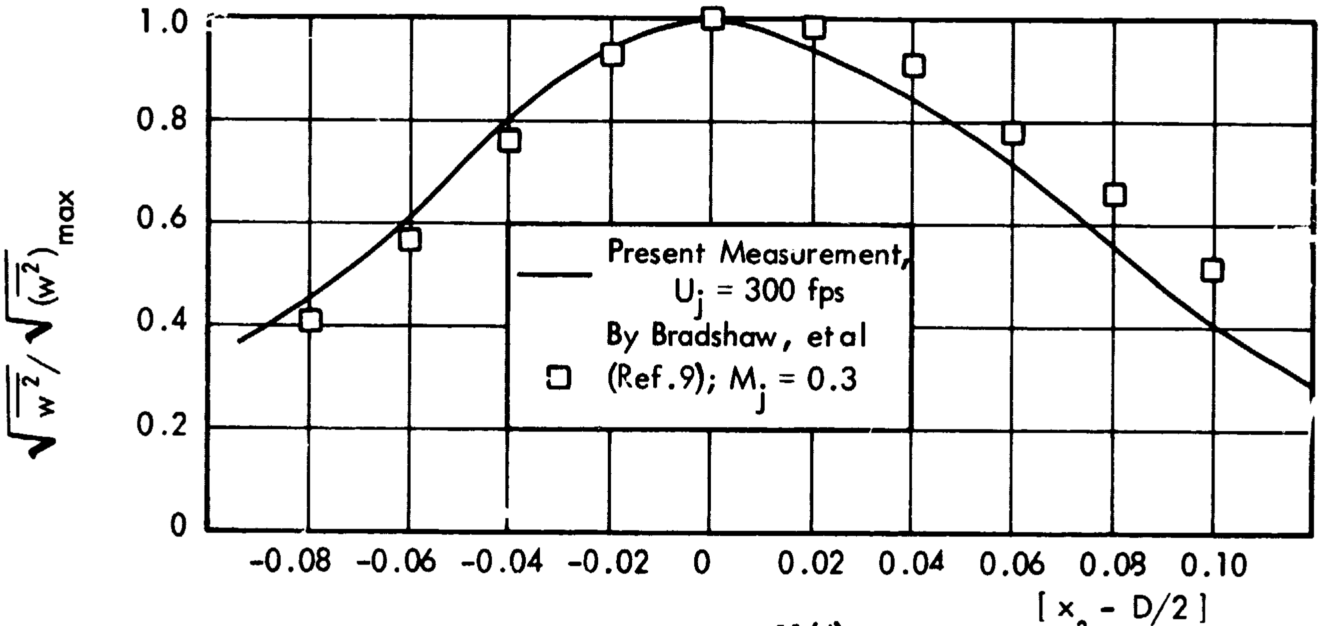

Figure 11(d)

Figure 11. Concluded

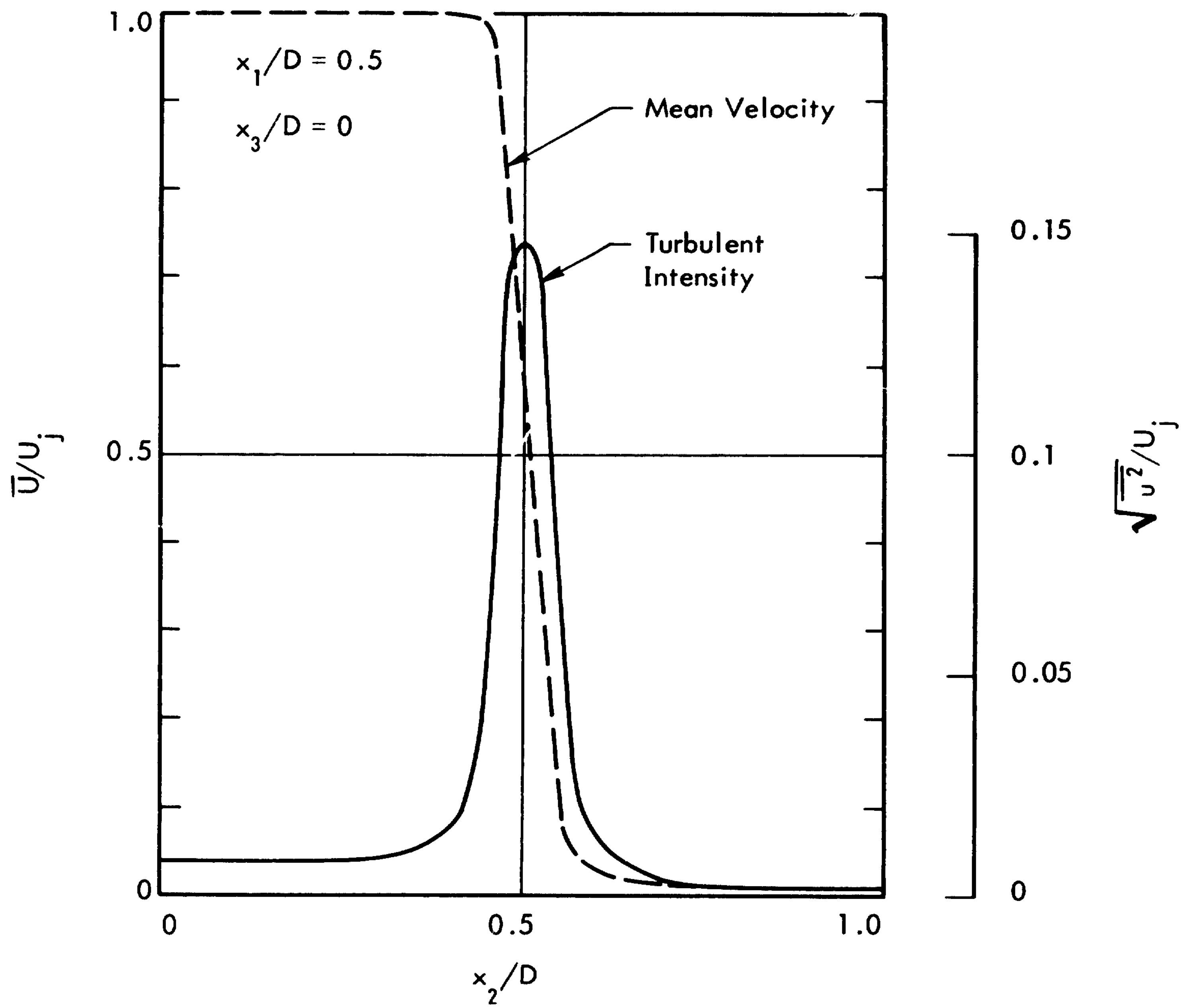

Figure 12. Turbulence Intensity Profile of $\sqrt{\overline{u^2}}$ Measured Across the Jet Flow, $x_1 = 0.5D$

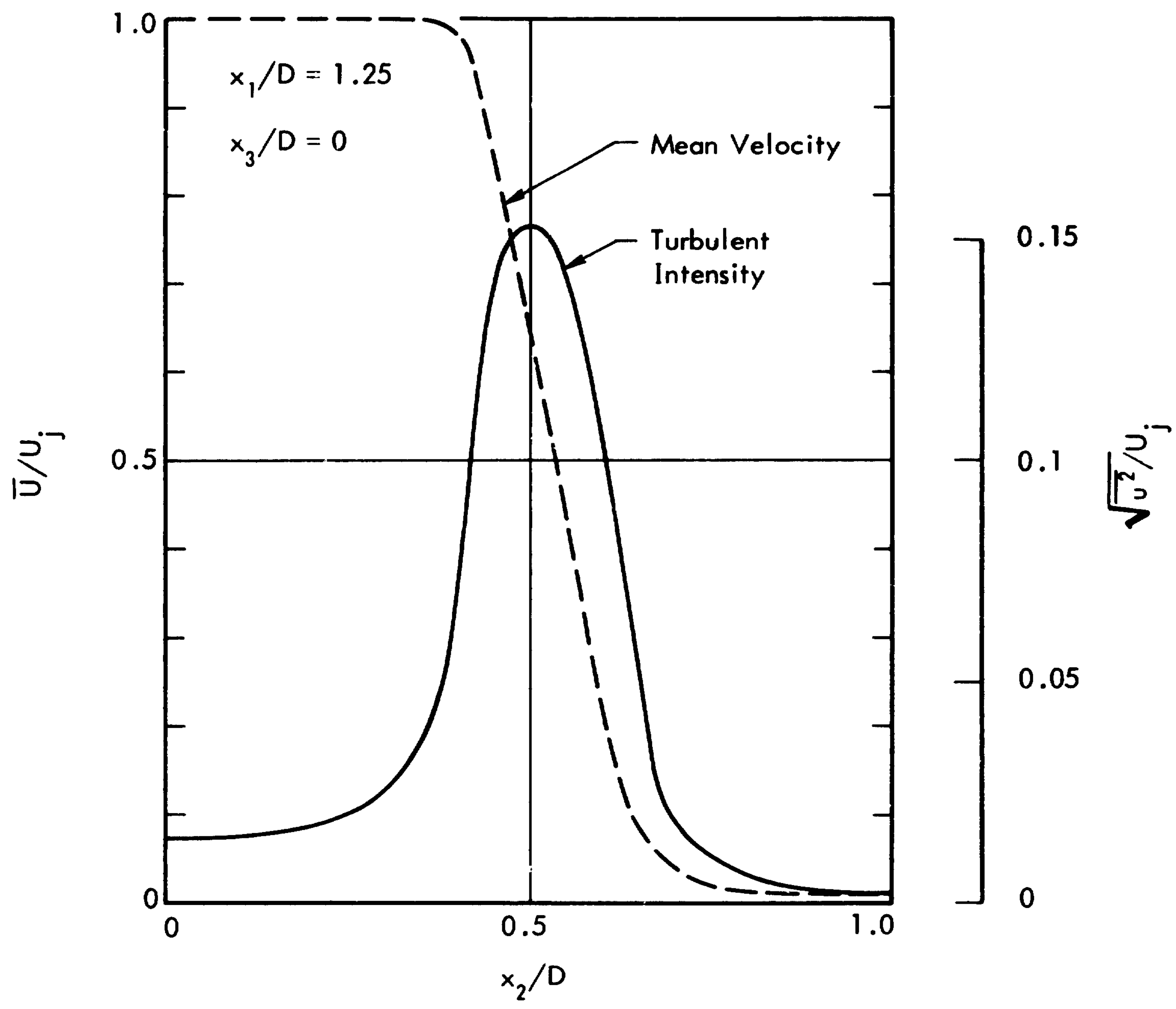

Figure 13. Turbulence Intensity Profile of $\sqrt{\overline{u^2}}$ Measured Across the Jet Flow, $x_1 = 1.25D$

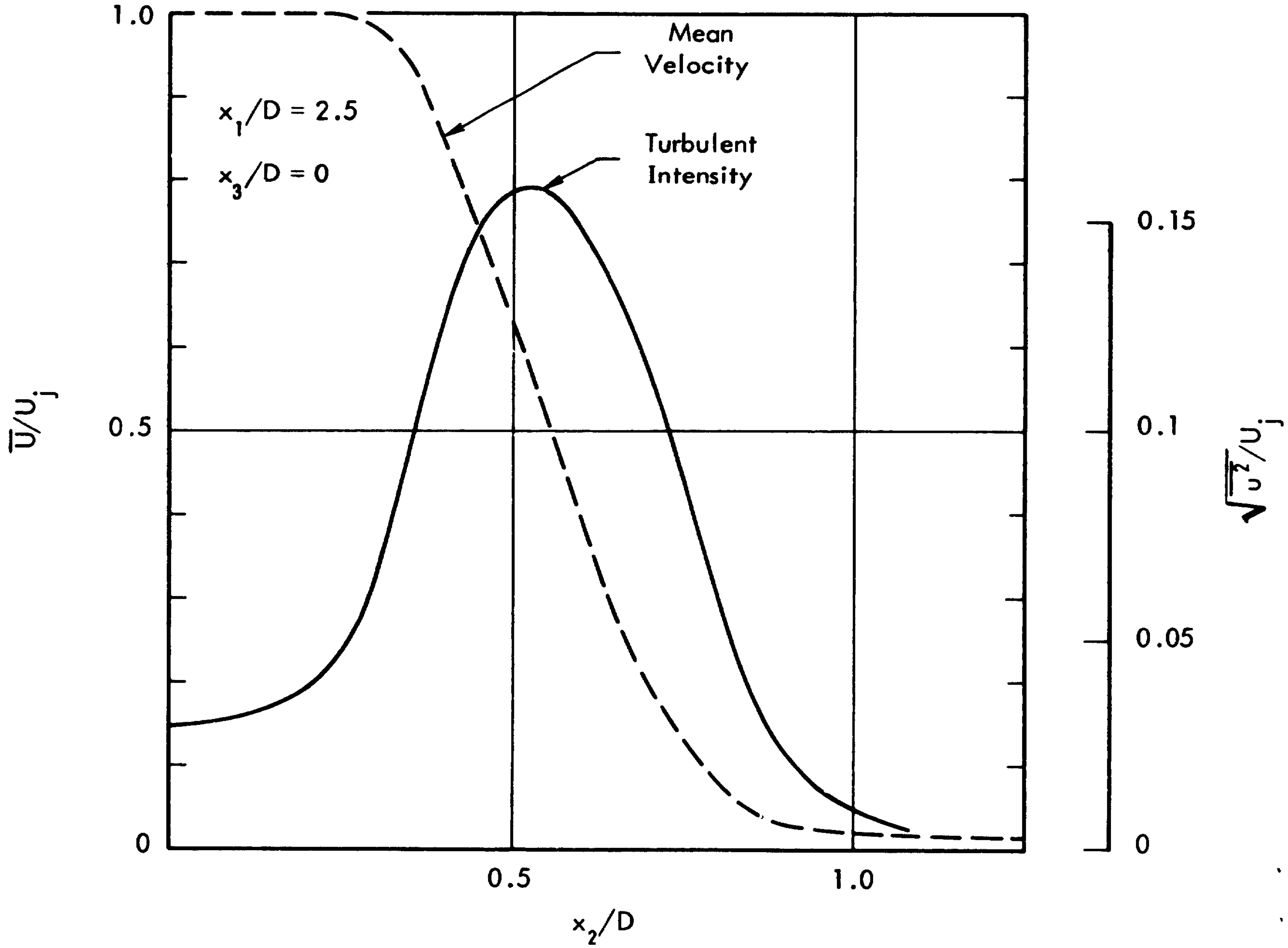

Figure 14. Turbulence Intensity Profile of $\sqrt{\overline{u^2}}$ Measured Across the Jet Flow, $x_1 = 2.5D$

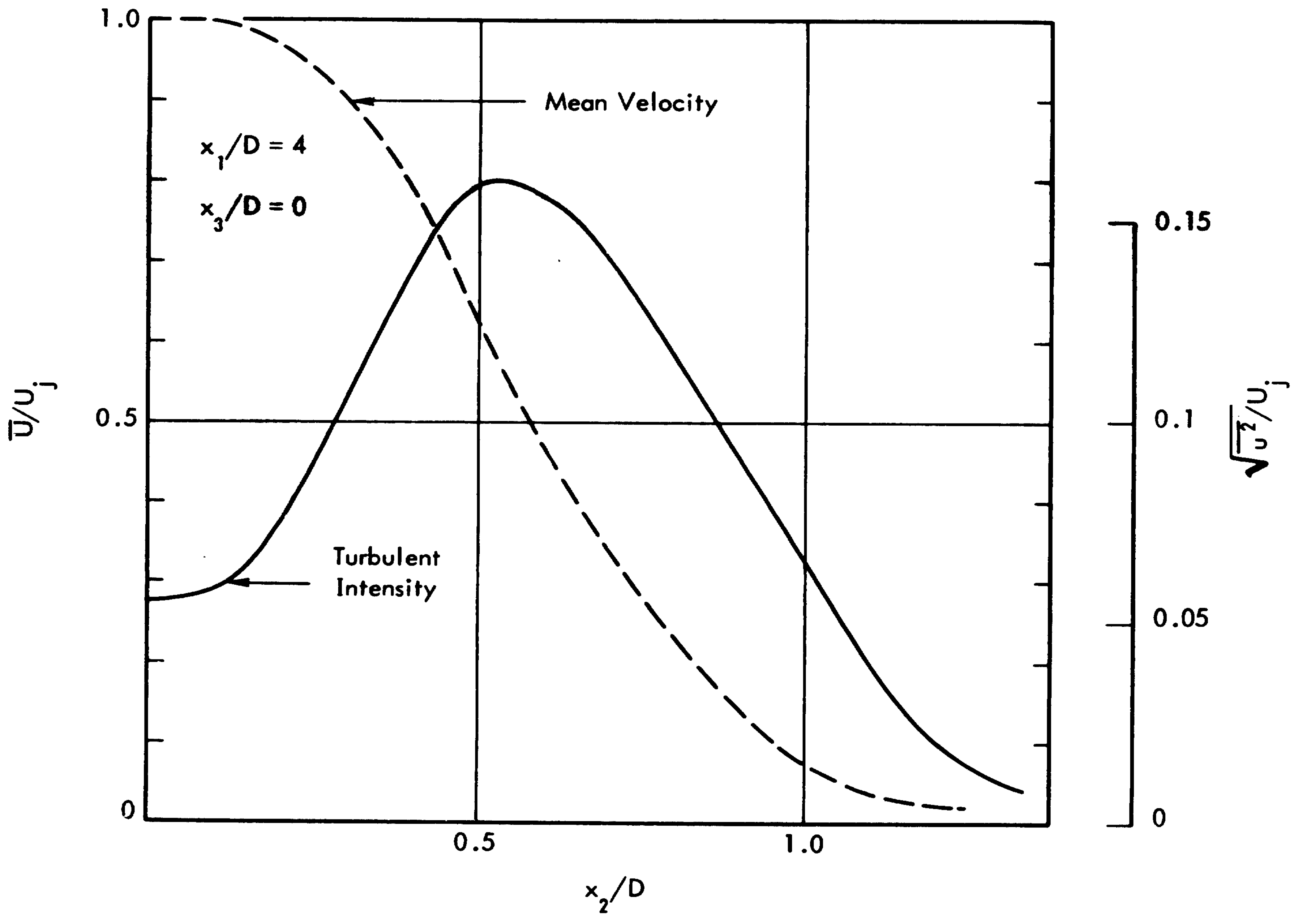

Figure 15. Turbulence Intensity Profile of $\sqrt{\overline{u^2}}$ Measured Across the Jet Flow, $x_1 = 4D$

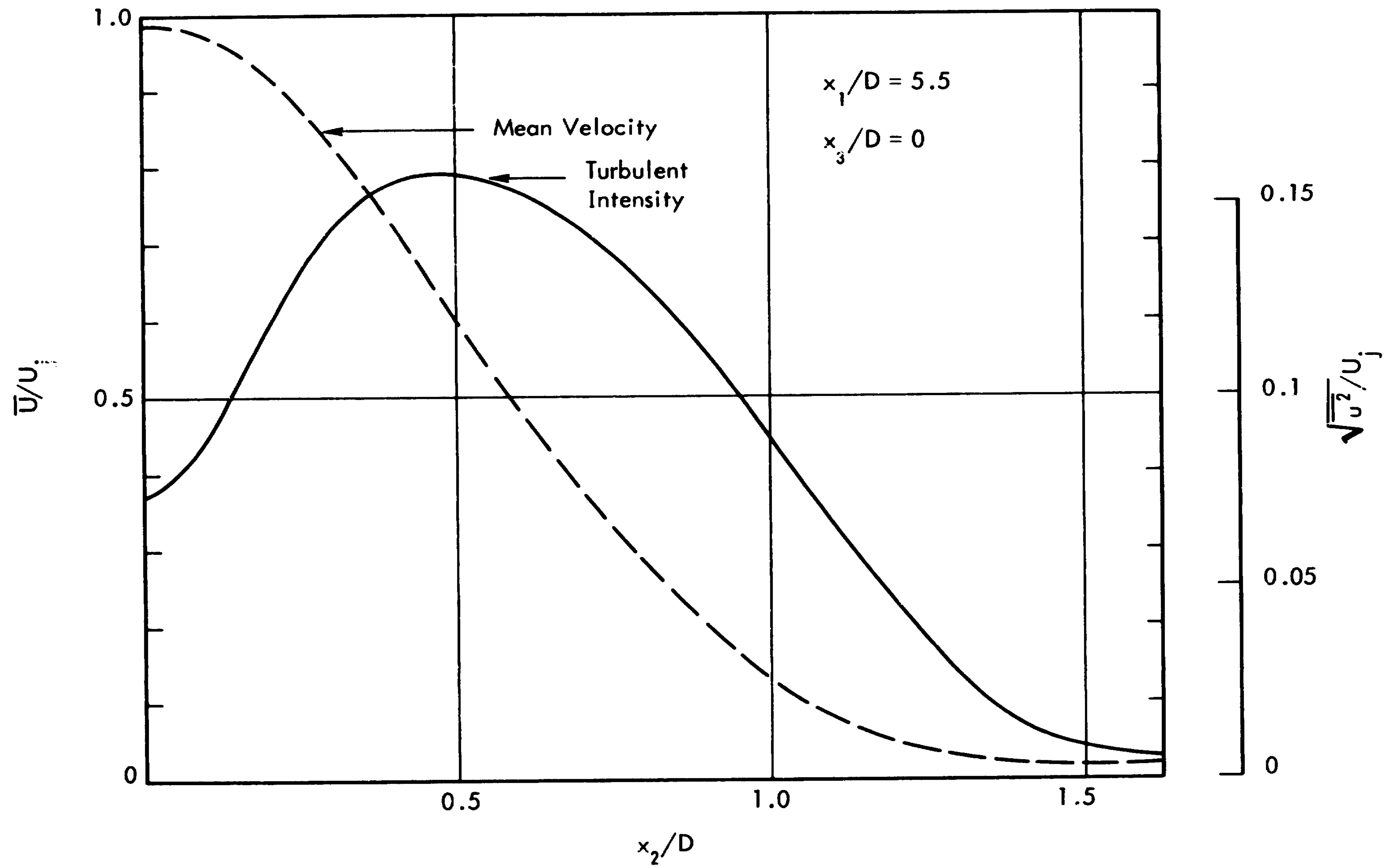

Figure 16. Turbulence Intensity Profile of $\sqrt{\overline{u^2}}$ Measured Across the Jet Flow, $x_1 = 5.5D$

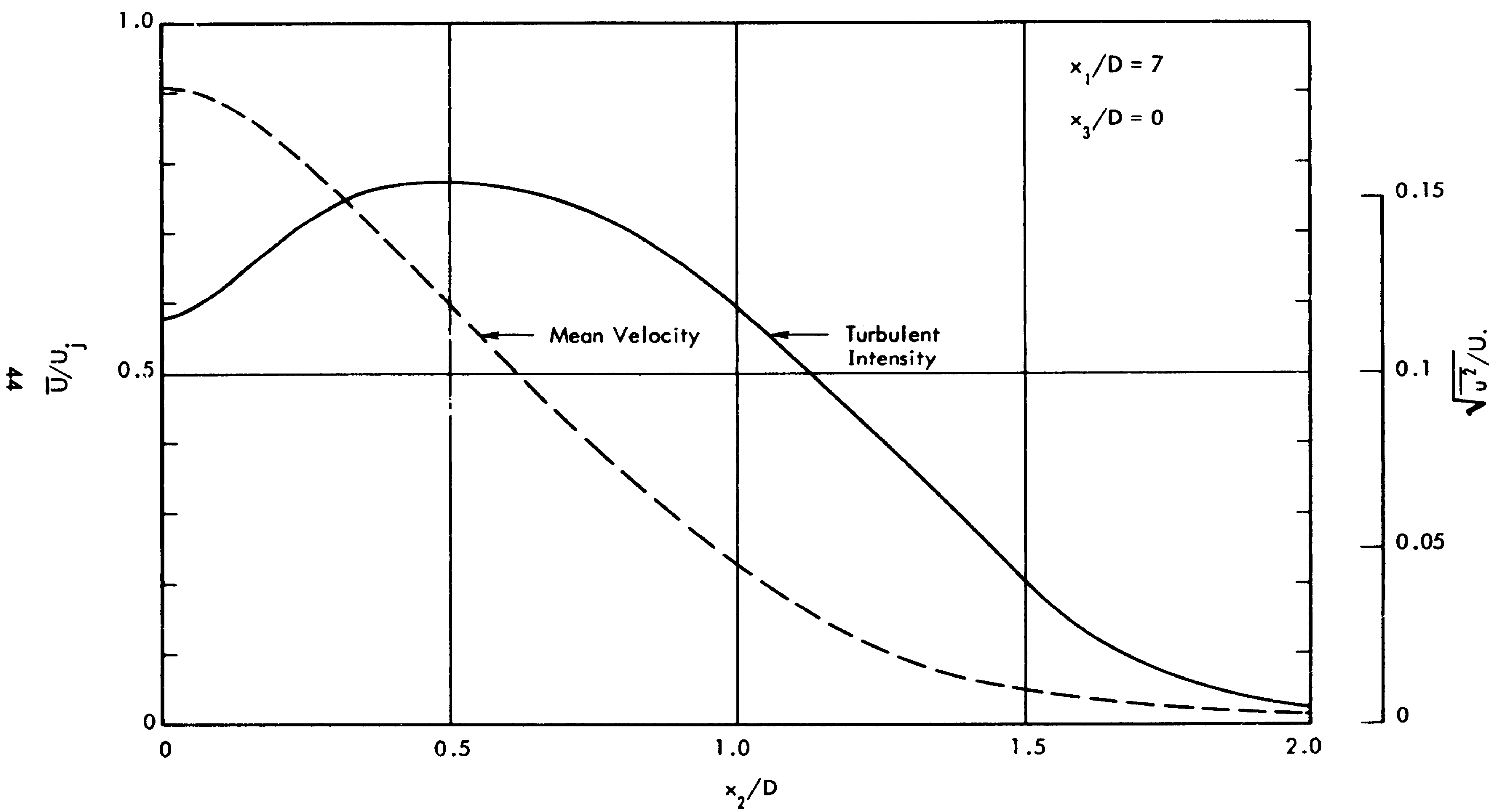

Figure 17. Turbulence Intensity Profile of $\sqrt{\overline{u^2}}$ Measured Across the Jet Flow, $x_1 = 7D$

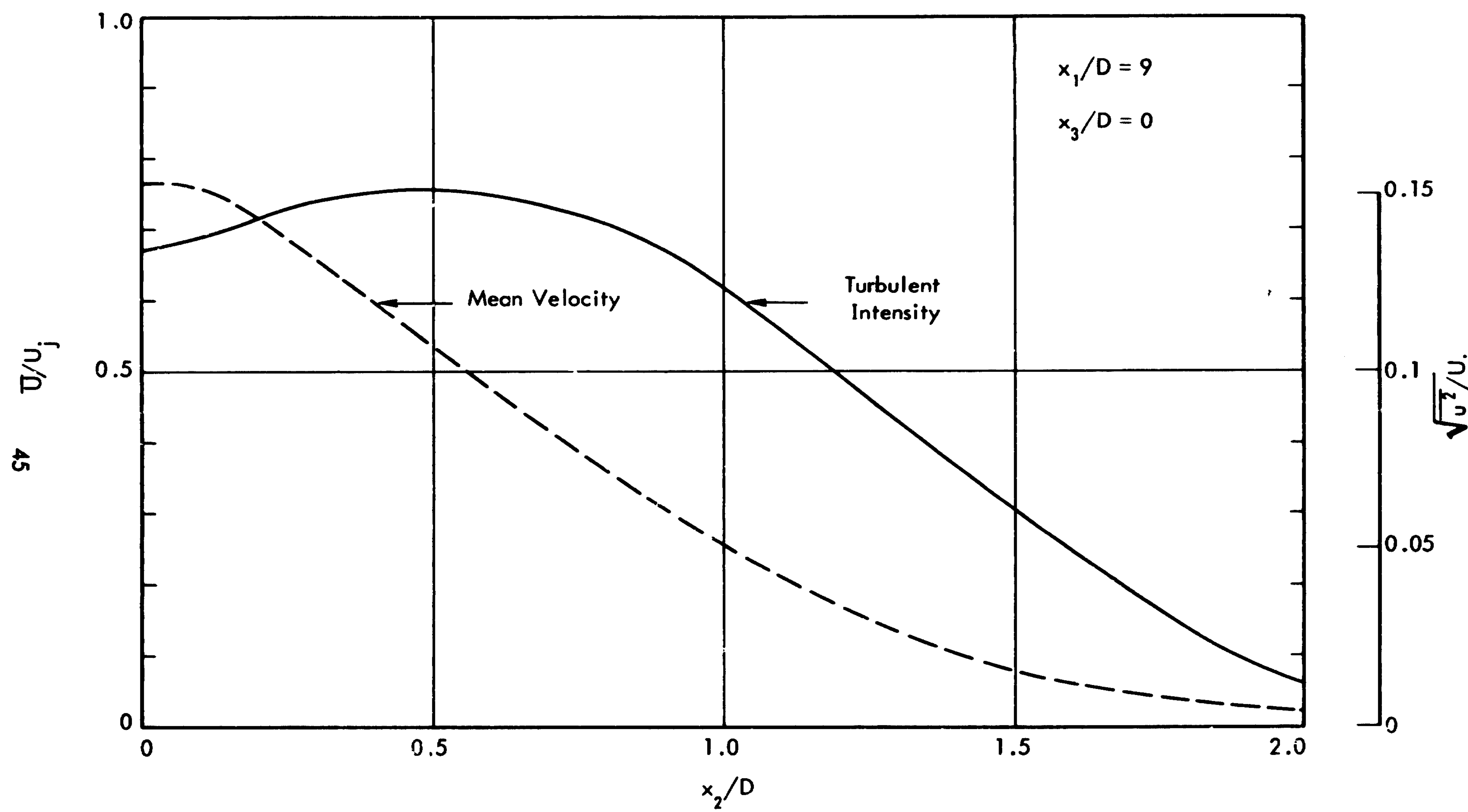

Figure 18. Turbulence Intensity Profile of $\sqrt{\overline{u^2}}$ Measured Across the Jet Flow, $x_1 = 9D$

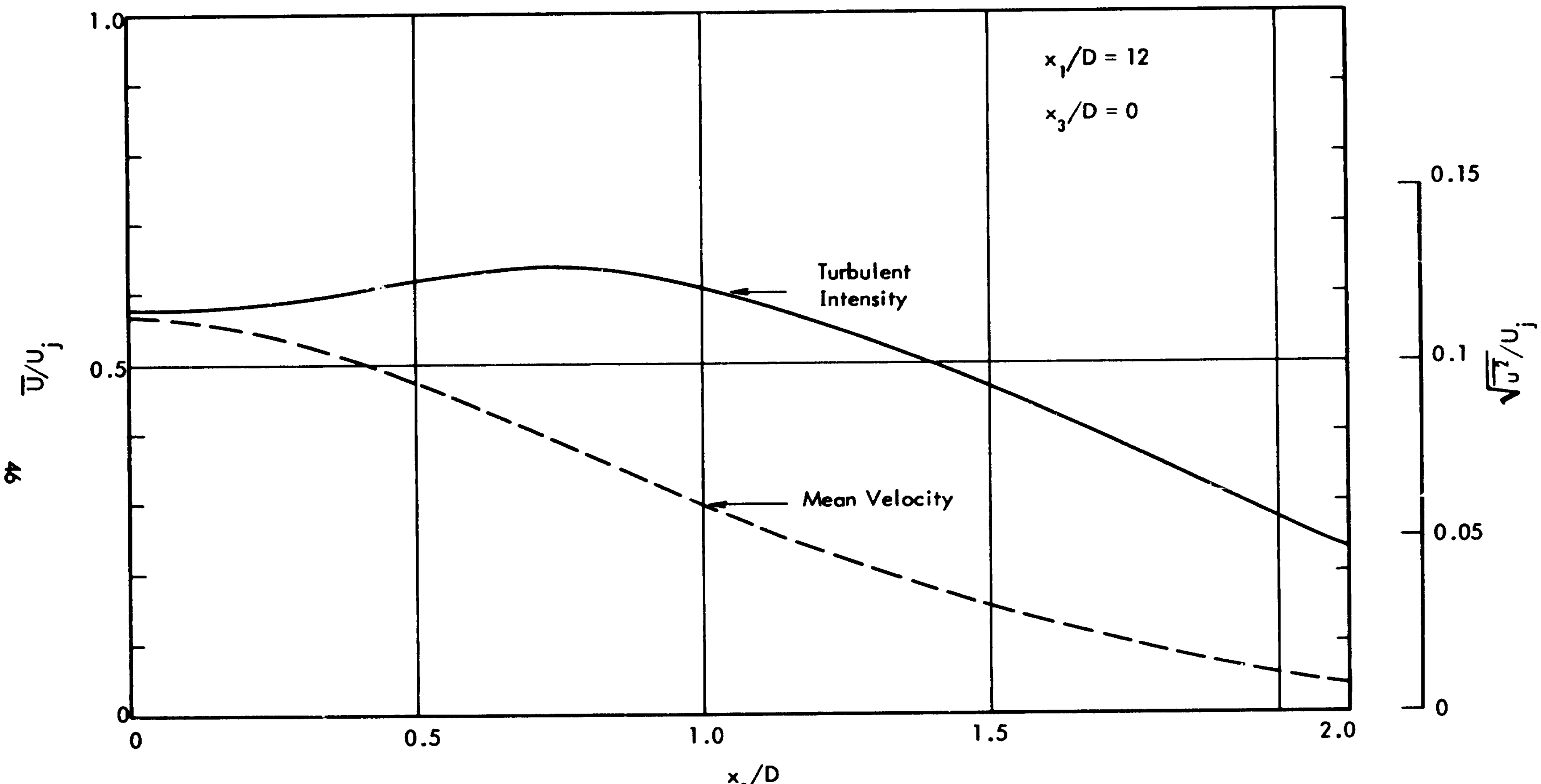

Figure 19. Turbulence Intensity Profile of $\sqrt{\overline{u^2}}$ Measured Across the Jet Flow, $x_1 = 12D$

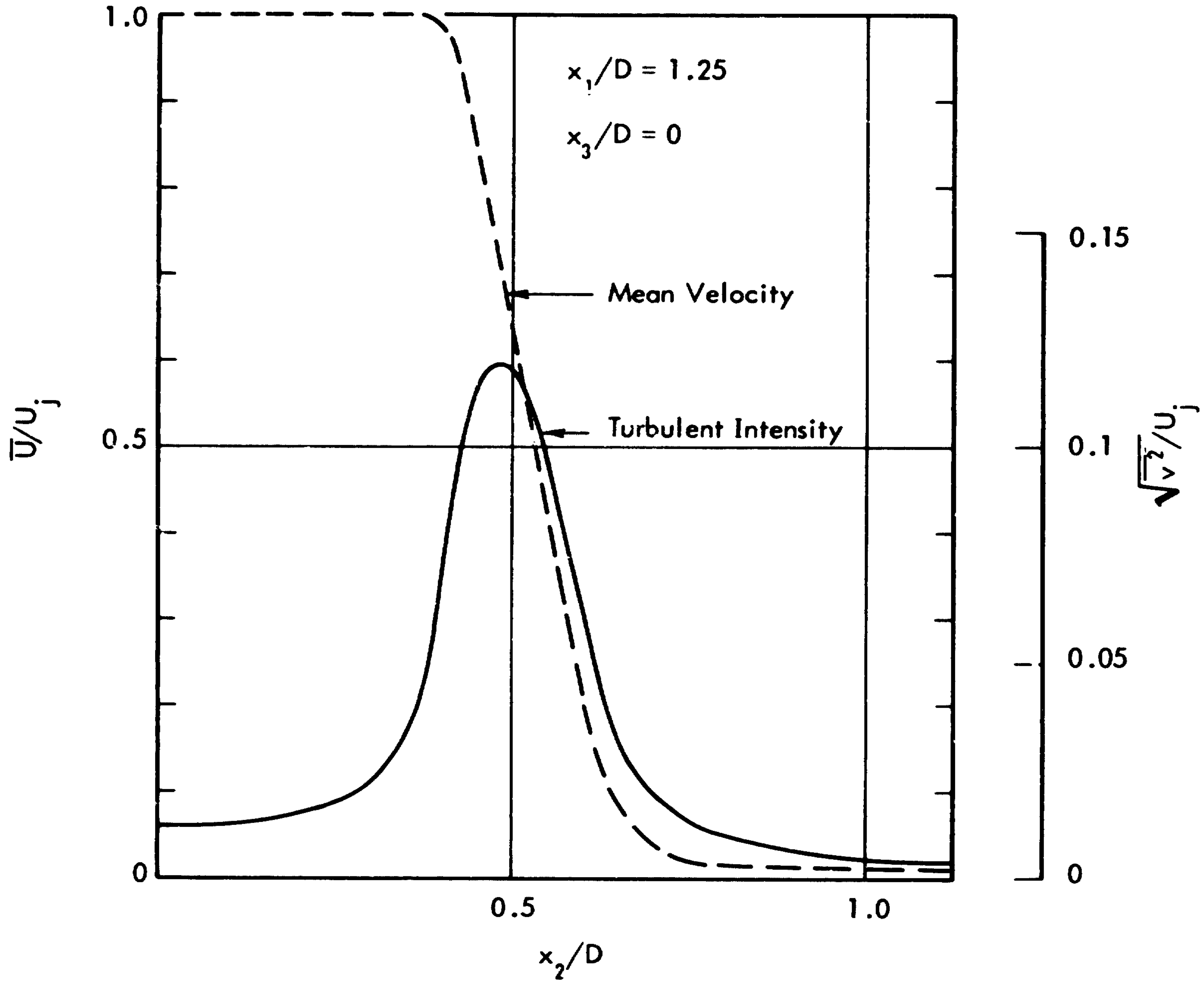

Figure 20. Turbulence Intensity Profile of $\sqrt{\overline{v^2}}$ Measured Across the Jet Flow, $x_1 = 1.25D$

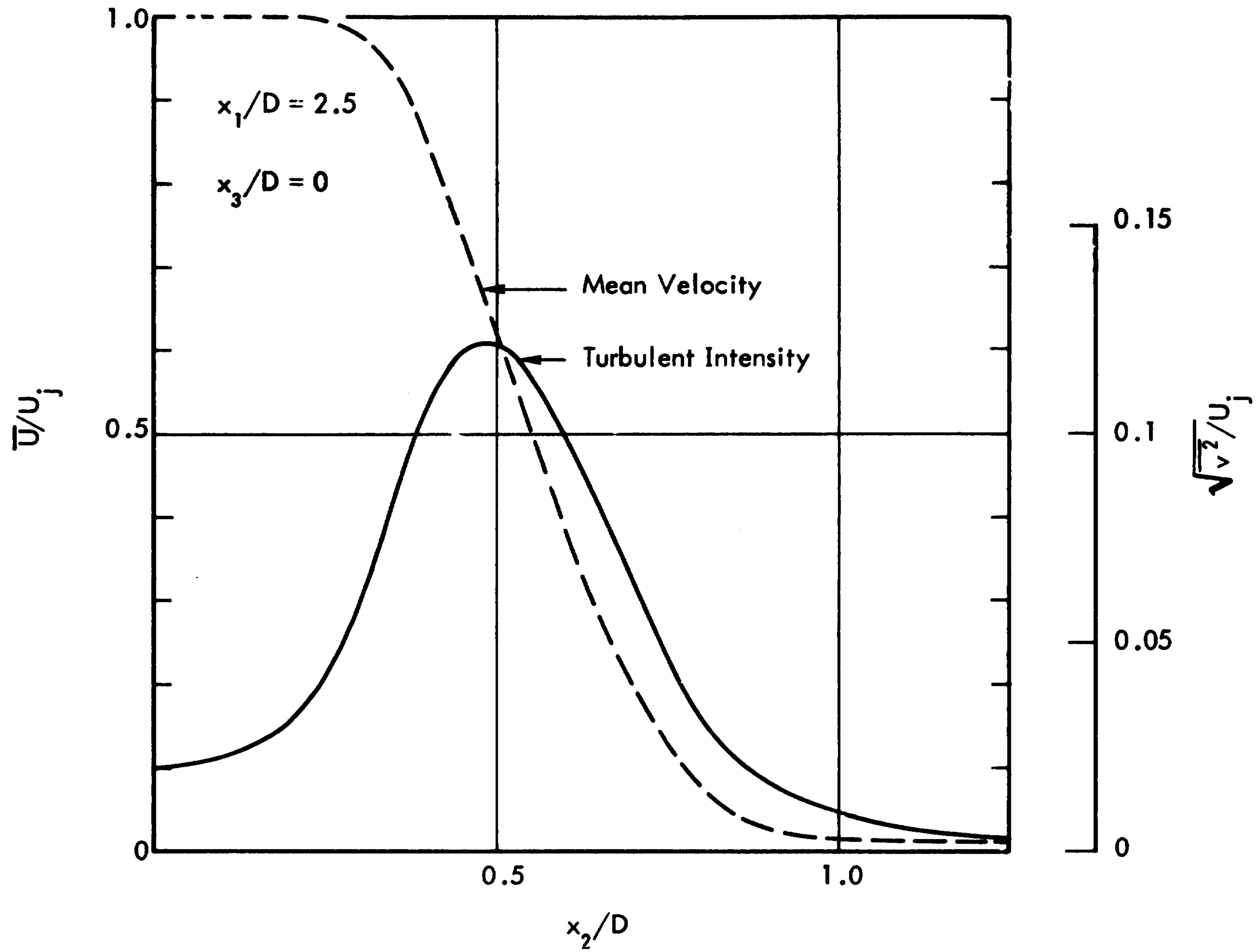

Figure 21. Turbulence Intensity Profile of $\sqrt{\overline{v^2}}$ Measured Across the Jet Flow, $x_1 = 2.5D$

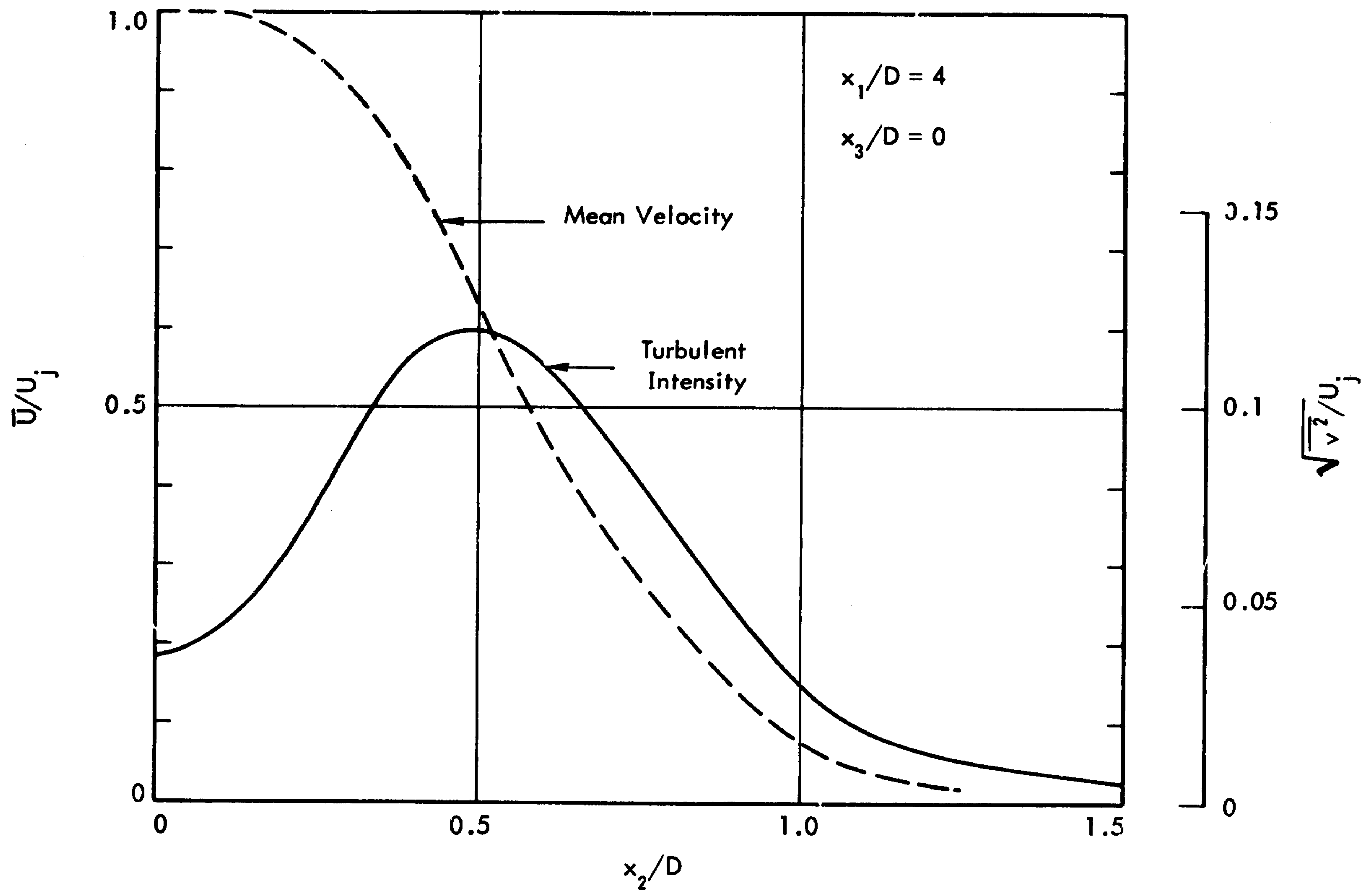

Figure 22. Turbulence Intensity Profile of $\sqrt{\overline{v^2}}$ Measured Across the Jet Flow, $x_1 = 4D$

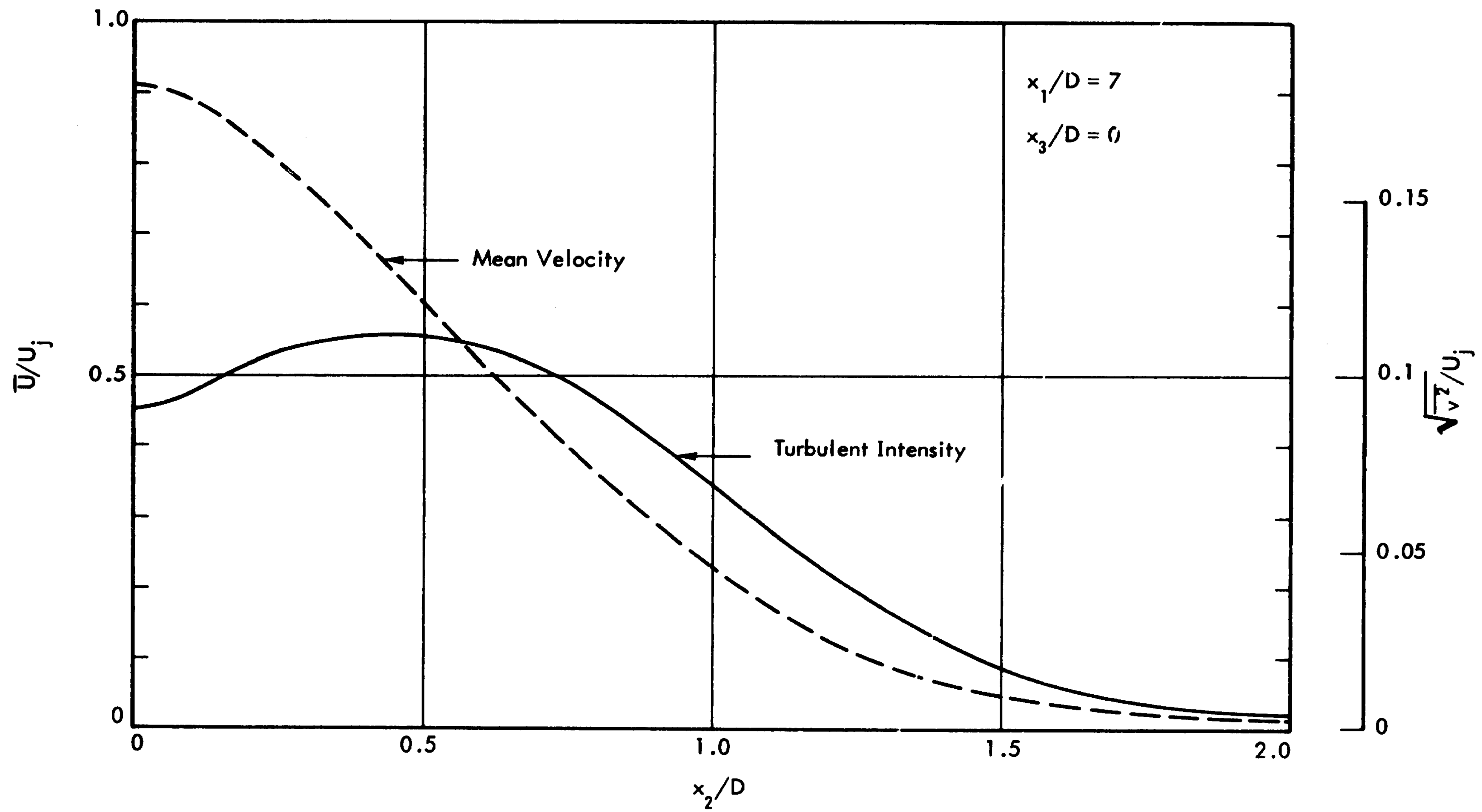

Figure 23. Turbulence Intensity Profile of $\sqrt{\overline{v^2}}$ Measured Across the Jet Flow, $x_1 = 7D$

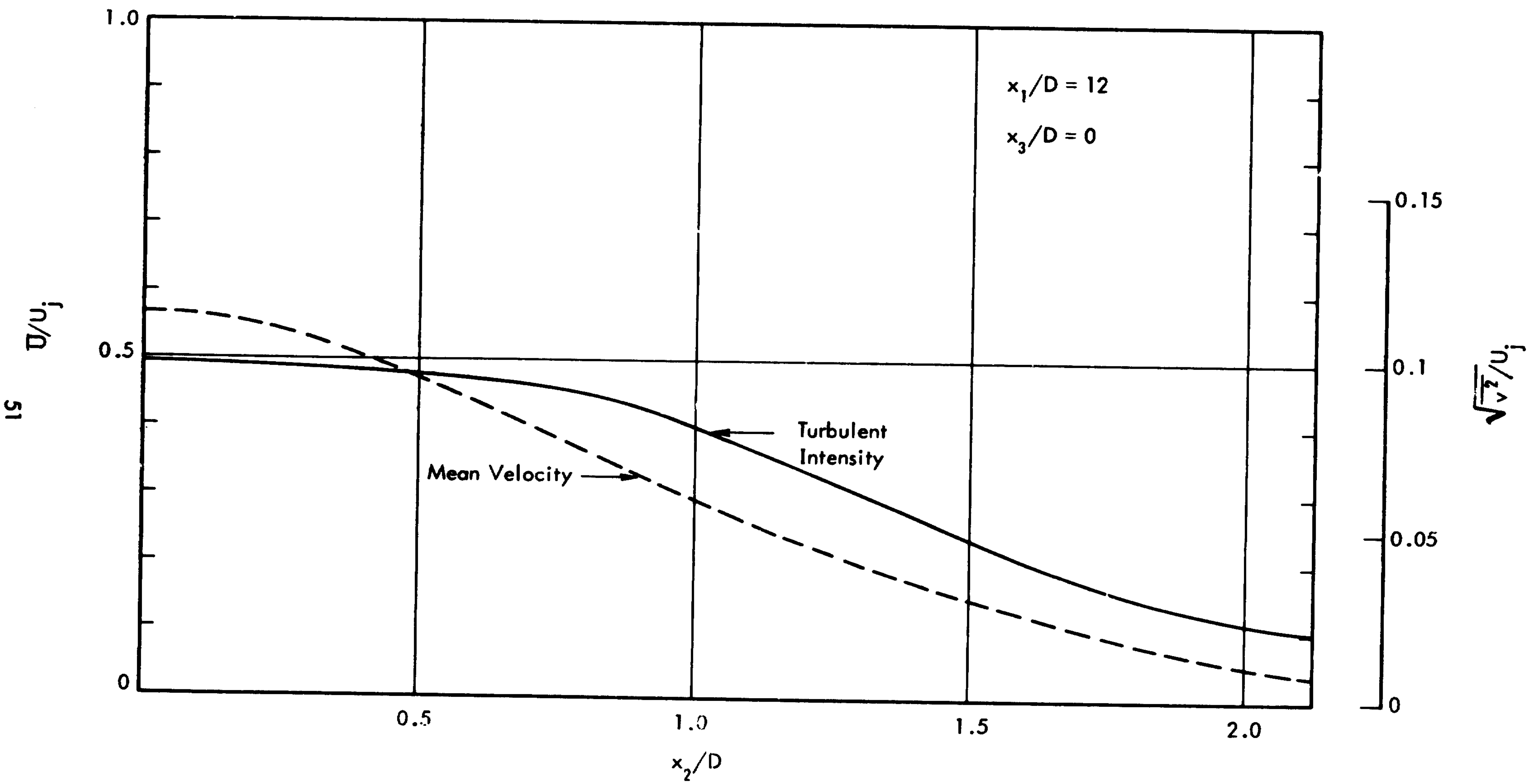

Figure 24. Turbulence Intensity Profile of $\sqrt{\overline{v^2}}$ Measured Across the Jet Flow, $x_1 = 12D$

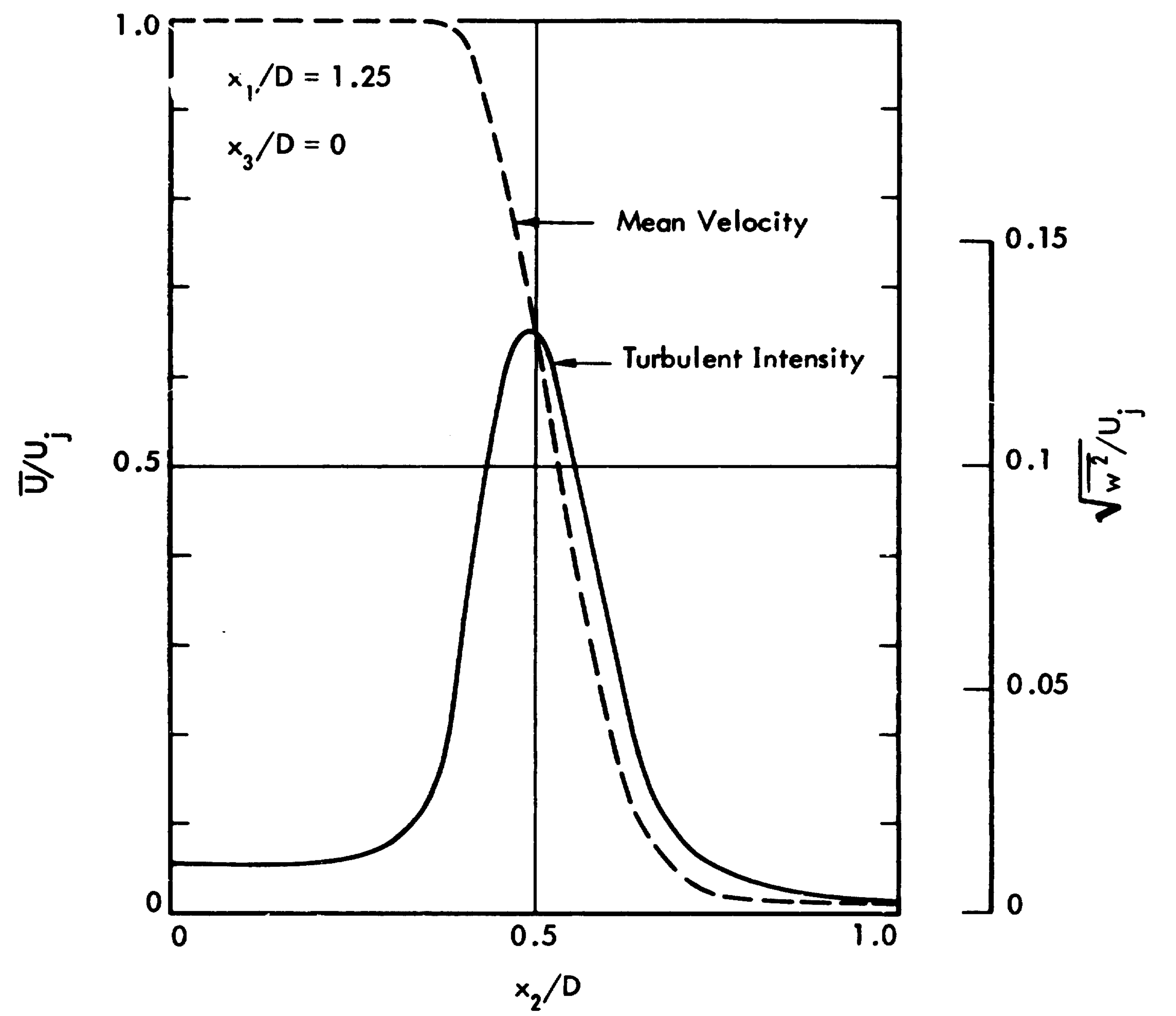

Figure 25. Turbulence Intensity Profile of $\sqrt{\overline{w^2}}$ Measured Across the Jet Flow, $x_1 = 1.25D$

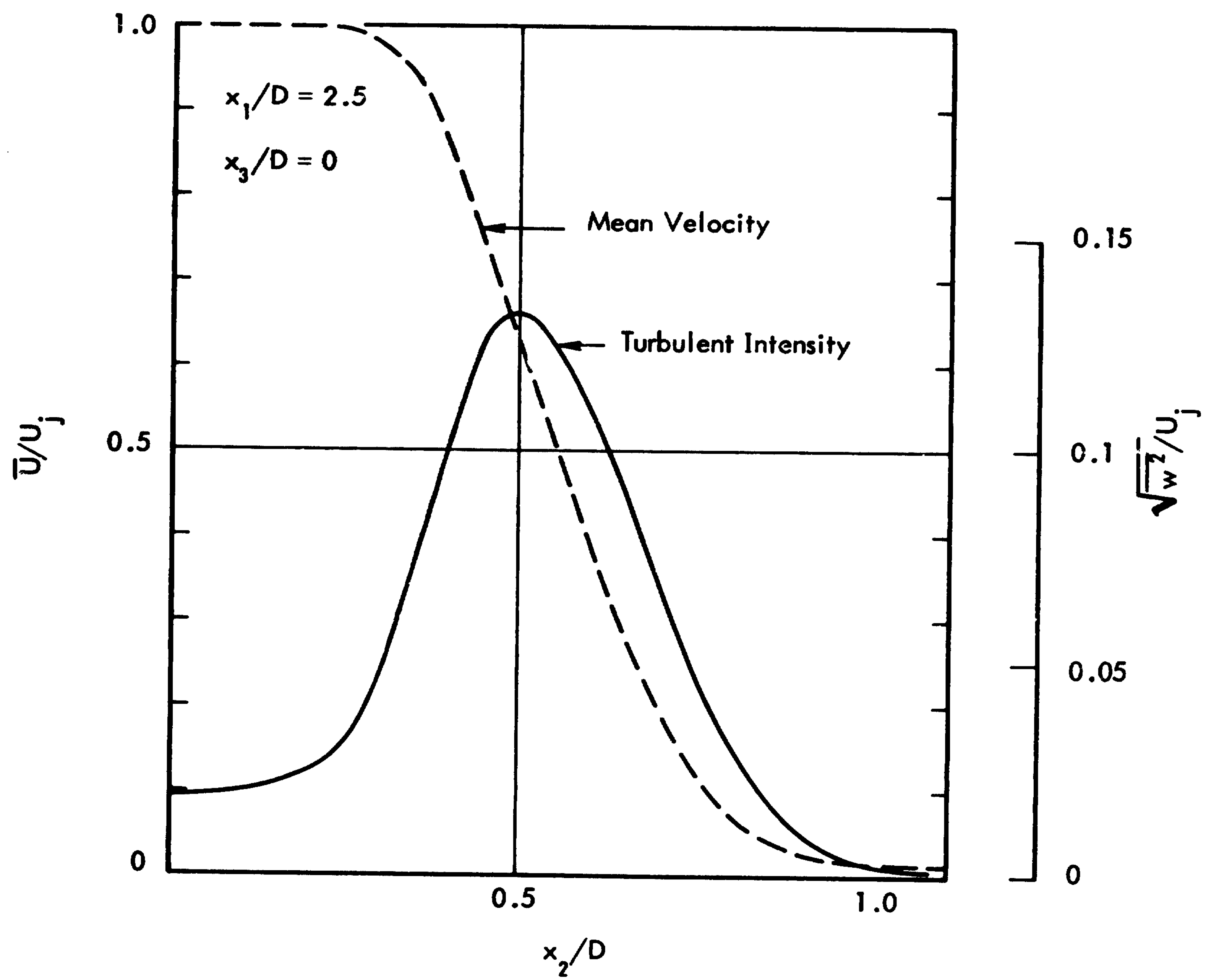

Figure 26. Turbulence Intensity Profile of $\sqrt{\overline{w^2}}$ Measured Across the Jet Flow, $x_1 = 2.5D$

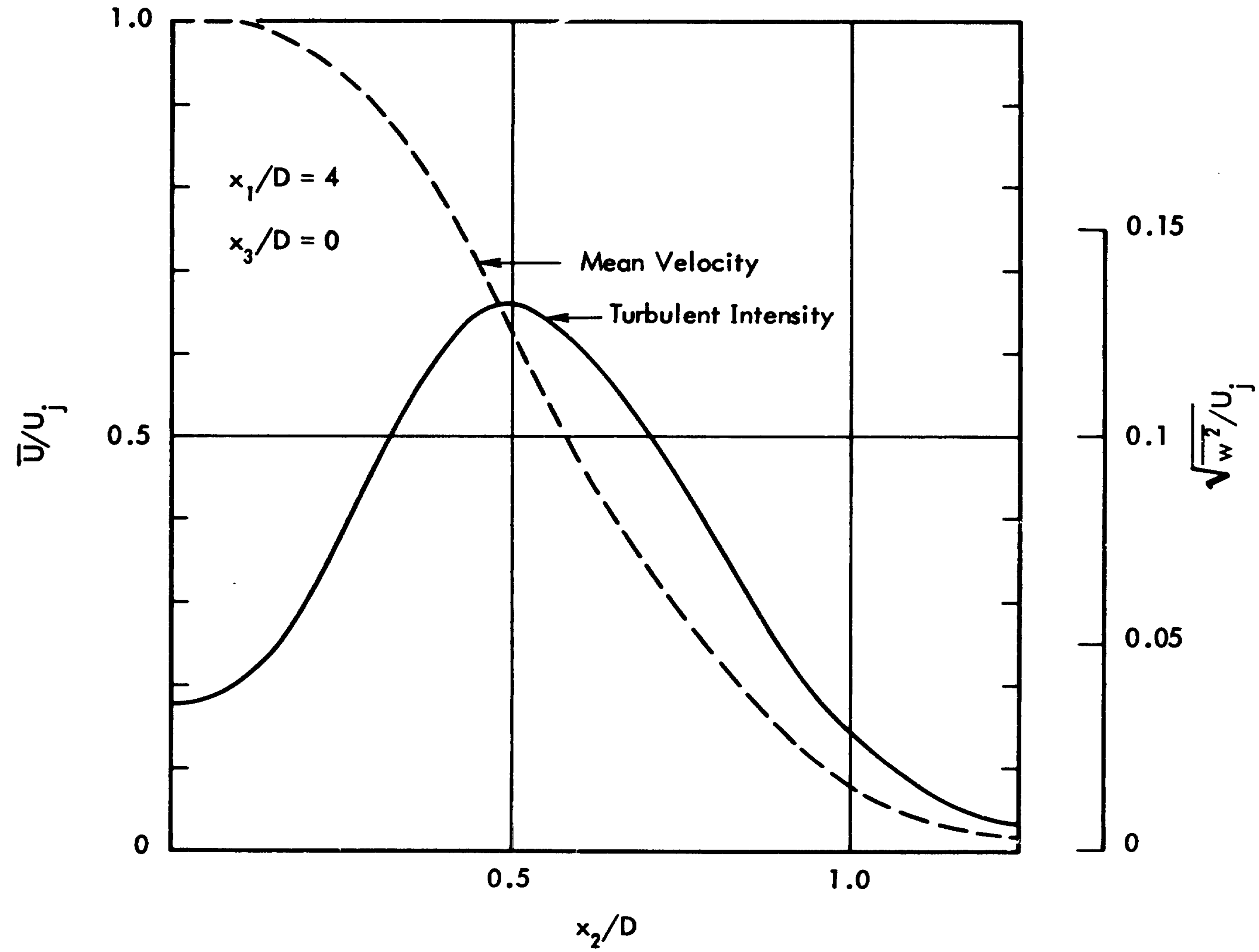

Figure 27. Turbulence Intensity Profile of $\sqrt{\overline{w^2}}$ Measured Across the Jet Flow, $x_1 = 4D$

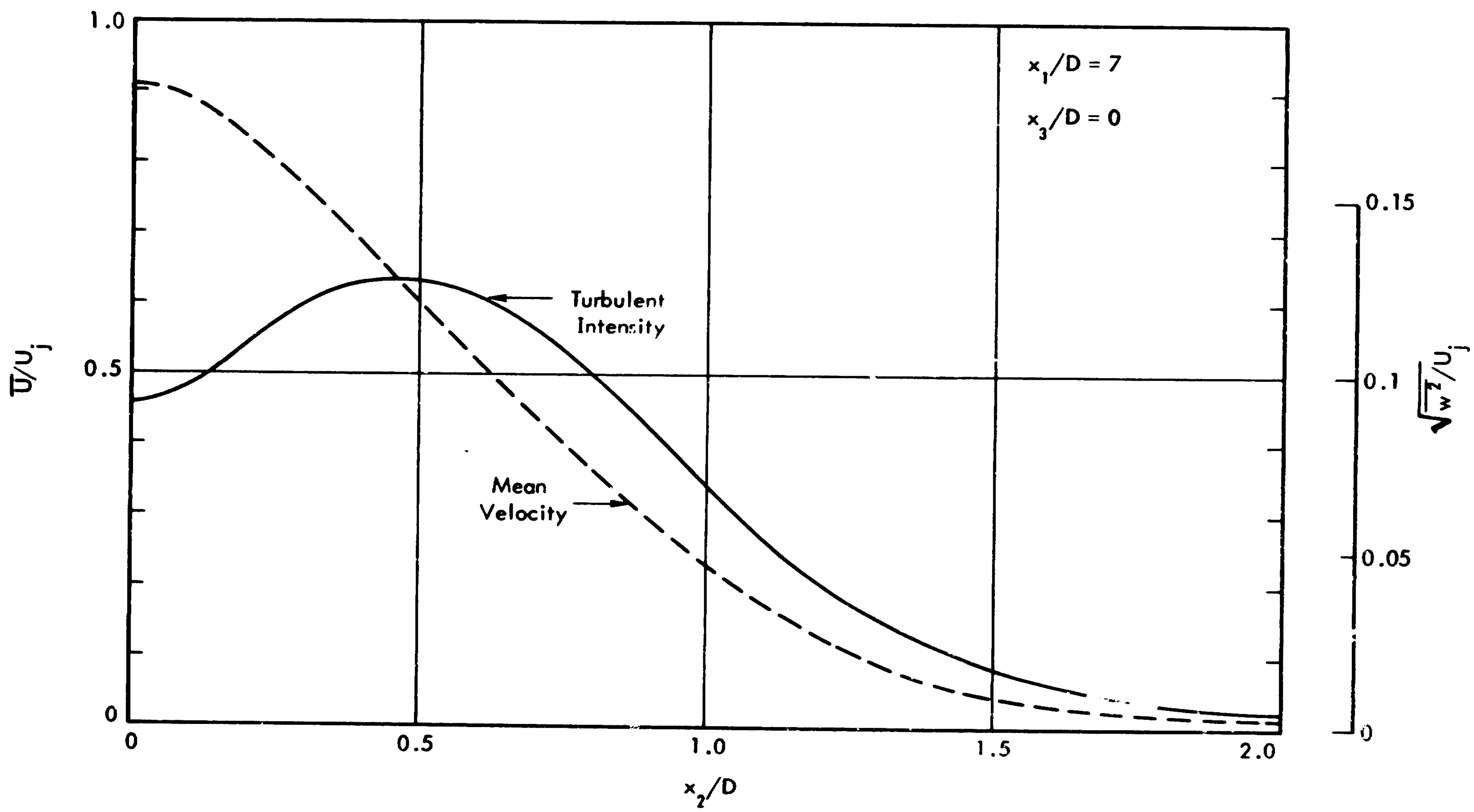

Figure 28. Turbulence Intensity Profile of $\sqrt{\overline{w^2}}$ Measured Across the Jet Flow, $x_1 = 7D$

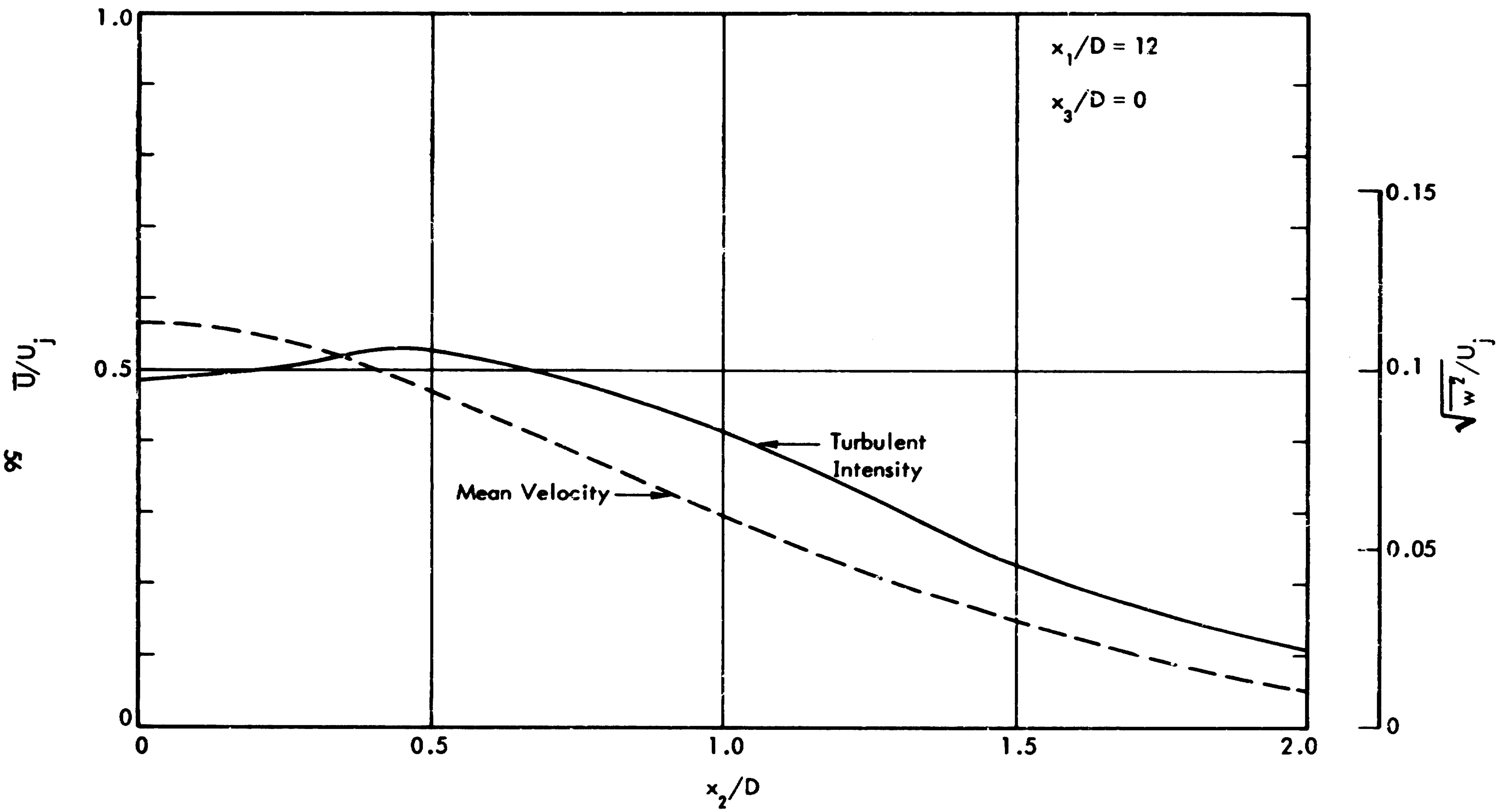

Figure 29. Turbulence Intensity Profile of $\sqrt{\overline{w^2}}$ Measured Acorss the Jet Flow, x_1 = 12 D

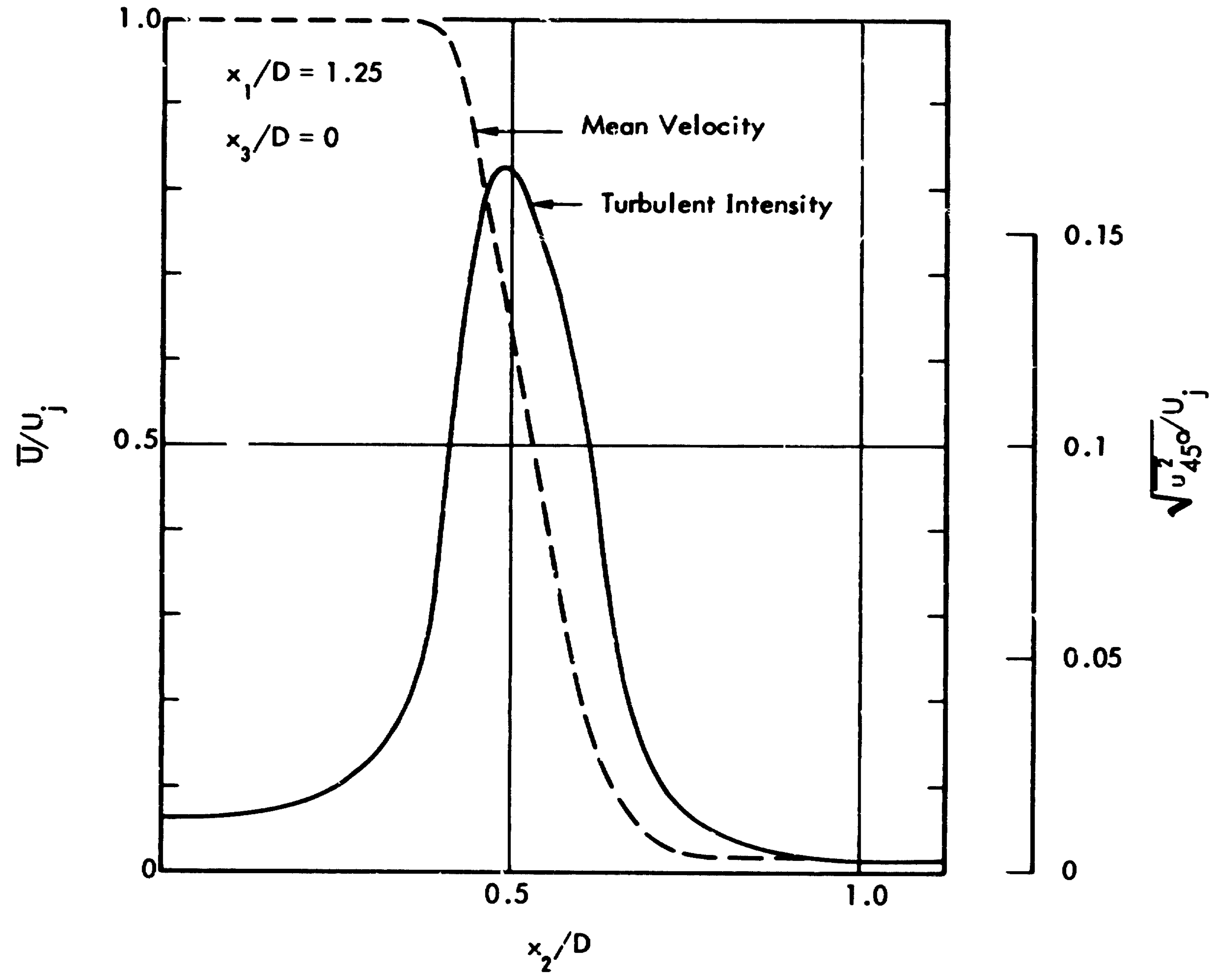

Figure 30. Turbulence Intensity Profile of $\sqrt{\overline{u^2_{45°}}}$ Measured Across the Jet Flow, $x_1 = 1.25D$

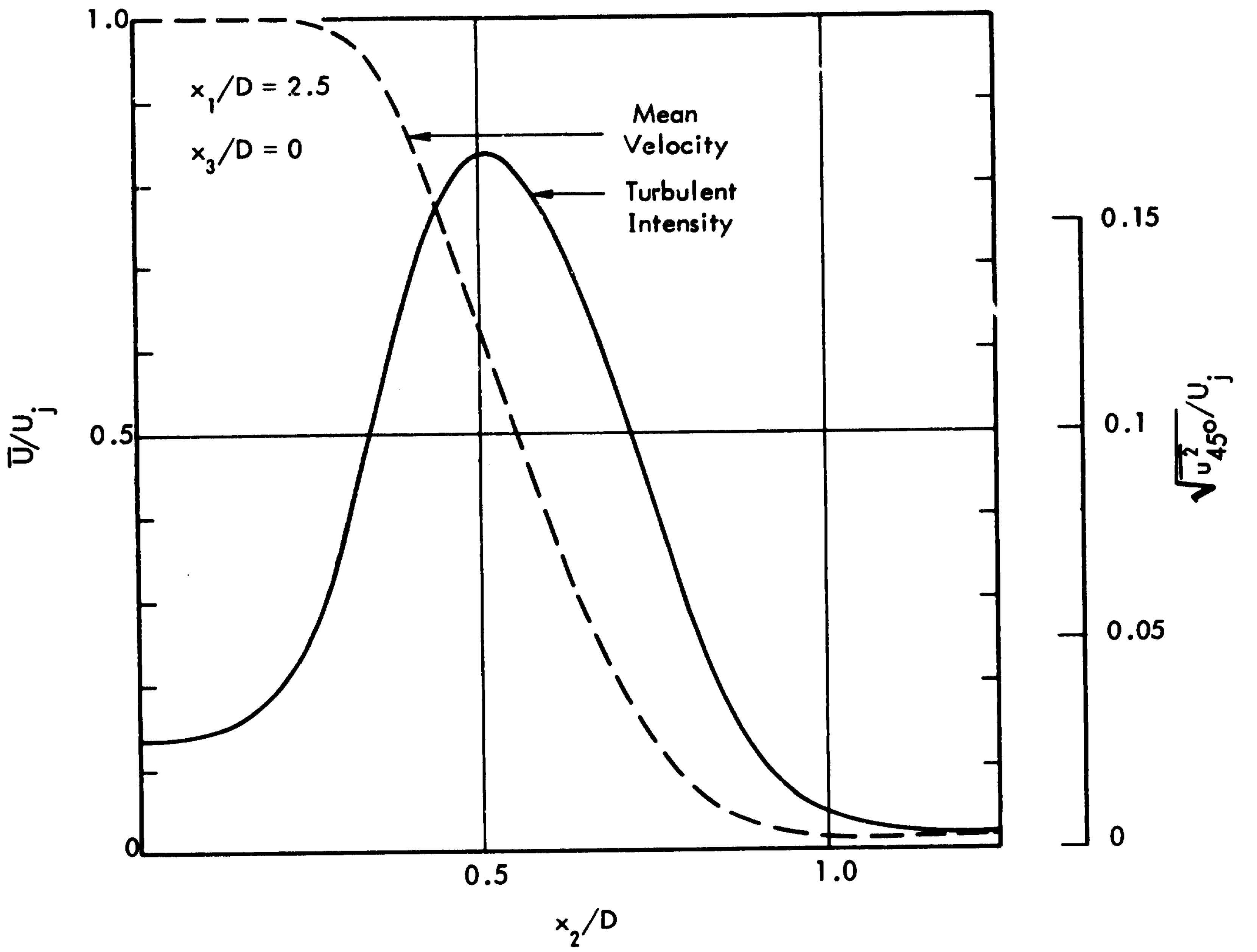

Figure 31. Turbulence Intensity Profile of $\sqrt{\overline{u^2_{45°}}}$ Measured Across the Jet Flow, $x_1 = 2.5D$

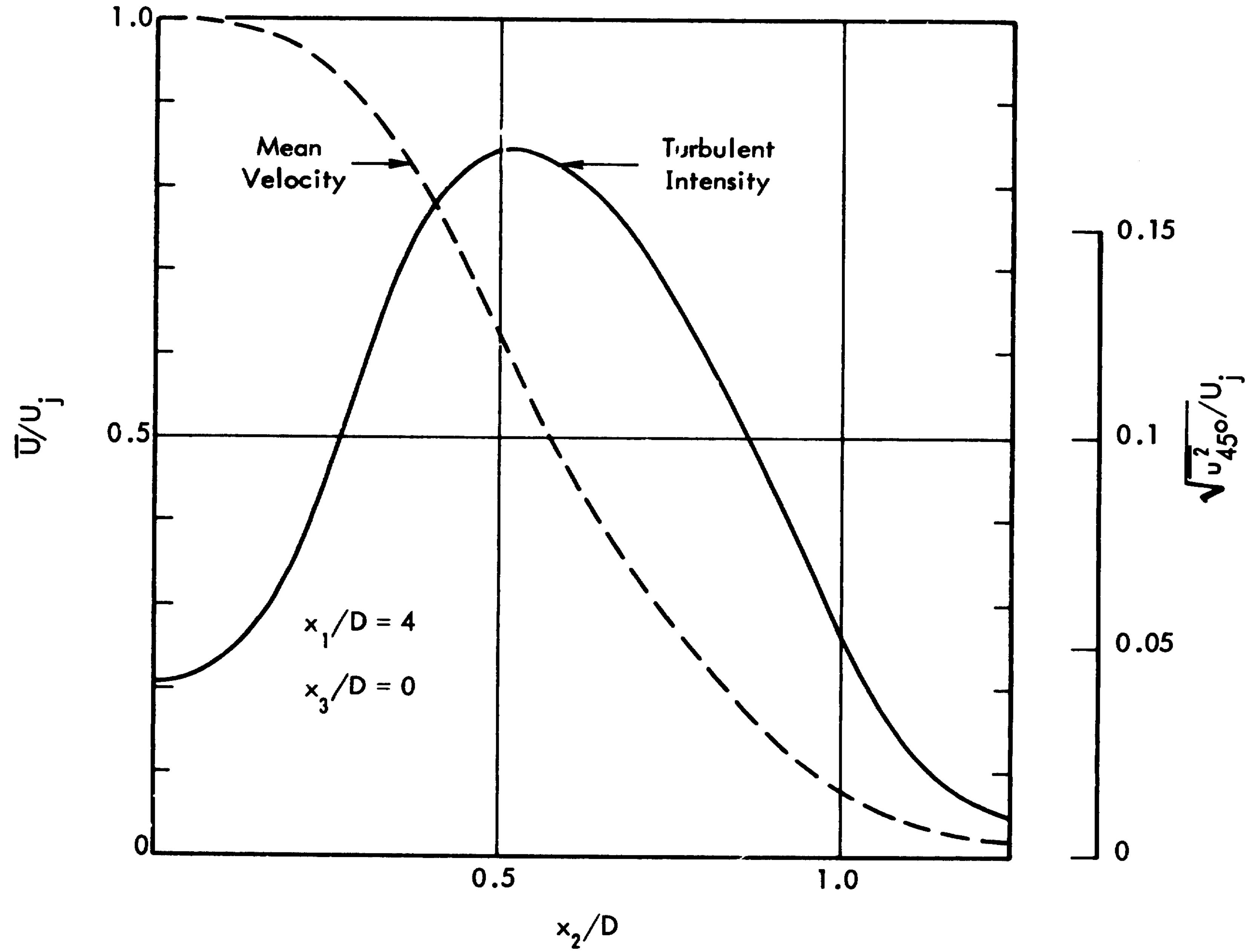

Figure 32. Turbulence Intensity Profile of $\sqrt{\overline{u^2_{45^o}}}$ Measured Across the Jet Flow, $x_1 = 4D$

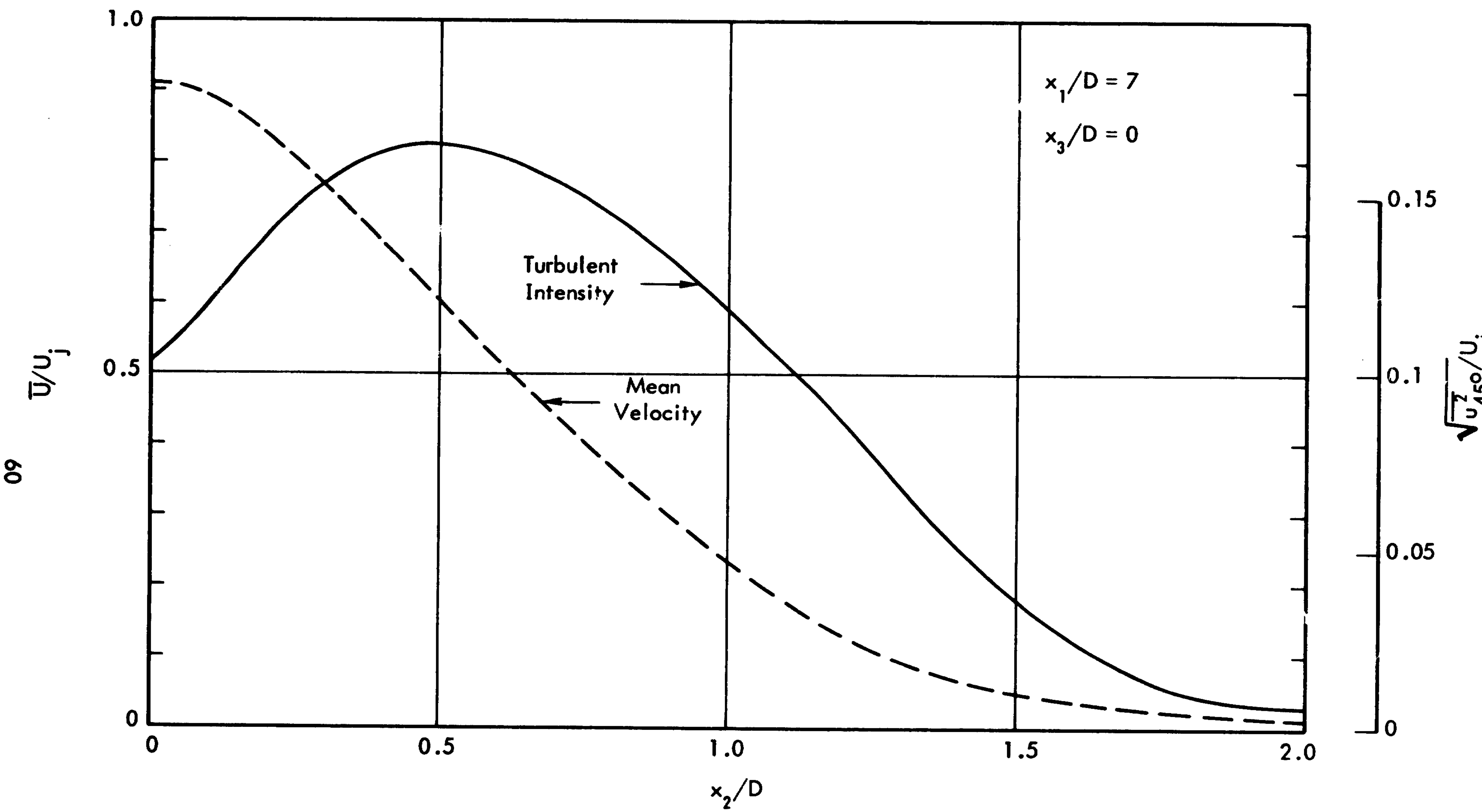

Figure 33. Turbulence Intensity Profile of $\sqrt{\overline{u^2_{45^\circ}}}$ Measured Across the Jet Flow, $x_1 = 7D$

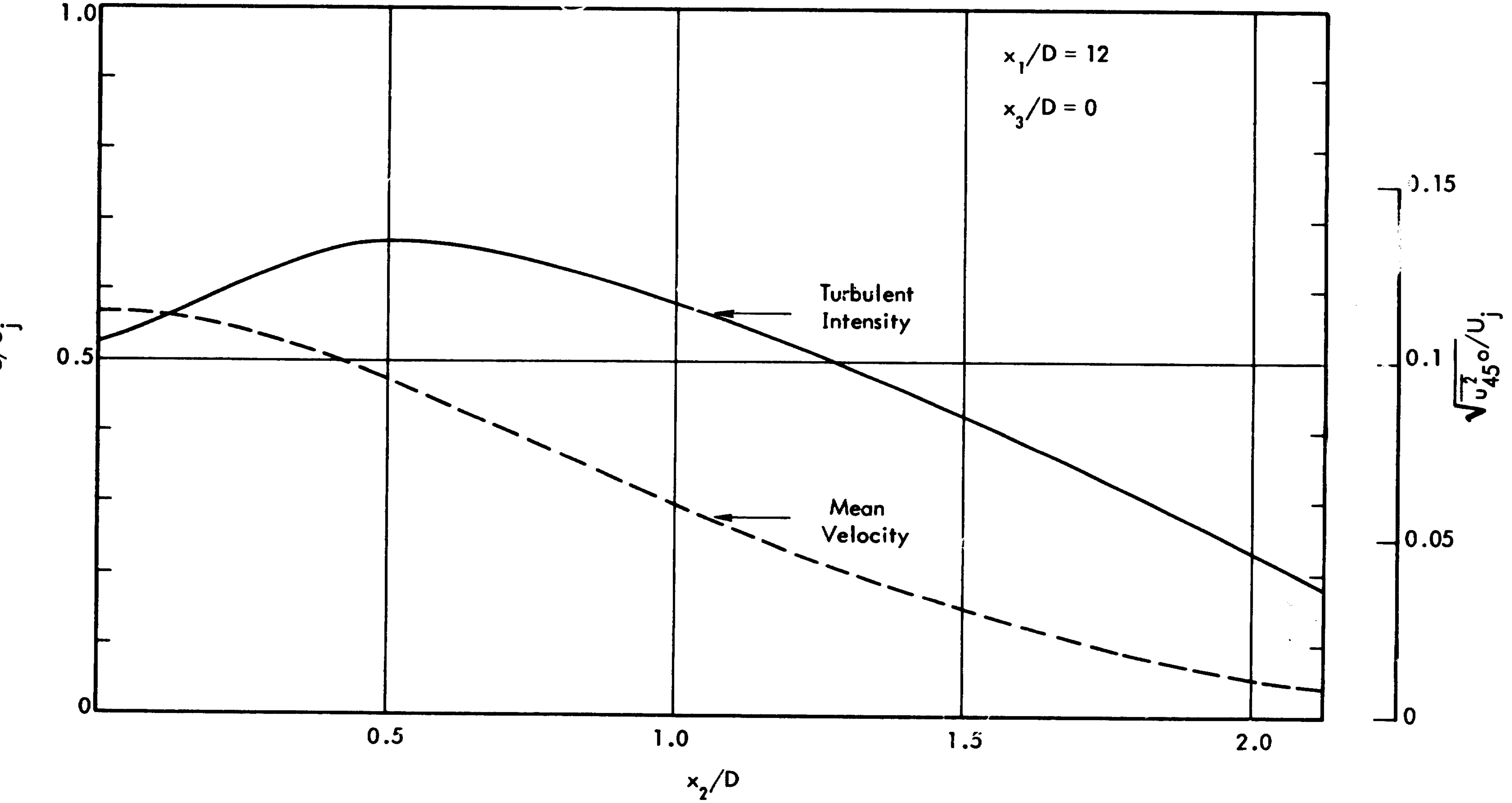

Figure 34. Turbulence Intensity Profile of $\sqrt{\overline{u^2_{45^o}}}$ Measured Across the Jet Flow, $x_1 = 12D$

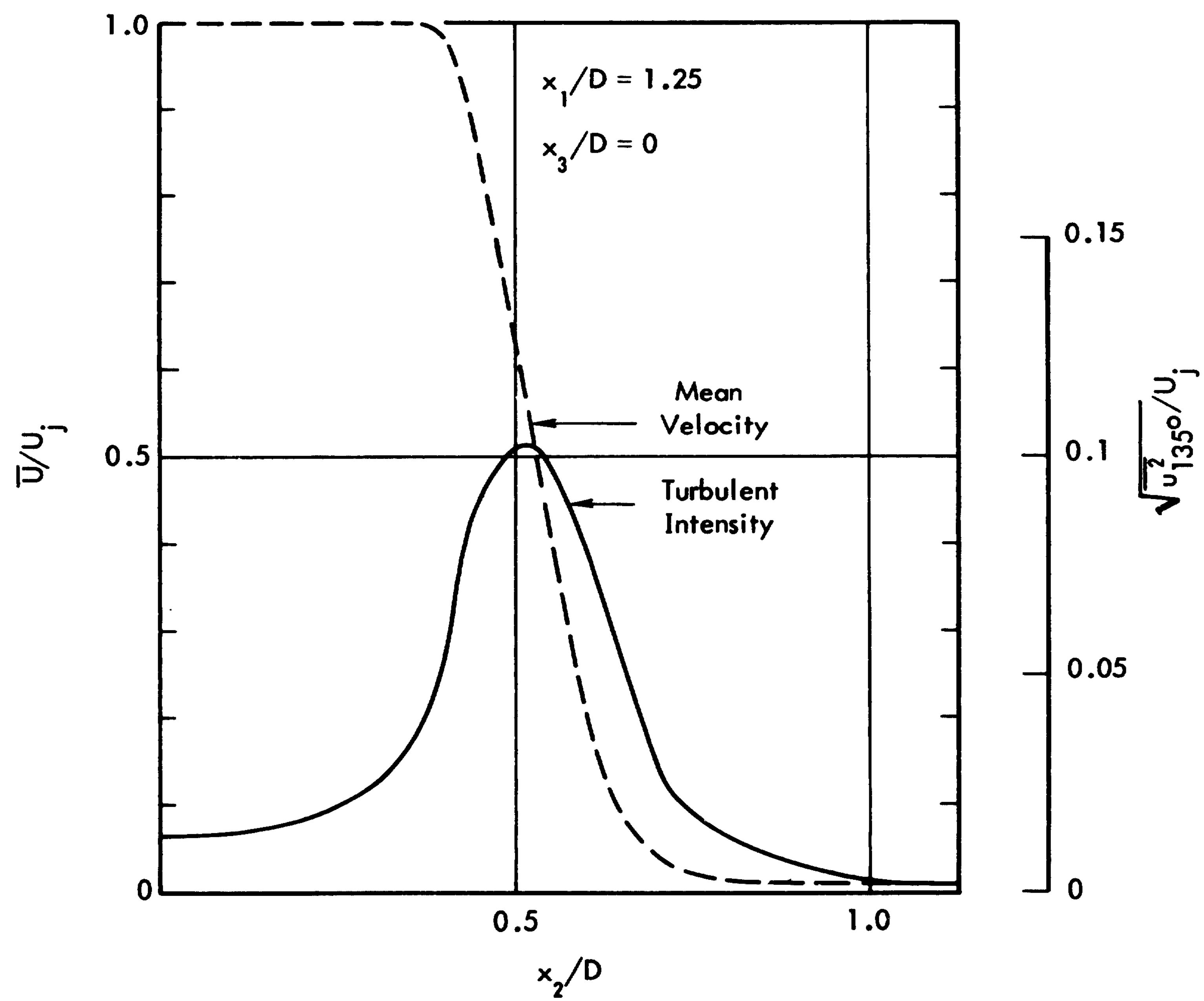

Figure 35. Turbulence Intensity Profile of $\sqrt{\overline{u^2_{135°}}}$ Measured Across the Jet Flow, $x_1 = 1.25D$

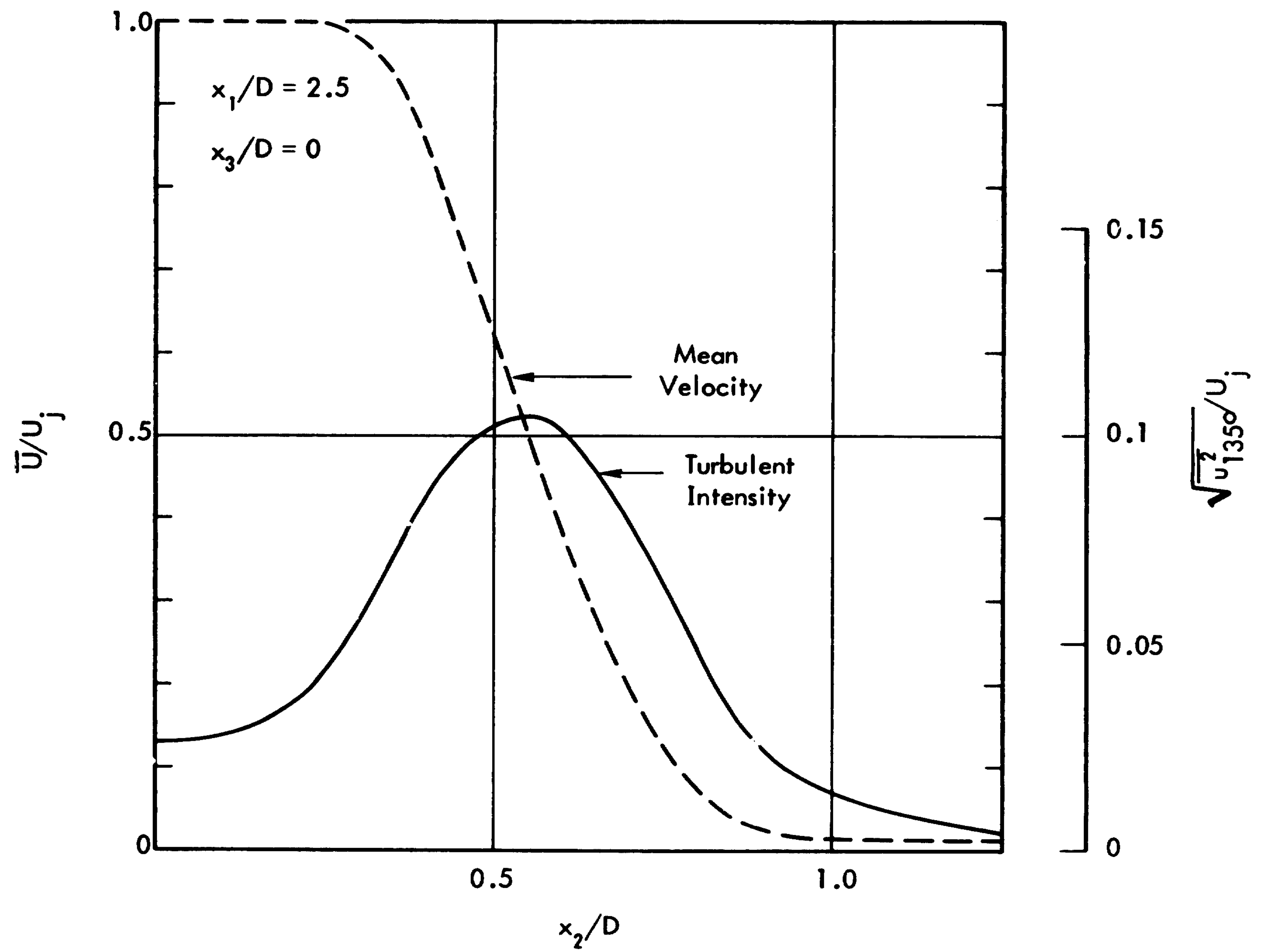

Figure 36. Turbulence Intensity Profile of $\sqrt{\overline{u^2_{135°}}}$ Measured Across the Jet Flow, $x_1 = 2.5D$

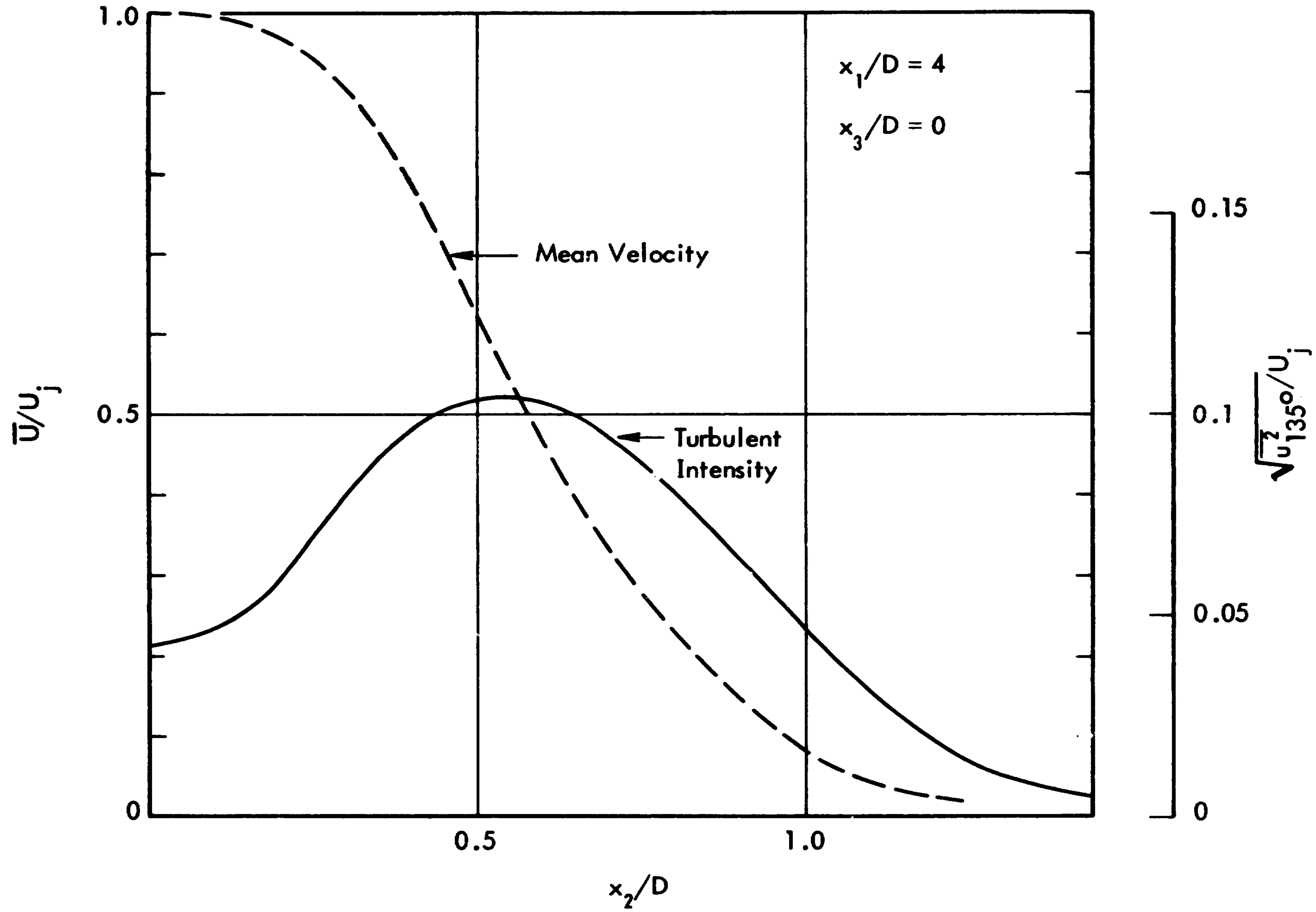

Figure 37. Turbulence Intensity Profile of $\sqrt{\overline{u^2_{135^o}}}$ Measured Across the Jet Flow, $x_1 = 4D$

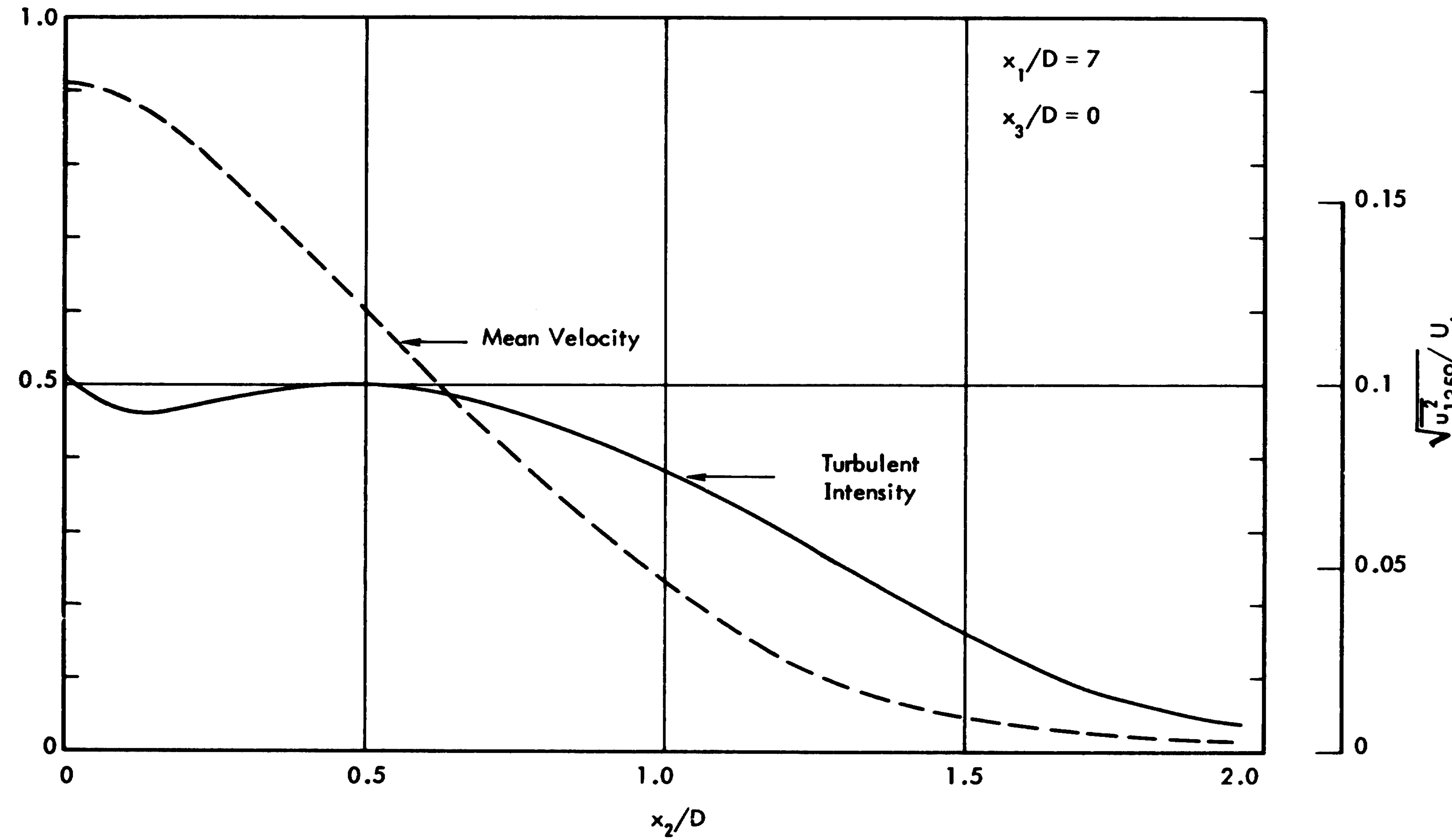

Figure 38. Turbulence Intensity Profile of $\sqrt{\overline{u^2_{135°}}}$ Measured Acorss the Jet Flow, $x_1 = 7D$

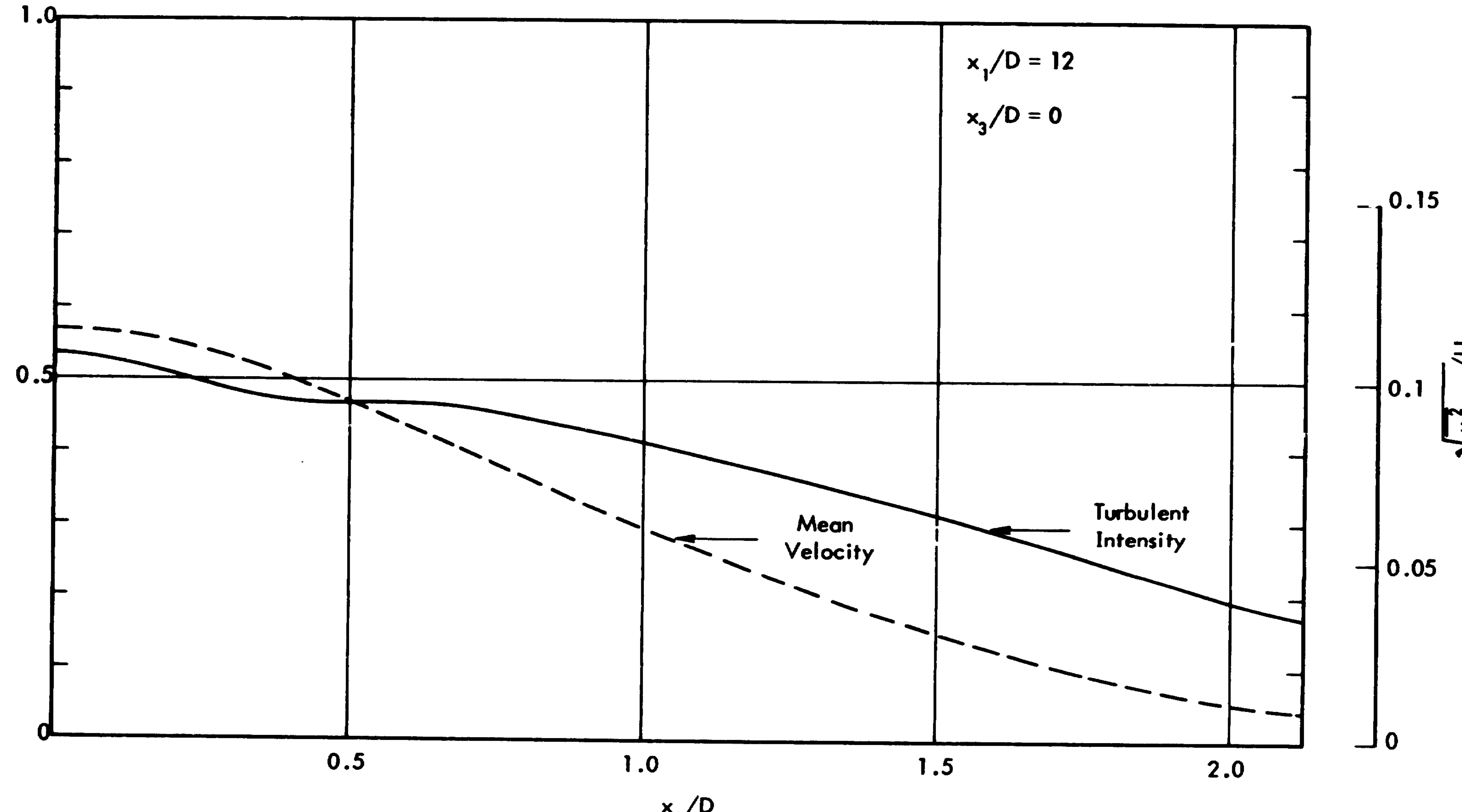

Figure 39. Turbulence Intensity Profile of $\sqrt{u^2_{135°}}$ Measured Across the Jet Flow, $x_1 = 12D$

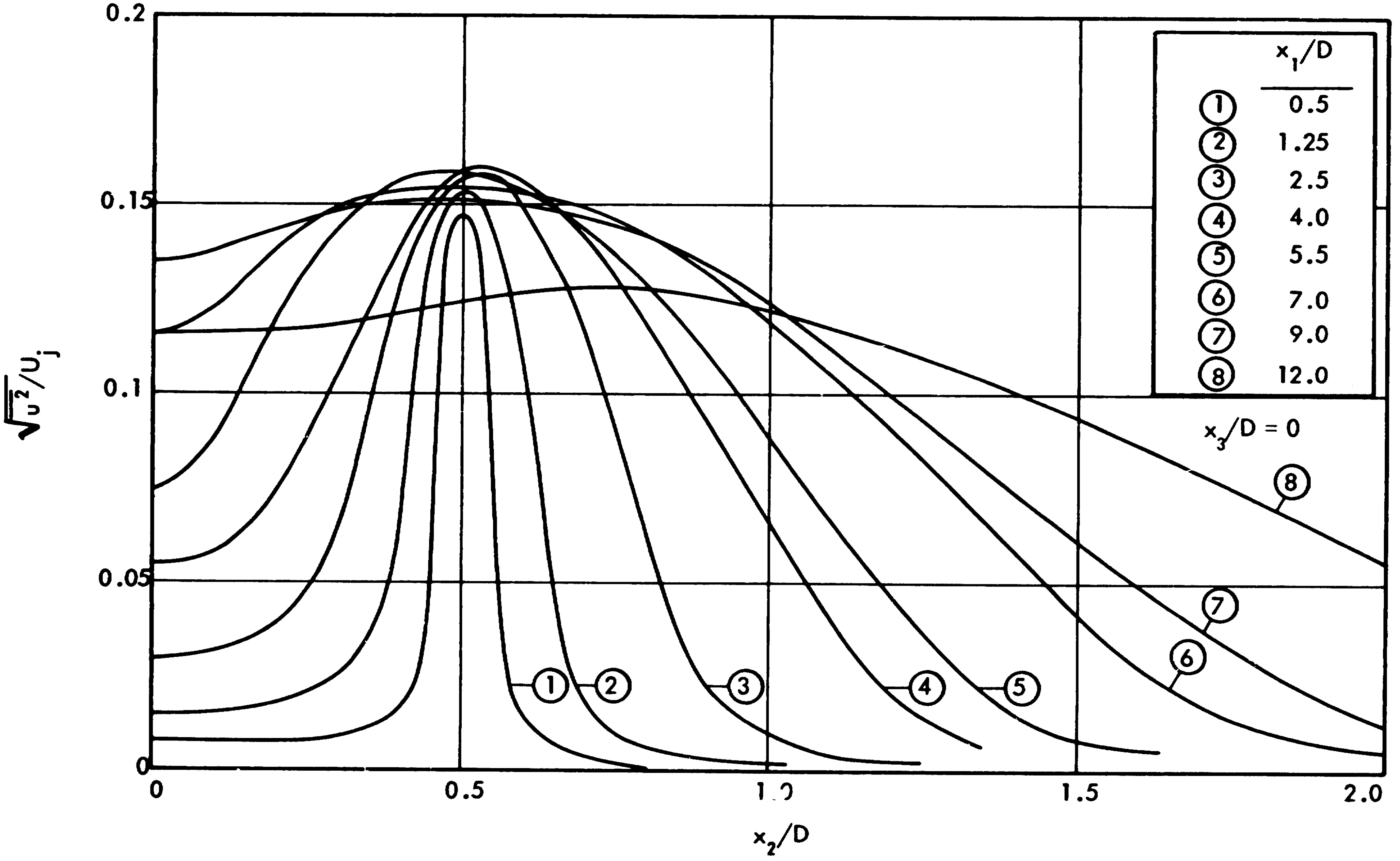

Figure 40. Comparison of Turbulence Intensity Profile of $\sqrt{\overline{u^2}}$ at Different Distances to the Jet Exit

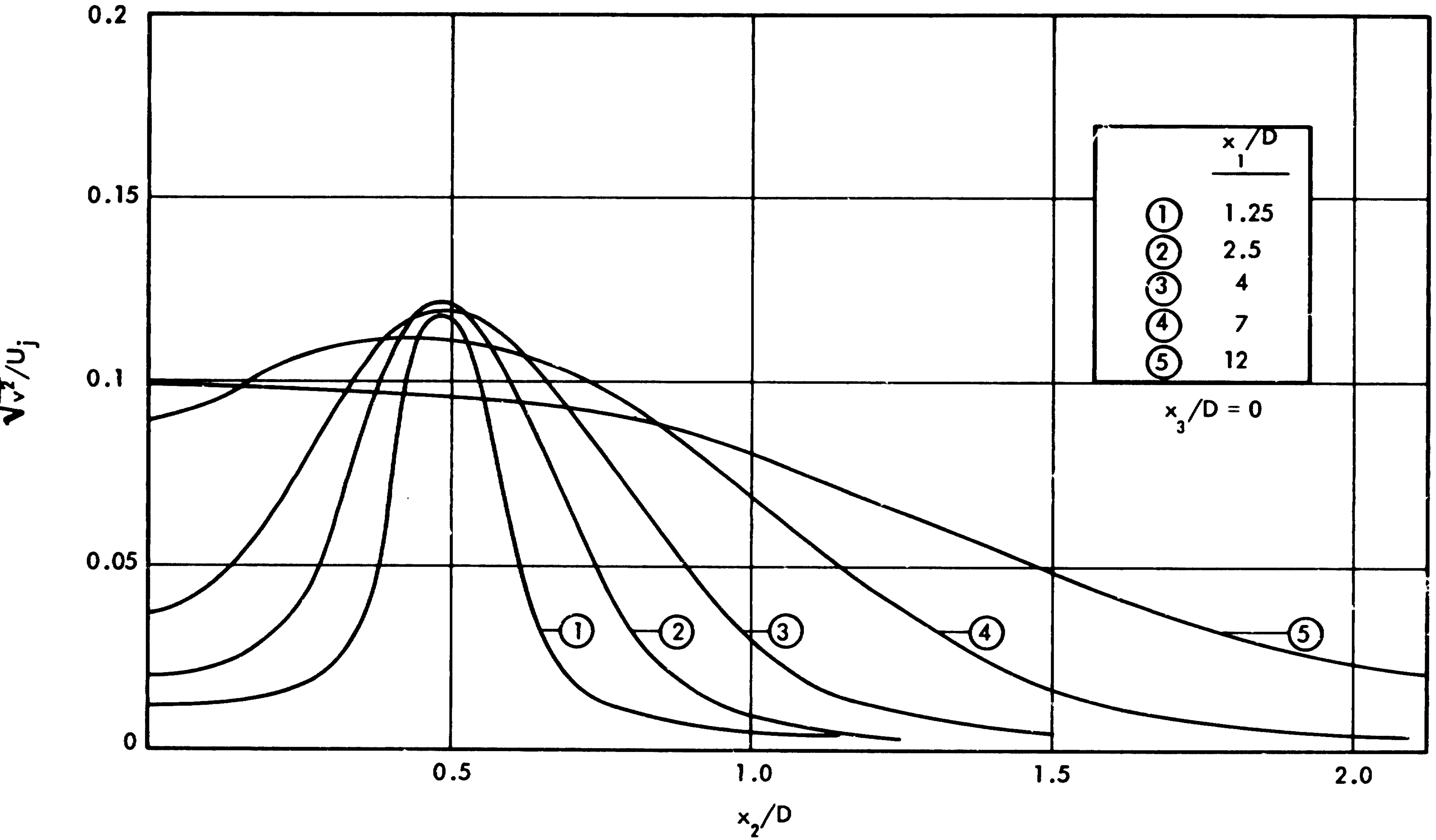

Figure 41. Comparison of Turbulence Intensity Profile of $\sqrt{\overline{v^2}}$ at Different Distances to the Jet Exit

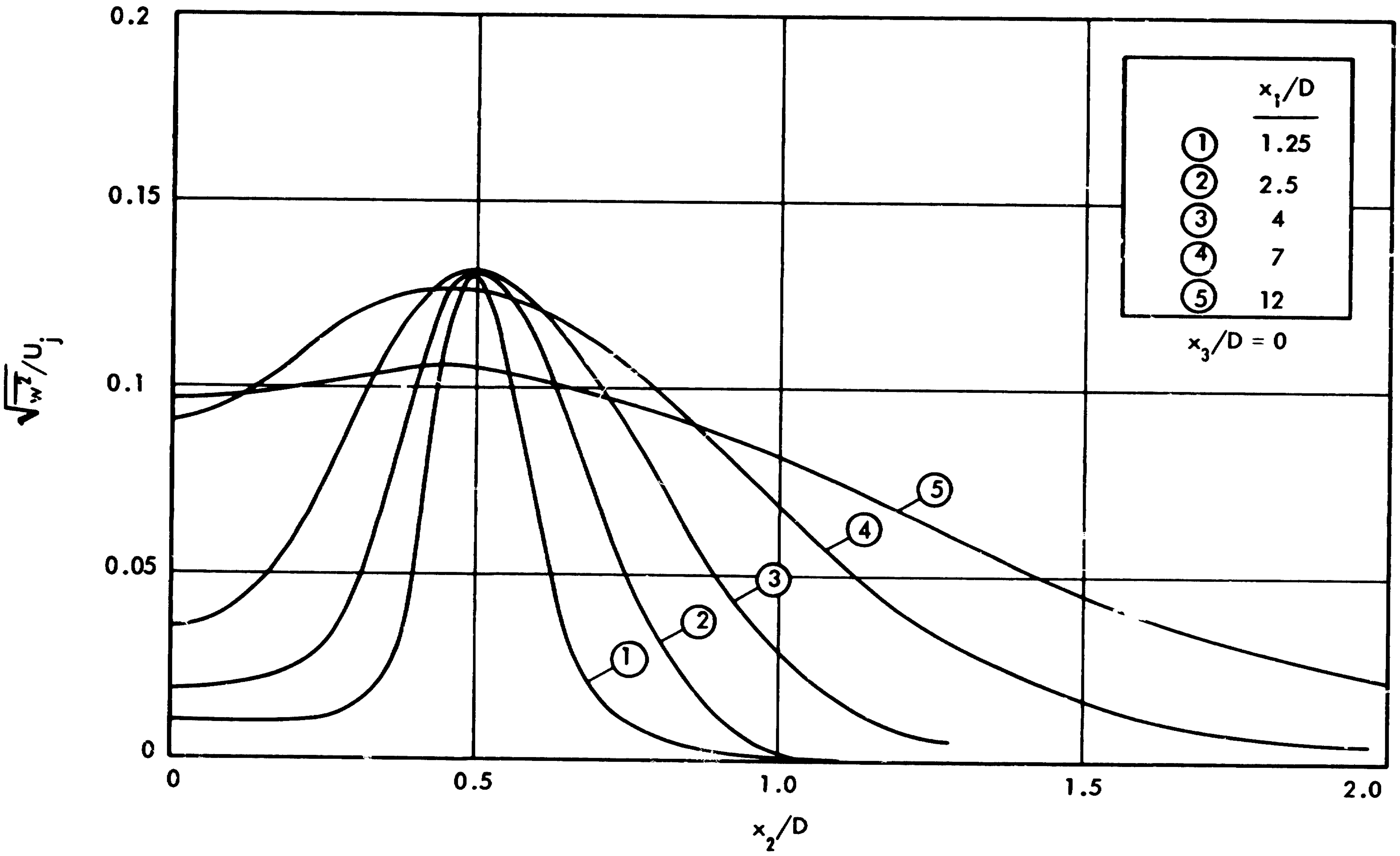

Figure 42. Comparison of Turbulence Intensity Profile of $\sqrt{\overline{w^2}}$ at Different Distances to the Jet Exit

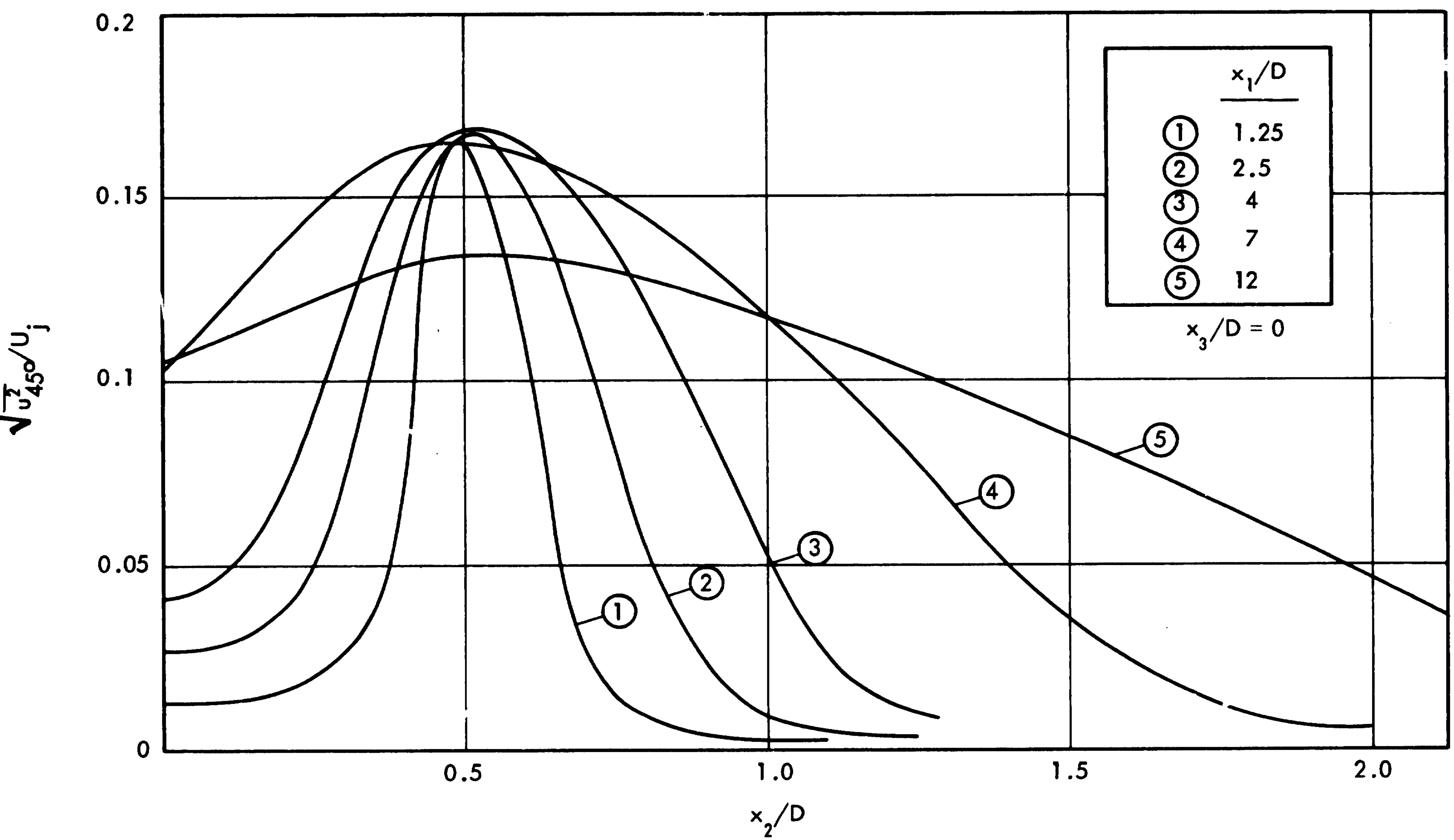

Figure 43. Comparison of Turbulence Intensity Profile of $\sqrt{\overline{u^2_{45°}}}$ at Different Distances to the Jet Exit

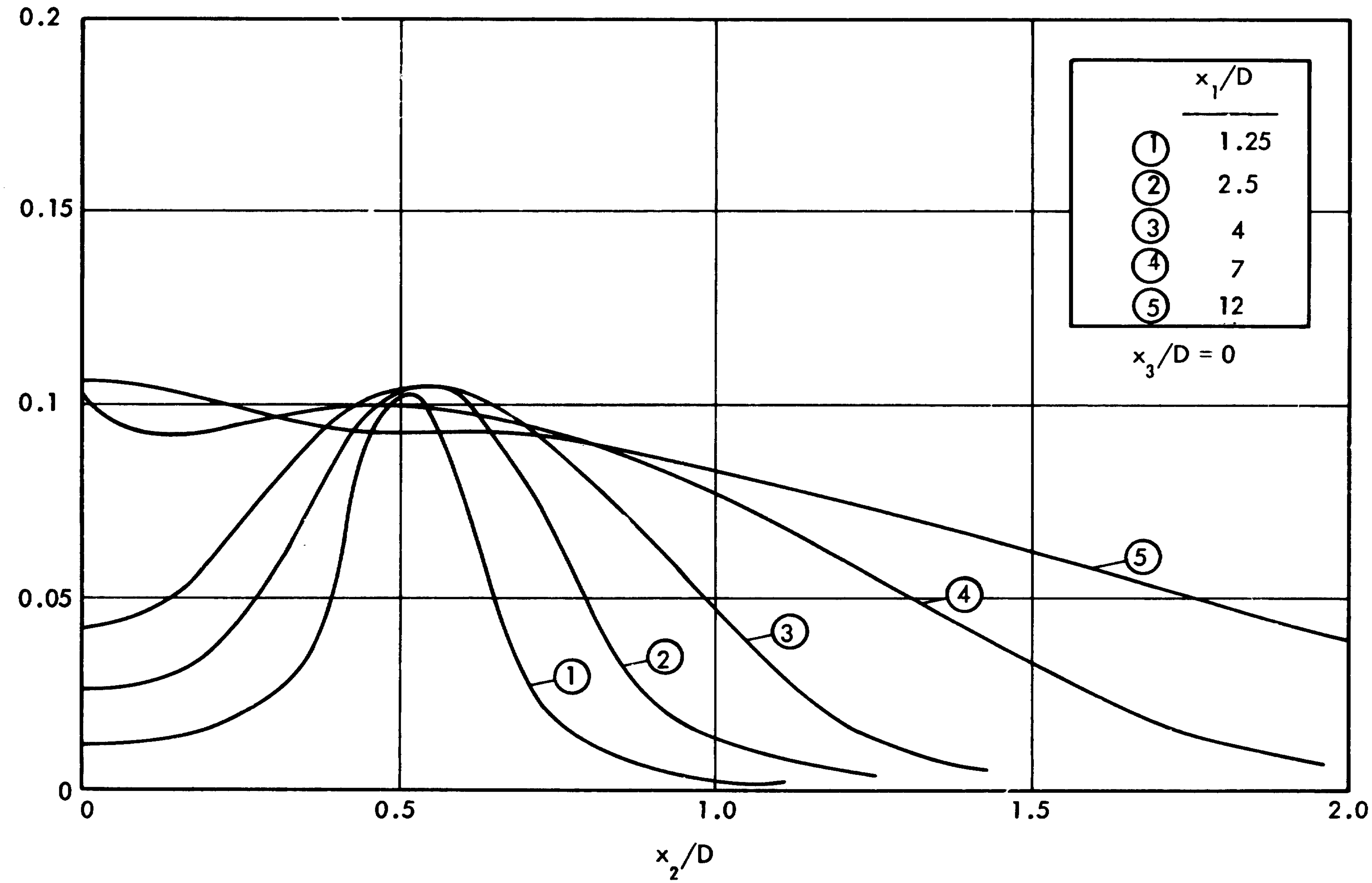

Figure 44. Comparison of Turbulence Intensity Profile of $\sqrt{\overline{u^2_{135^o}}}$ at Different Distances to the Jet Exit

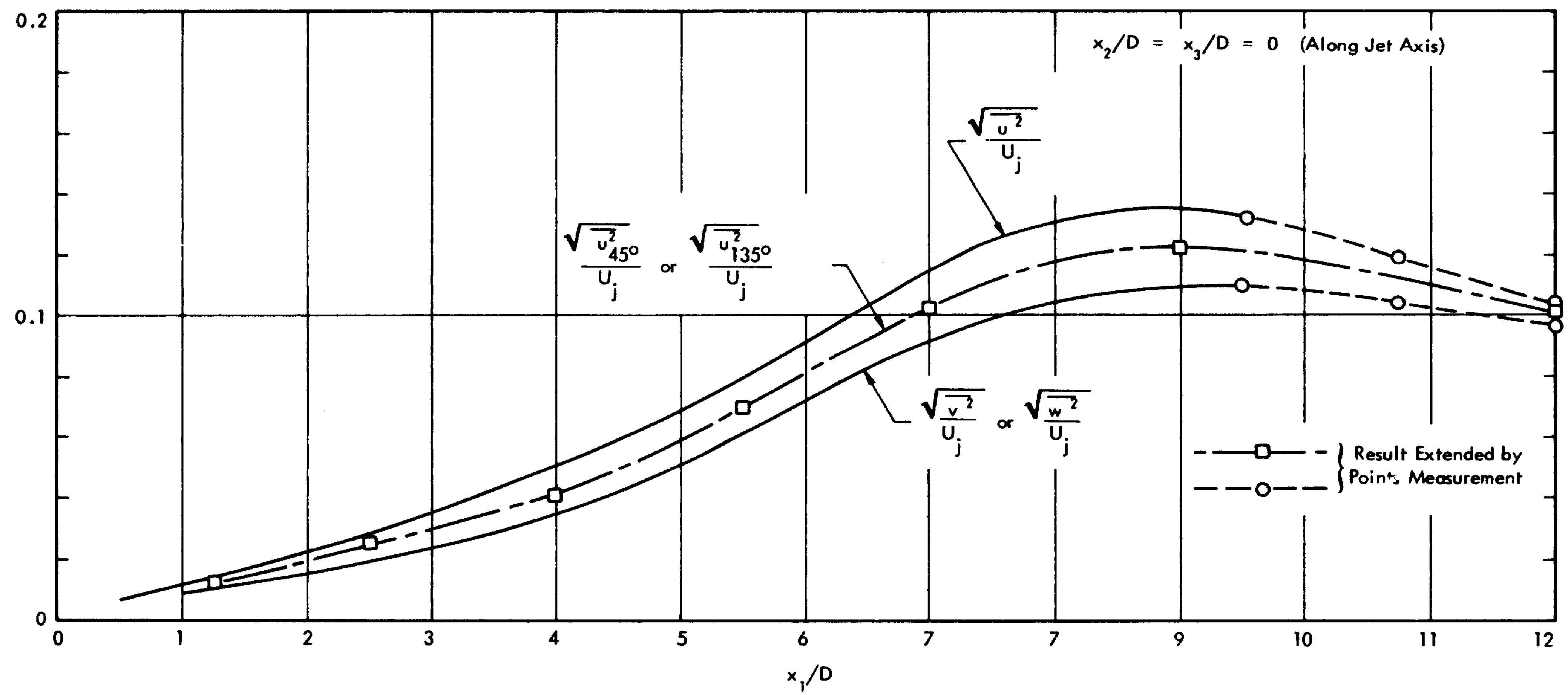

Figure 45. Turbulence Intensity Profiles of Different Velocity Components Measured Along the Jet Flow, I

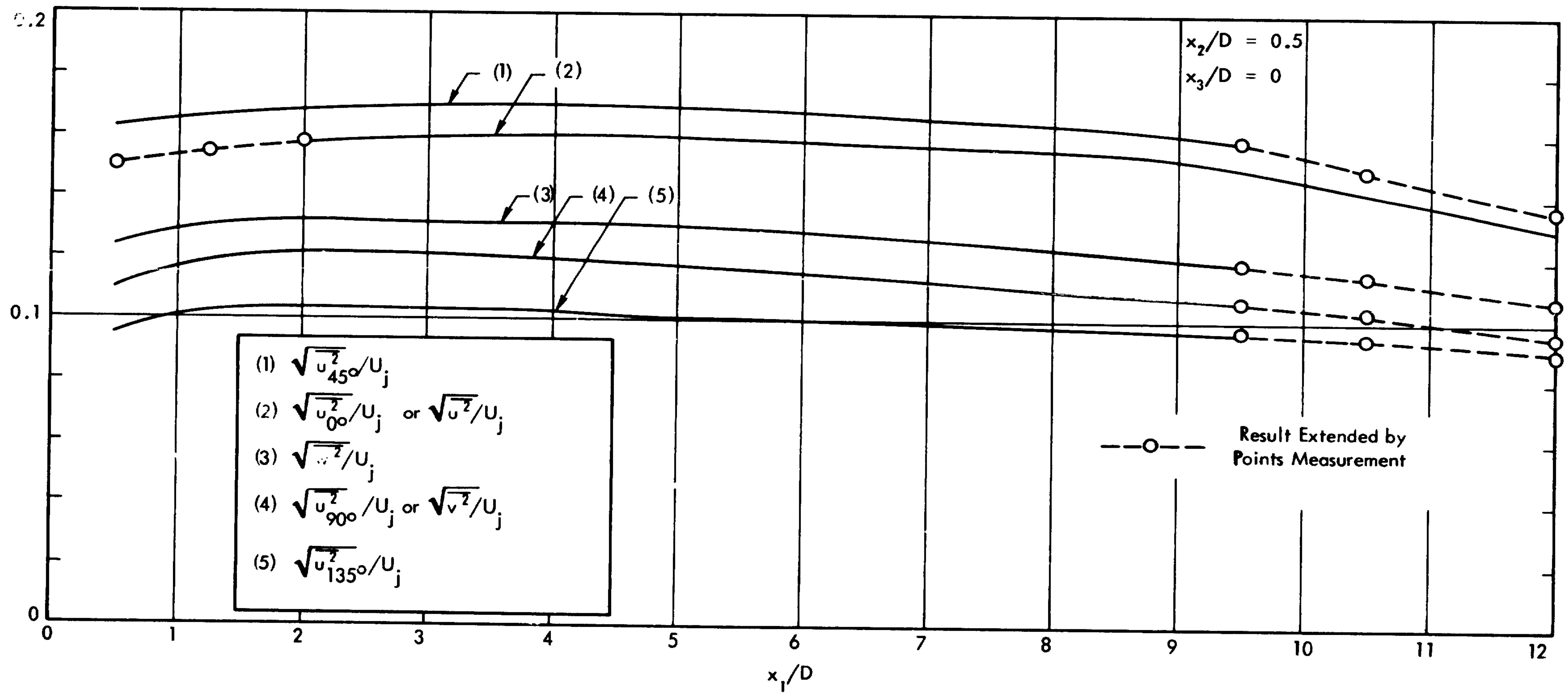

Figure 46. Turbulence Intensity Profiles of Different Velocity Components Measured Along the Jet Flow, II

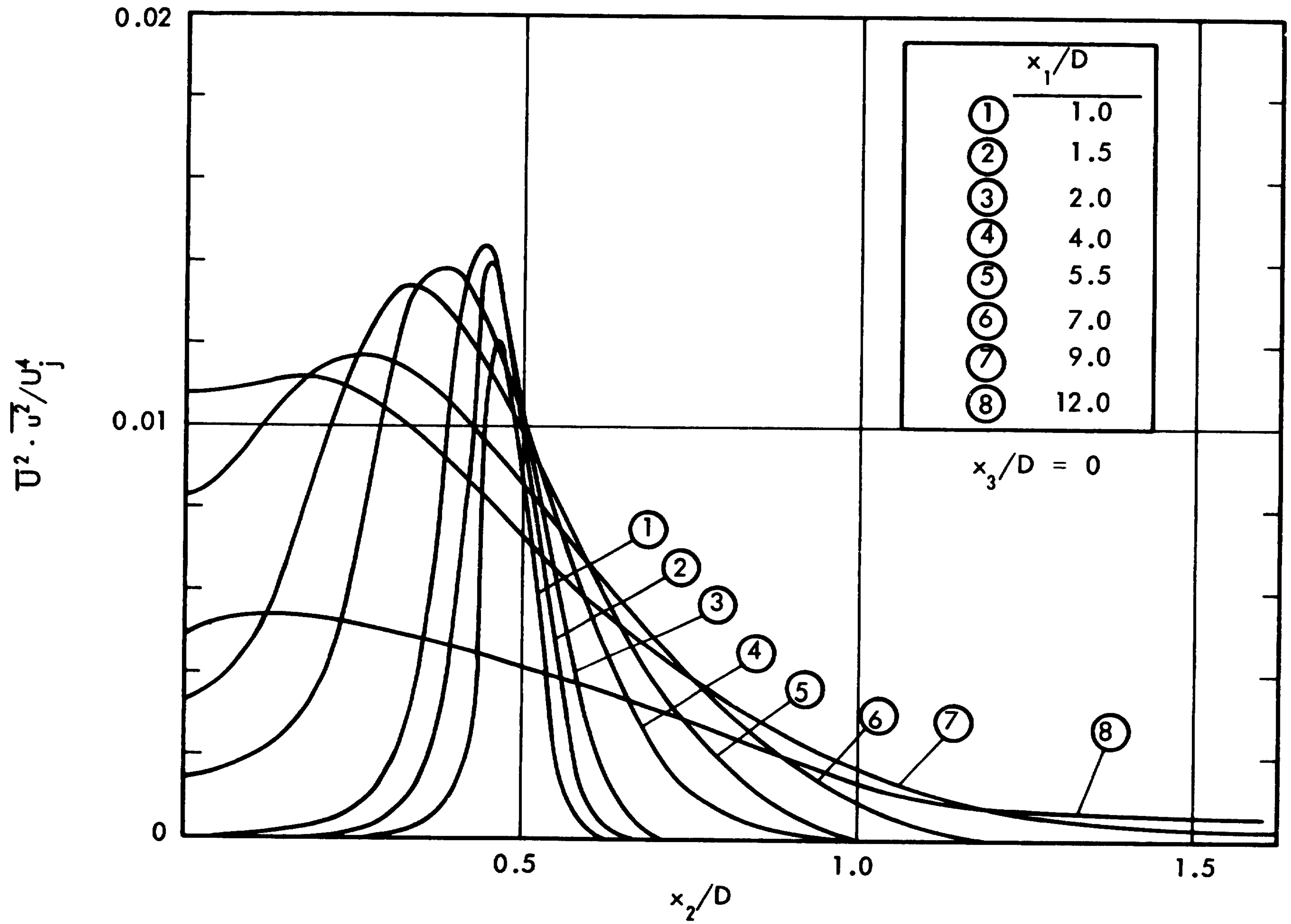

Figure 47. Profiles of Noise Source Intensity Factor, $\overline{U}^2 \cdot \overline{u^2}$, at Different Distances to the Jet Exit

NOTE:

1. Jet Exit Speed:

   (a) to (e) 300 fps
   (f) 100 fps

2. Hot-Wire Position:

	(a)	(b)	(c)	(d)	(e)	(f)
x_1/D	0.5	1.25	2.5	4	5	1.25

   $x_2/D = x_3/D = 0$ (Jet Centerline)

3. Oscilloscope Sweeping Time:

   (a) to (e) 5 Milli-Sec/cm
   (f) 10 Milli-Sec/cm

4. Oscilloscope Sensitivity:

   The same in all 6 cases: 1 volt/cm

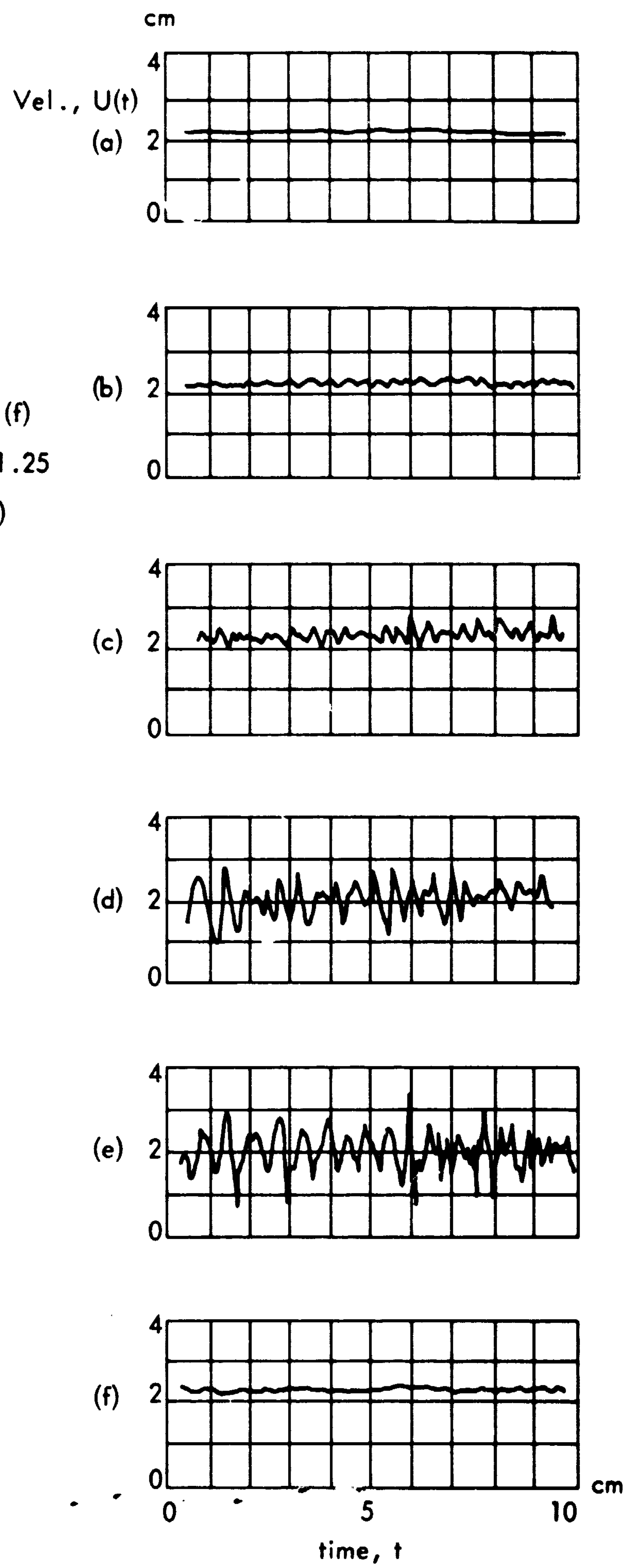

Figure 48. Oscilloscope Trace of the Hot-Wire Signal of the Growing Instability Along the Jet Centerline Inside the Potential Core

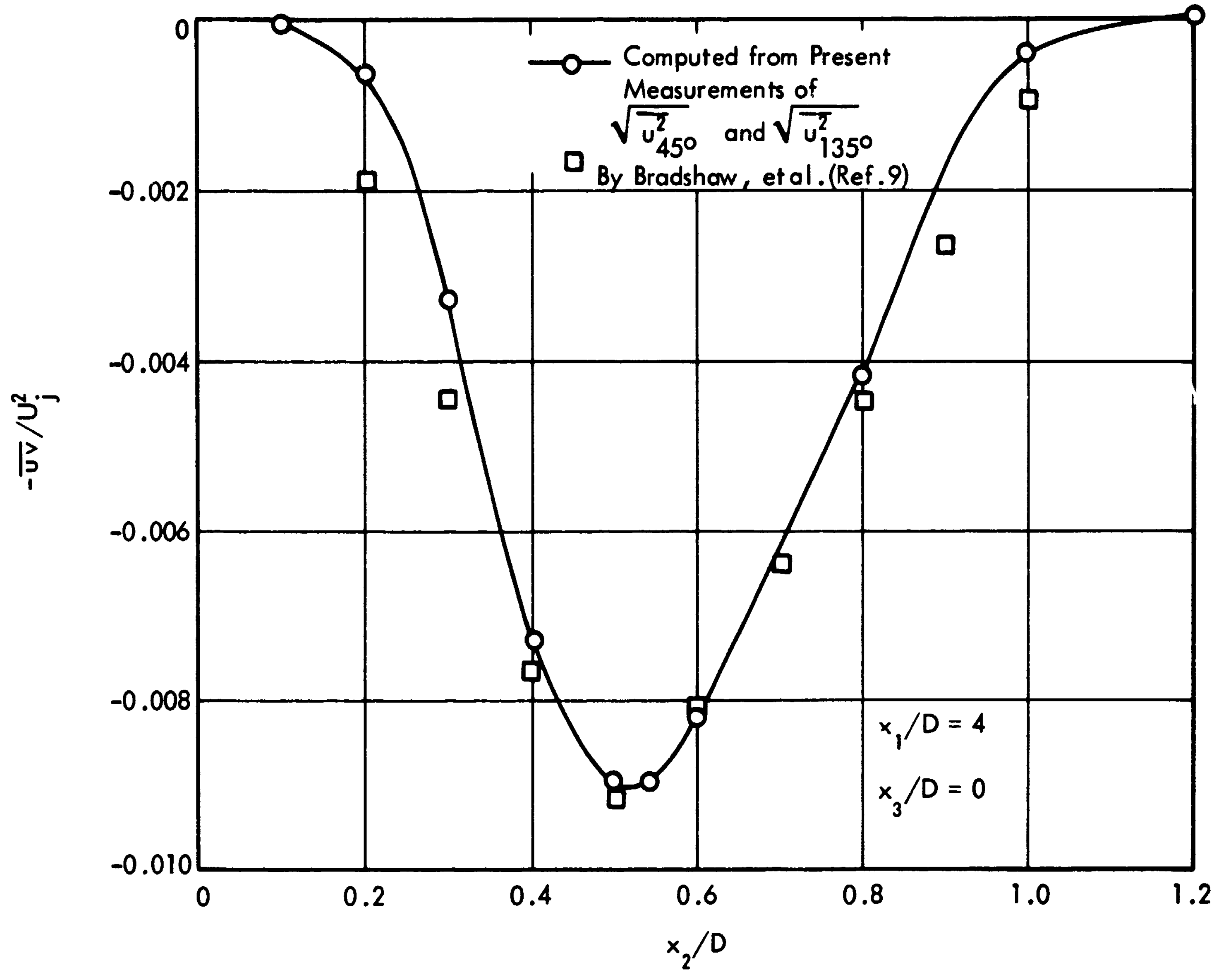

Figure 49. Turbulent Shear Stress, $-\overline{uv}$: $x_1 = 4D$, $x_3 = 0$

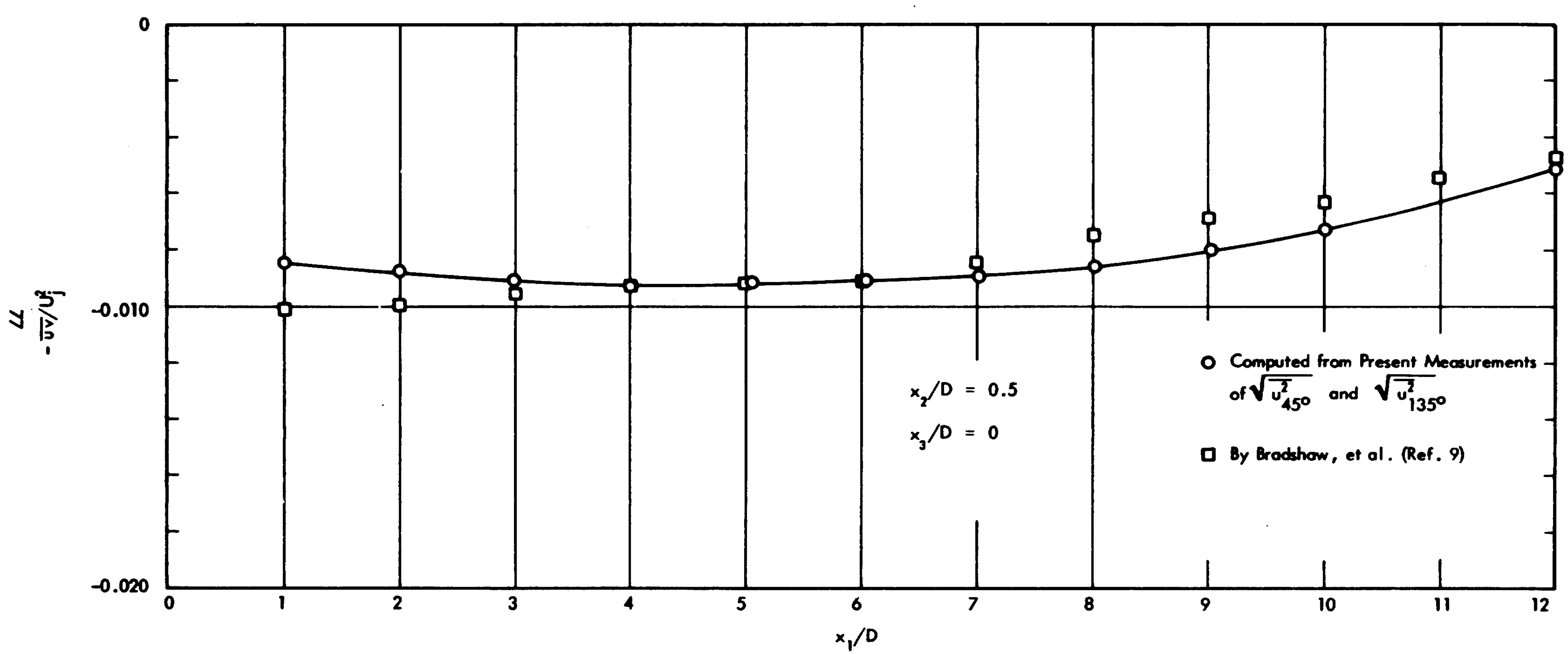

Figure 50. Turbulent Shear Stress, $-\overline{uv}$: $x_2 = 0.5D$, $x_3 = 0$

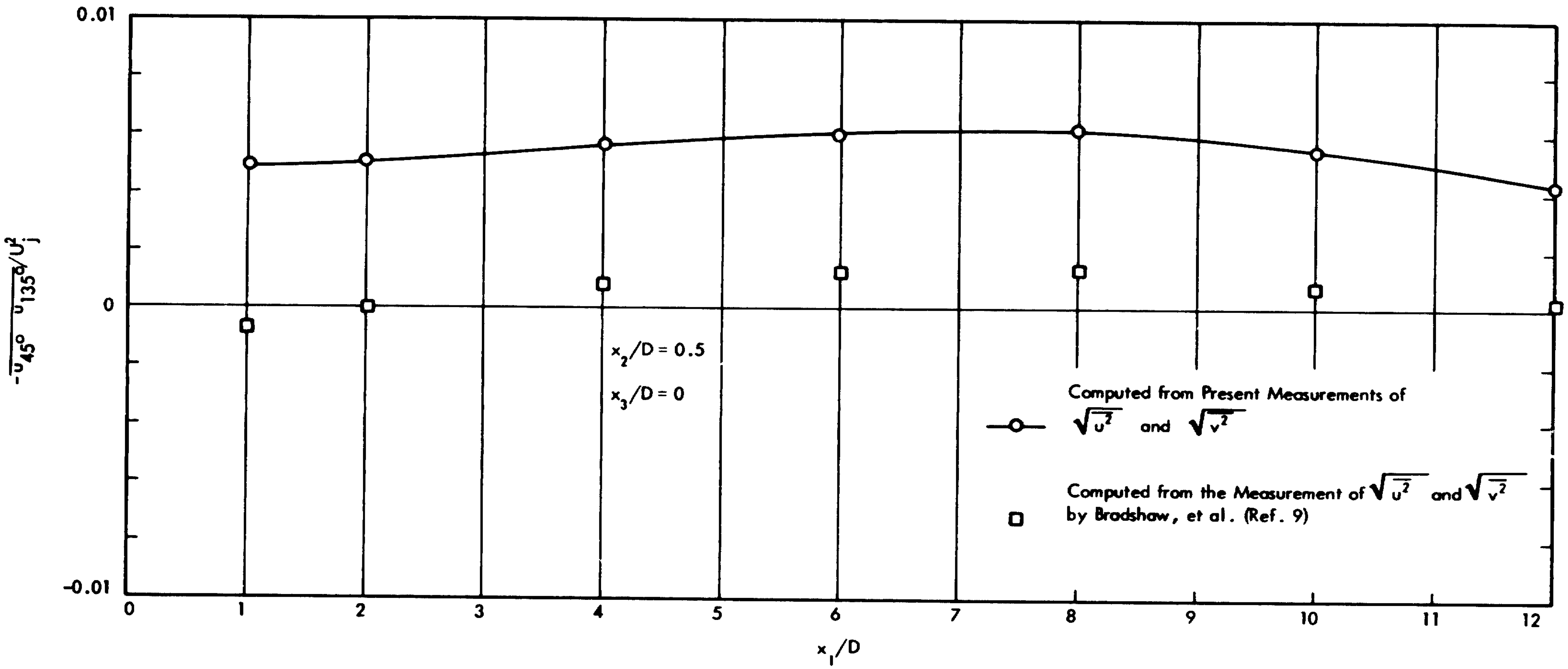

Figure 51. Turbulent Shear Stress, $\overline{-u_{45°}, u_{135°}}$: $x_2 = 0.5D$, $x_3 = 0$

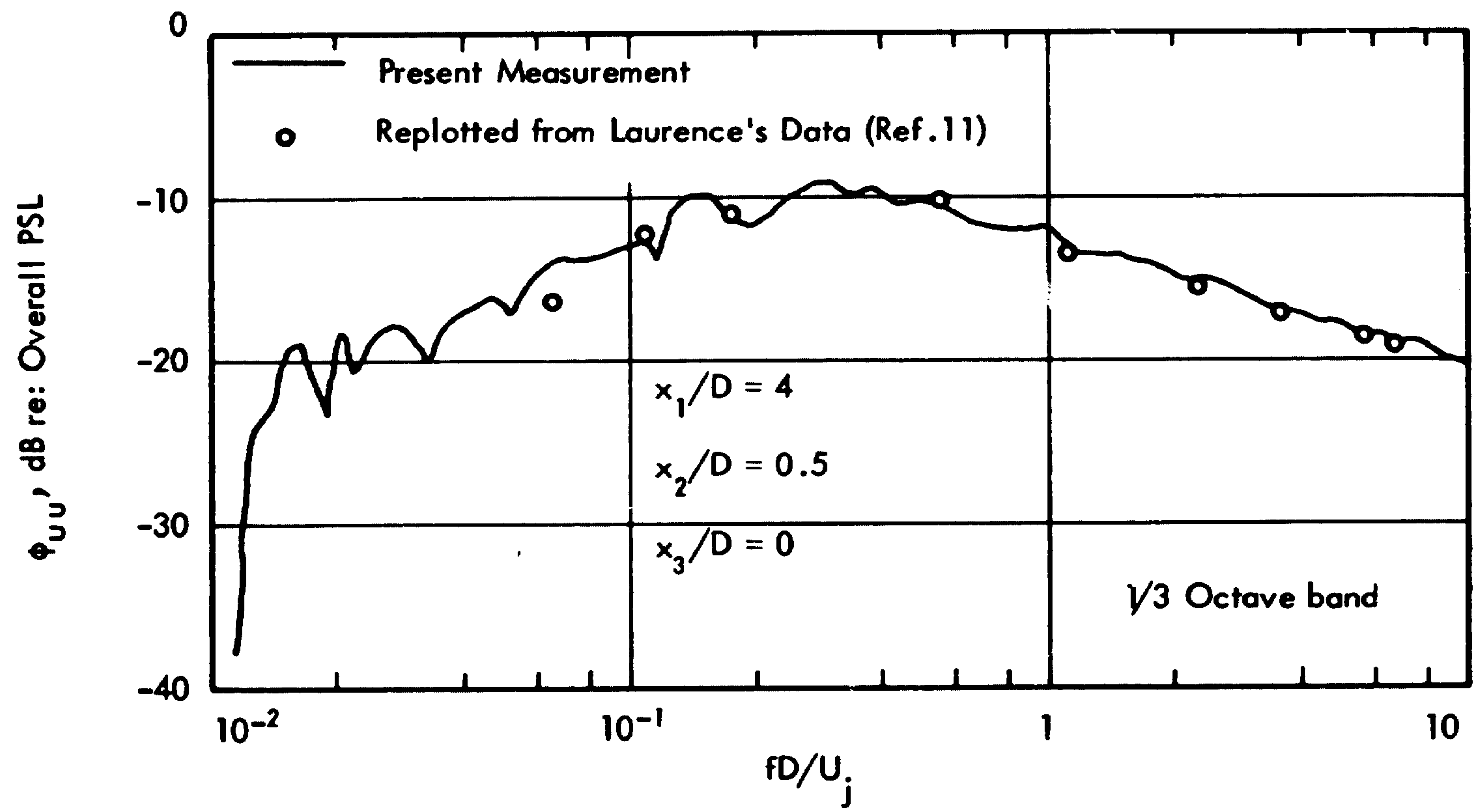

Figure 52. Comparison of One-Third Octave Band Spectra for u-Component with Previous work

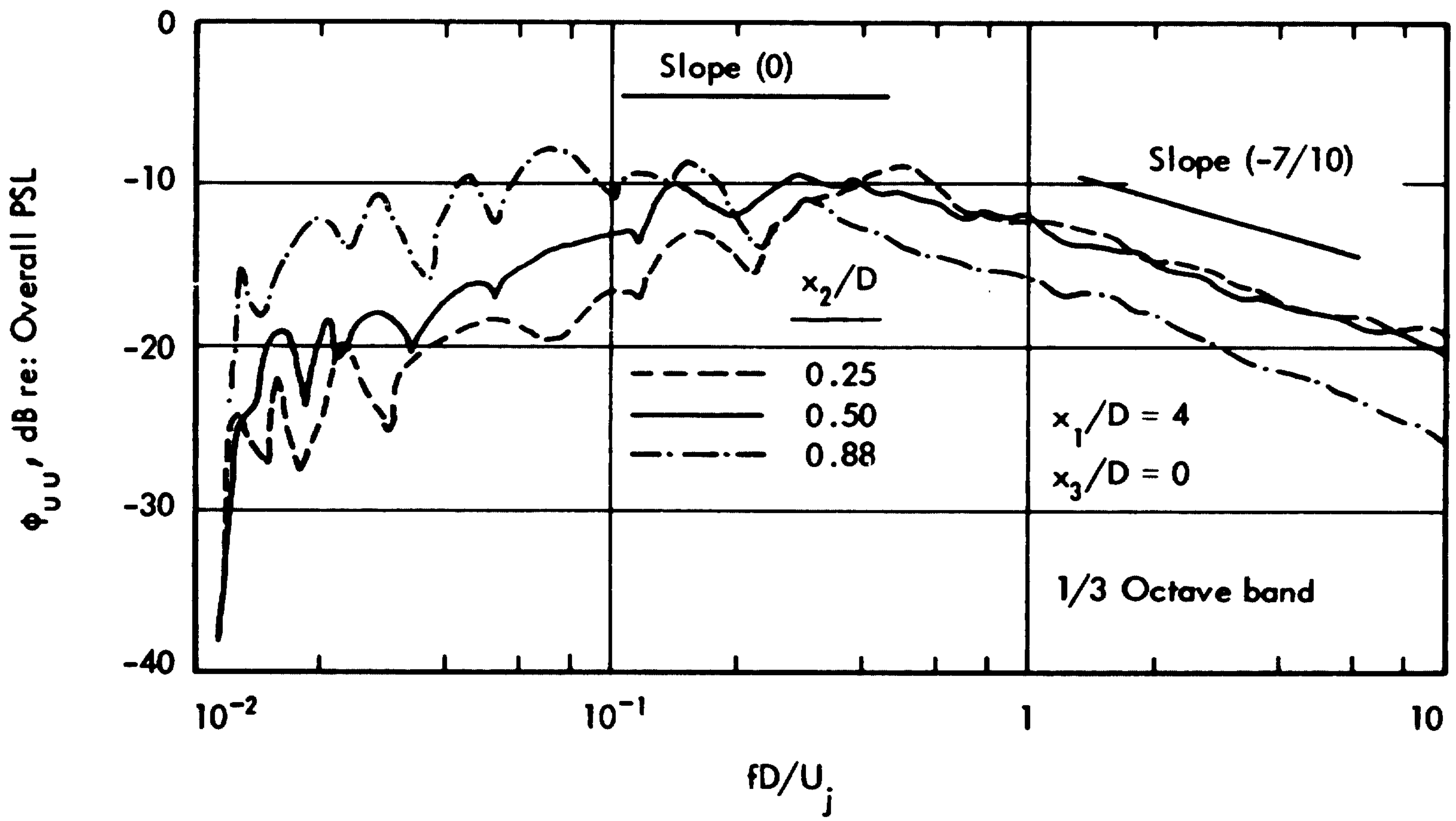

Figure 53. One-Third Octave Band Spectra for u-Component, I

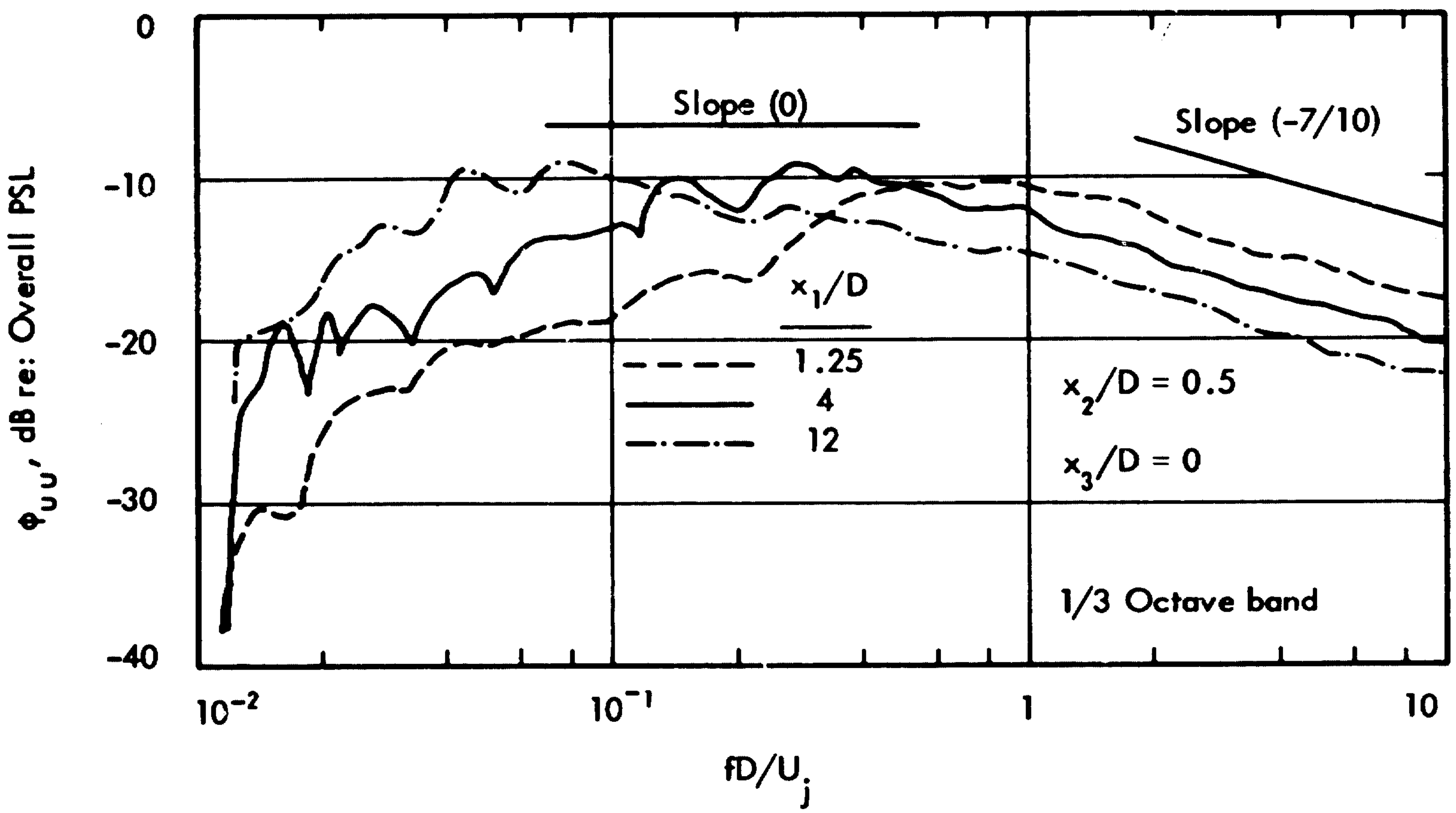

Figure 54. One-Third Octave Band Spectra for u-Component, II

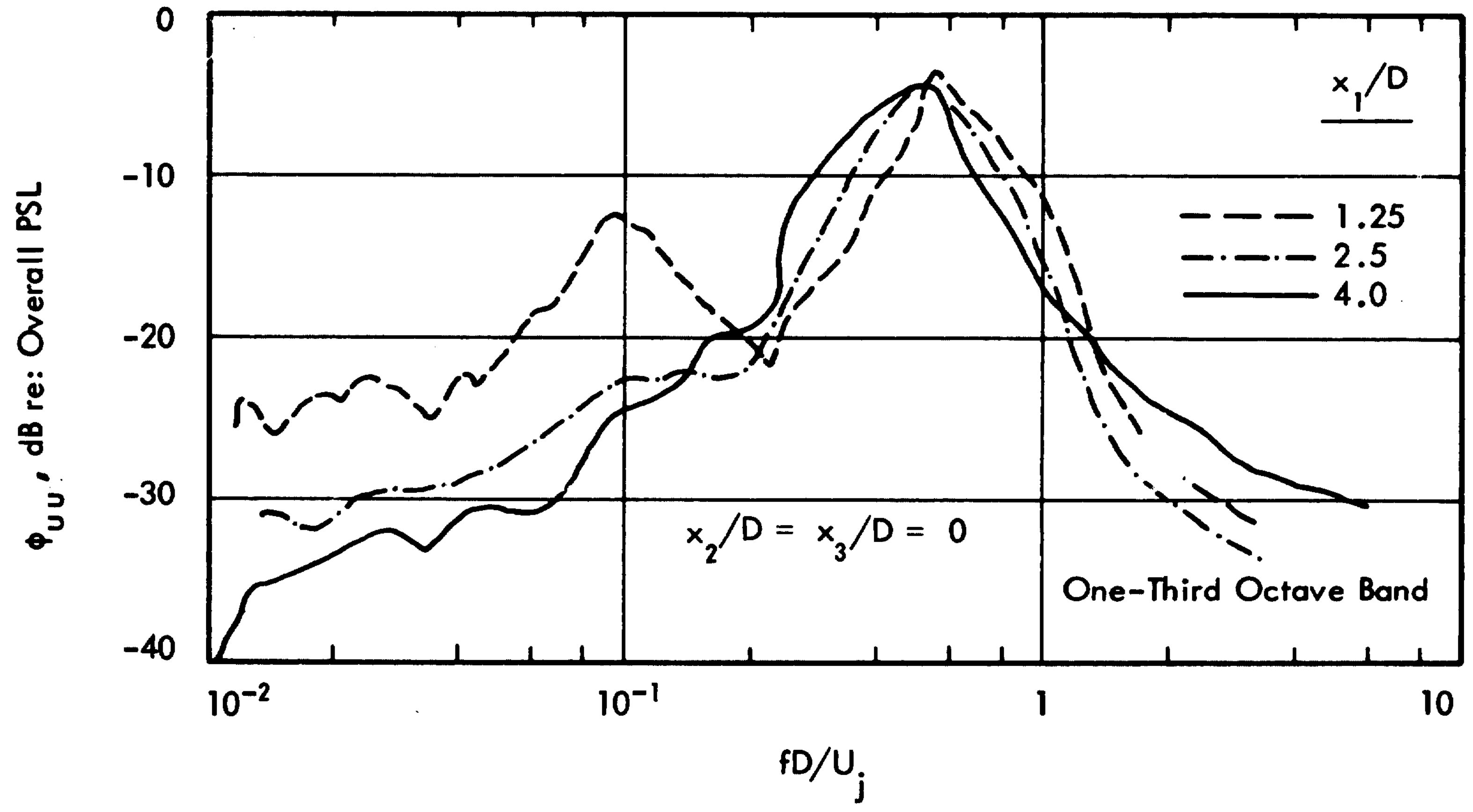

Figure 55. One-Third Octave Band Spectra for u-Component, III

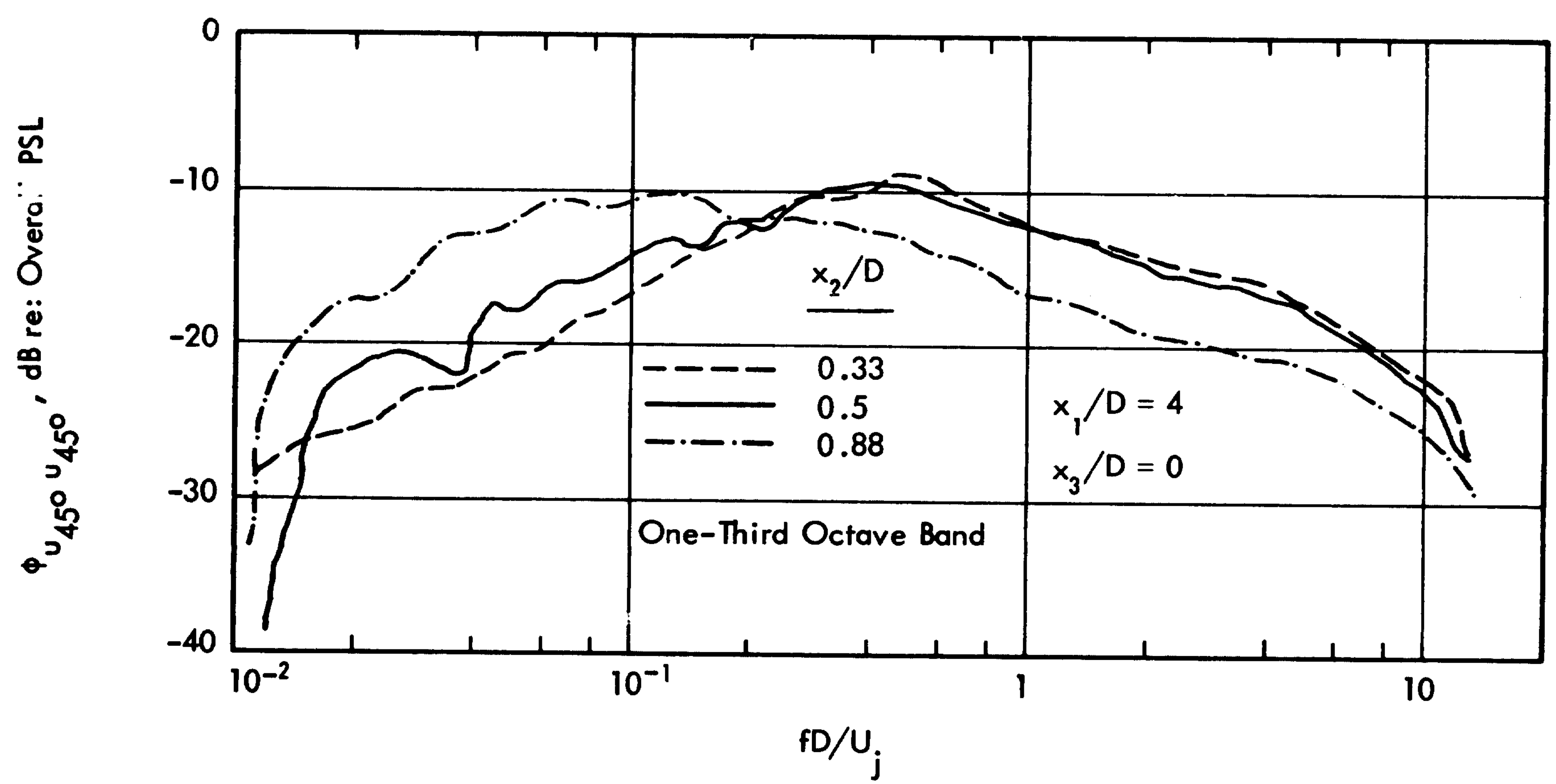

Figure 56. One-Third Octave Band Spectra for u_{45^o} - Component

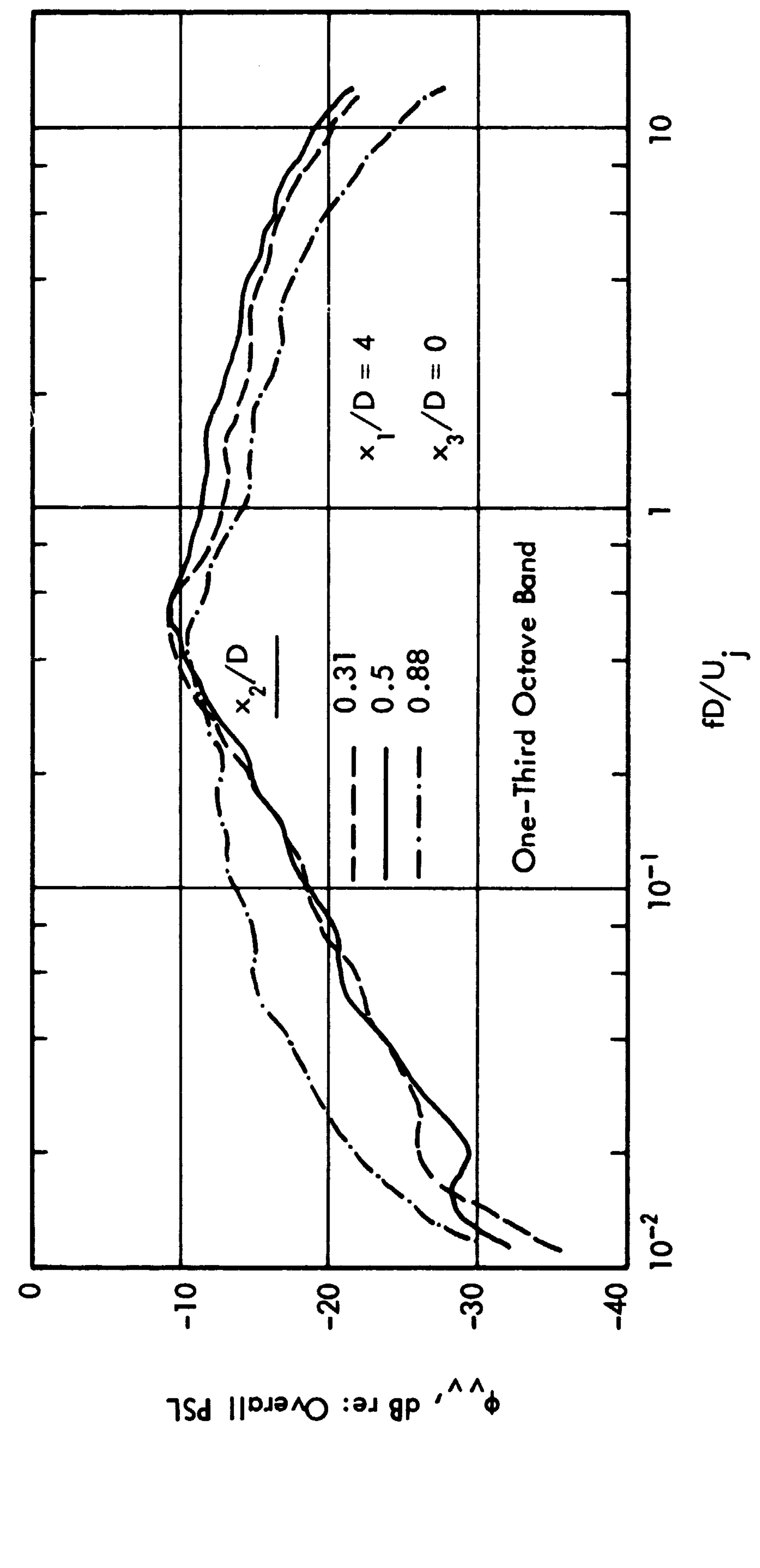

Figure 57. One-Third Octave Band Spectra for v-Component

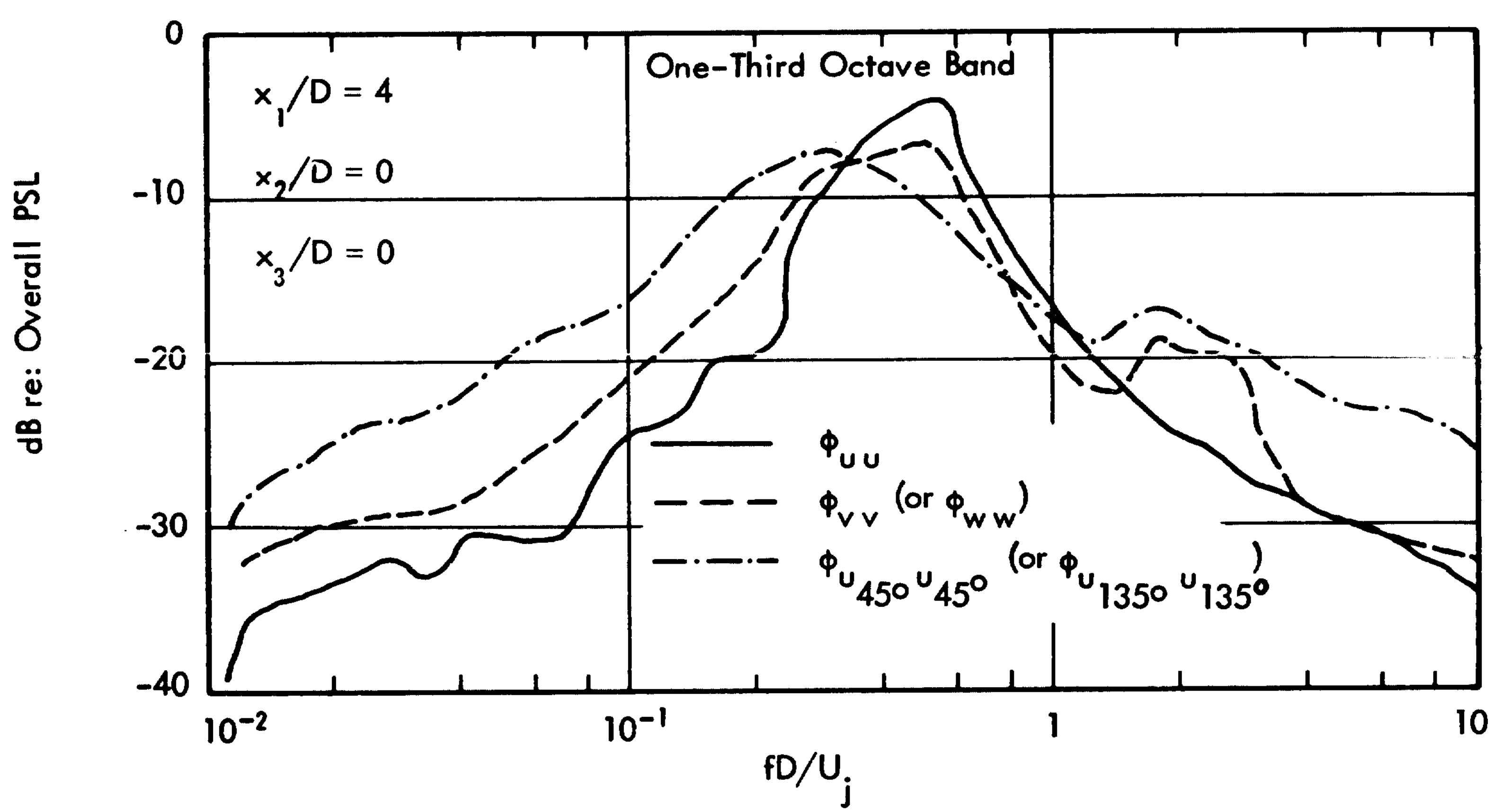

Figure 58. Comparison of One-Third Octave Band Spectra for Different Velocity Components, I

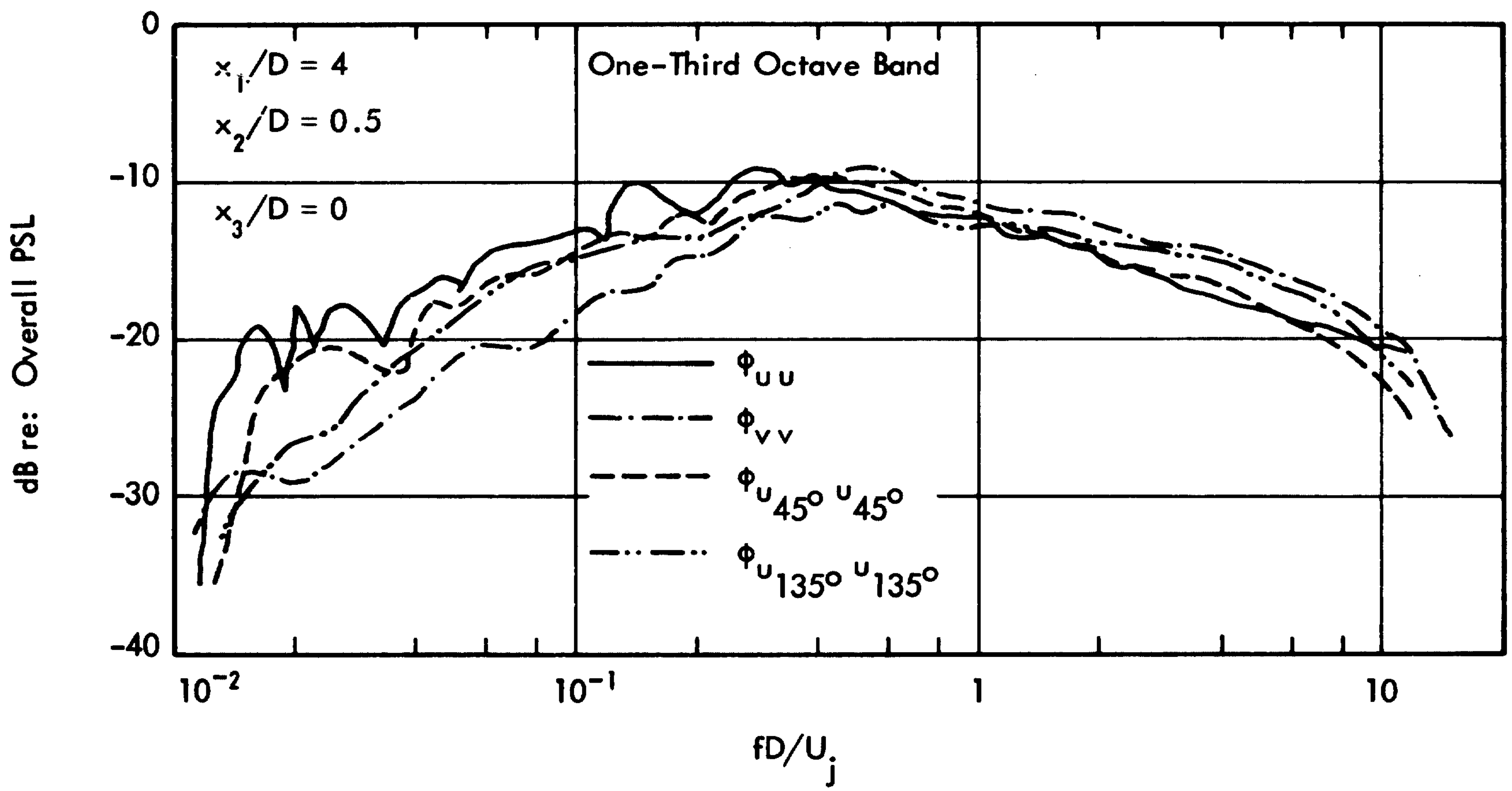

Figure 59. Comparison of One-Third Octave Band Spectra for Different Velocity Components, II

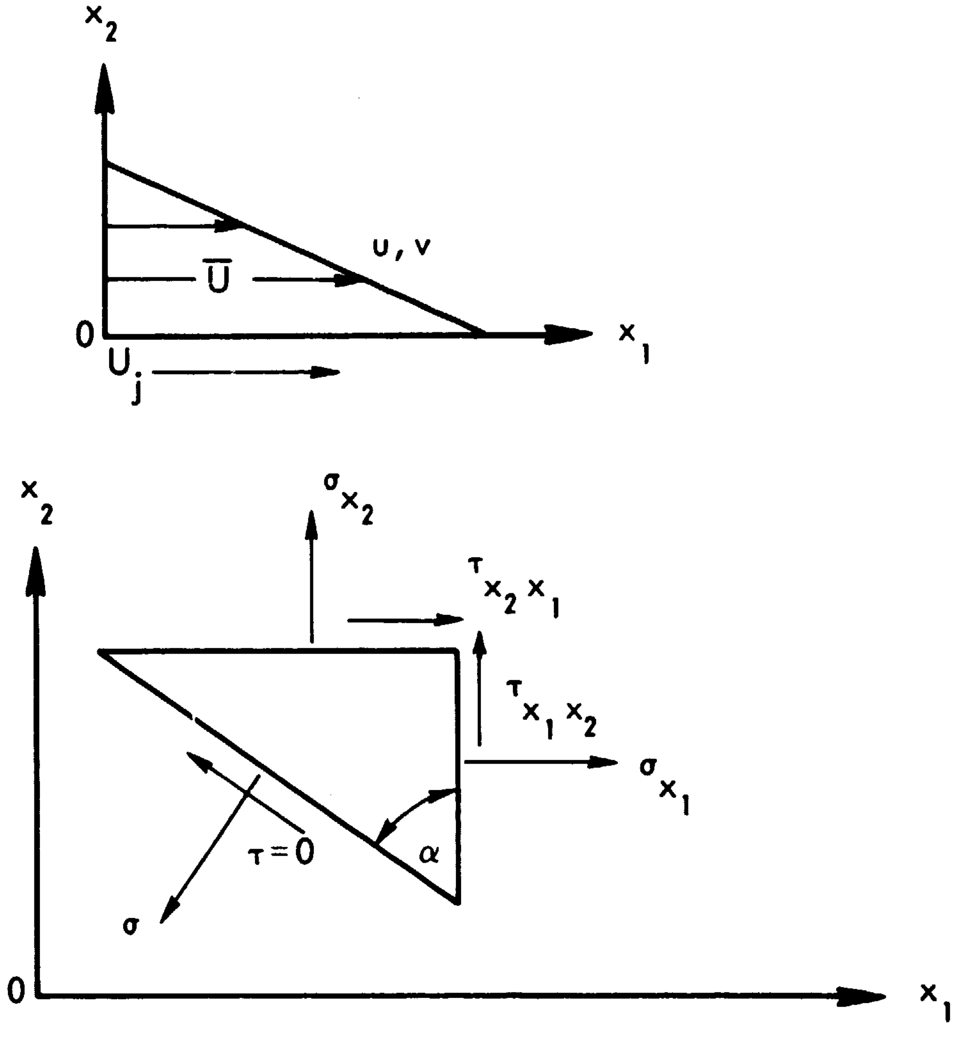

$$\sigma_{x_1} = -\overline{p} + 2\mu \frac{\partial \overline{U}}{\partial x_1} - \rho \overline{u^2}$$

$$\sigma_{x_2} = -\overline{p} + 2\mu \frac{\partial \overline{V}}{\partial x_2} - \rho \overline{v^2}$$

$$\tau_{x_1 x_2} = \tau_{x_2 x_1} = \mu \left(\frac{\partial \overline{U}}{\partial x_2} + \frac{\partial \overline{V}}{\partial x_1} \right) - \rho \overline{uv}$$

$$\alpha = \frac{1}{2} \tan^{-1} \left(\frac{2 \tau_{x_1 x_2}}{\sigma_{x_1} - \sigma_{x_2}} \right)$$

$$\sigma = \sigma_{x_1} \cos^2 \alpha + \sigma_{x_2} \sin^2 \alpha + \tau_{x_1 x_2} \sin 2\alpha$$

Figure 60. Principal Directions of Mean Stresses in a Shear Flow

APPENDIX

SPATIAL SEPARATIONS OF TWO POINTS WHERE DIFFERENT TURBULENT VELOCITY COMPONENTS HAVE BEEN RECORDED

$u_{\theta f}$ = Turbulent Fluctuation of Velocity Component u_θ Measured by Fixed Probe

$u_{\theta M}$ = Turbulent Fluctuation of Velocity Component u_θ Measured by Movable Probe

Run No.	Reel No.	Spacing (in.)			Channels of Recording					Remark
		ξ_1	ξ_2	ξ_3	$u_{\theta F}$	$u_{\theta M}$	$u^2_{\theta F}$	$u^2_{\theta M}$	Voice	
1	1	0	0.22	0	1	2	3	4	14	
2	1	0	0.33	0	1	2	3	4	14	
3	1	0	0.44	0	1	2	3	4	14	
4	1	0	0.55	0	1	2	3	4	14	
5	1	0	0.66	0	1	2	3	4	14	
6	1	0	0.77	0	1	2	3	4	14	
7	1	0	1.5	0	5	6	7	8	13	
8	1	0	2.0	0	5	6	7	9	13	Rerun
9	1	0	2.5	0	5	6	7	8	13	
10	1	0	3.0	0	5	6	7	8	13	
11	1	0	3.5	0	5	6	7	8	13	
12	2	0	-0.22	0	1	2	3	4	14	
13	2	0	-0.33	0	1	2	3	4	14	
14	2	0	-0.44	0	1	2	3	4	14	
15	2	0	-0.55	0	1	2	3	4	14	
16	2	0	-0.66	0	1	2	3	4	14	
17	2	0	-0.77	0	1	2	3	4	14	
18	2	0	-1.5	0	1	2	3	4	14	
19	2	0	-2.0	0	1	2	3	4	14	
20	2	0	-2.5	0	1	2	3	4	14	
21	2	0	-3.0	0	1	2	3	4	14	
22	2	0	-3.5	0	1	2	3	4	14	

Run No.	Reel No.	Spacing (in.)			Channels of Recording					Remark
		ξ_1	ξ_2	ξ_3	$u_0 \circ F$	$u_0 \circ M$	$u_0^2 \circ F$	$u_0^2 \circ M$	Voice	
23	2	0	-4.0	0	1	2	3	4	14	
24	2	0	0	-0.22	1	2	3	4	14	
25	2	0.1	0	-0.22	1	2	3	4	14	
26	2	0.2	0	-0.22	5	6	7	8	13	
27	2	0.4	0	-0.22	5	6	7	8	13	
28	2	0.6	0	-0.22	5	6	7	8	13	
29	2	0.8	0	-0.22	5	6	7	8	13	
30	2	1.5	0	-0.22	5	6	7	8	13	
31	2	2	0	-0.22	5	6	7	8	13	
32	2	2.5	0	-0.22	5	6	7	8	13	
33	2	3.0	0	-0.22	5	6	7	8	13	
34	2	4.0	0	-0.22	5	6	7	8	13	
35	2	-0.2	0	-0.22	5	6	7	8	13	
36	2	-0.4	0	-0.22	5	6	7	8	13	
37	2	-0.6	0	-0.22	5	6	7	8	13	
38	2	-0.8	0	-0.22	5	6	7	8	13	
39	3	-1.5	0	-0.22	5	6	7	8	13	
40	3	-2.0	0	-0.22	5	6	7	8	13	
41	3	-2.5	0	-0.22	5	6	7	8	13	
42	3	-3.0	0	-0.22	5	6	7	8	13	
43	3	-4.0	0	-0.22	5	6	7	8	13	
44	3	0	0	-0.43	5	6	7	8	13	
45	3	0.4	0	-0.43	5	6	7	8	13	
46	3	0.8	0	-0.43	5	6	7	8	13	
47	3	1.5	0	-0.43	5	6	7	8	13	
48	3	2.0	0	-0.43	5	6	7	8	13	
49	3	2.5	0	-0.43	5	6	7	8	13	
50	3	3.0	0	-0.43	5	6	7	8	13	

Run No.	Reel No.	Spacing (in.)			Channels of Recording					Remark
		ξ_1	ξ_2	ξ_3	$u_{0°F}$	$u_{0°M}$	$u^2_{0°F}$	$u^2_{0°M}$	Voice	
51	3	4.0	0	-0.43	5	6	7	8	13	
52	3	0	0	-0.64	1	2	3	4	14	
53	3	0.4	0	-0.64	1	2	3	4	14	
54	3	0.8	0	-0.64	1	2	3	4	14	
55	3	1.5	0	-0.64	1	2	3	4	14	
56	3	2.0	0	-0.64	1	2	3	4	14	
57	3	2.5	0	-0.64	1	2	3	4	14	
58	3	3.0	0	-0.64	1	2	3	4	14	
59	3	4.0	0	-0.64	1	2	3	4	14	
60	3	0	0	-0.85	1	2	3	4	14	
61	3	0	0	-1.06	1	2	3	4	14	
62	3	0	0	-1.27	1	2	3	4	14	
63	3	0	0	-1.8	1	2	3	4	14	
64	3	0	0	+2.3	1	2	3	4	14	
65	3	0	0	+2.83	1	2	3	4	14	
66	3	0	0	+3.55	1	2	3	4	14	

Run No.	Reel No.	Spacing (in.)			Channels of Recording					Remark
		ξ_1	ξ_2	ξ_3	$u_{90°F}$	$u_{90°M}$	$u^2_{90°F}$	$u^2_{90°M}$	Voice	
67	4	0	-0.22	0	1	2	3	4	14	
68	4	0	-0.33	0	1	2	3	4	14	
69	4	0	-0.44	0	1	2	3	4	14	
70	4	0	-0.55	0	1	2	3	4	14	
71	4	0	-0.77	0	1	2	3	4	14	
72	4	0	-1.5	0	1	2	3	4	14	
73	4	0	-2.0	0	1	2	3	4	14	
74	4	0	-2.5	0	1	2	3	4	14	
75	4	0	-3.0	0	1	2	3	4	14	

Run No.	Reel No.	Spacing (in.)			Channels of Recording					Remark
		ξ_1	ξ_2	ξ_3	$u_{90°F}$	$u_{90°M}$	$u^2_{90°F}$	$u^2_{90°M}$	Voice	
76	4	0	-4.0	0	1	2	3	4	14	
77	4	0	+0.22	0	1	2	3	4	14	
78	4	0	0.33	0	1	2	3	4	14	
79	4	0	0.44	0	1	2	3	4	14	
80	4	0	0.55	0	1	2	3	4	14	
81	4	0	0.77	0	5	6	7	8	13	
82	4	0	1.5	0	5	6	7	8	13	
83	4	0	2.0	0	5	6	7	8	13	
84	4	0	2.5	0	5	6	7	8	13	
85	4	0	3.0	0	5	6	7	8	13	
86	4	0	3.5	0	5	6	7	8	13	
87	4	0	0	-0.22	5	6	7	8	13	
88	4	0.1	0	-0.22	5	6	7	8	13	
89	4	0.2	0	-0.22	5	6	7	8	13	
90	4	0.4	0	-0.22	5	6	7	8	13	
91	4	0.6	0	-0.22	5	6	7	8	13	
92	4	0.8	0	-0.22	5	6	7	8	13	
93	4	1.5	0	-0.22	5	6	7	8	13	
94	4	2.0	0	-0.22	5	6	7	8	13	
95	4	2.5	0	-0.22	5	6	7	8	13	
96	4	3.0	0	-0.22	5	6	7	8	13	
97	5	4.0	0	-0.22	1	2	3	4	14	
98	5	-0.2	0	-0.22	1	2	3	4	14	
99	5	-0.4	0	-0.22	1	2	3	4	14	
100	5	-0.6	0	-0.22	1	2	3	4	14	
101	5	-0.8	0	-0.22	1	2	3	4	14	
102	5	-1.5	0	-0.22	1	2	3	4	14	
103	5	-2.0	0	-0.22	1	2	3	4	14	

Run No.	Reel No.	Spacing (in.)			Channels of Recording					Remark
		ξ_1	ξ_2	ξ_3	$u_{90°F}$	$u_{90°M}$	$u^2_{90°F}$	$u^2_{90°M}$	Voice	
104	5	-2.5	0	-0.22	1	2	3	4	14	
105	5	-3.0	0	-0.22	1	2	3	4	14	
106	5	-4.0	0	-0.22	1	2	3	4	14	
107	5	0	0	-0.43	1	2	3	4	14	
108	5	0.2	0	-0.43	1	2	3	4	14	
109	5	0.4	0	-0.43	1	2	3	4	14	
110	5	0.8	0	-0.43	1	2	3	4	14	
111	5	1.5	0	-0.43	1	2	3	4	14	
112	5	2.0	0	-0.43	1	2	3	4	14	
113	5	2.5	0	-0.43	5	6	7	8	13	
114	5	3.0	0	-0.43	5	6	7	8	13	
115	5	0	0	-0.64	5	6	7	8	13	
116	5	0.4	0	-0.64	5	6	7	8	13	
117	5	0.8	0	-0.64	5	6	7	8	13	
118	5	1.5	0	-0.64	5	6	7	8	13	
119	5	2.0	0	-0.64	5	6	7	8	13	
120	5	2.5	0	-0.64	5	6	7	8	13	
121	5	3.0	0	-0.64	5	6	7	8	13	
122	5	0	0	-0.85	5	6	7	8	13	
123	5	0	0	-1.06	5	6	7	8	13	
124	5	0	0	-1.5	5	6	7	8	13	
125	5	0	0	+2.0	5	6	7	8	13	
126	5	0	0	+2.5	5	6	7	8	13	
127	5	0	0	+3.0	5	6	7	8	13	
128	6	0	0	+4.0	5	6	7	8	13	
129	6	0.22	0.22	0	5	6	7	8	13	
130	6	0.42	0.42	0	5	6	7	8	13	
131	6	0.82	0.82	0	5	6	7	8	13	

Run No.	Reel No.	Spacing (in.)			Channels of Recording					Remark
		ξ_1	ξ_2	ξ_3	$u_{45^\circ F}$	$u_{45^\circ M}$	$u^2_{45^\circ F}$	$u^2_{45^\circ M}$	Voice	
132	6	0	0.22	0	5	6	7	8	13	
133	6	0	0.33	0	5	6	7	8	13	
134	6	0	0.44	0	5	6	7	8	13	
135	6	0	0.55	0	5	6	7	8	13	
136	6	0	0.77	0	5	6	7	8	13	
137	6	0	1.5	0	5	6	7	8	13	
138	6	0	2.0	0	5	6	7	8	13	
139	6	0	2.5	0	5	6	7	8	13	
140	6	0	3.0	0	5	6	7	8	13	
141	6	0	3.5	0	5	6	7	8	13	
142	6	0	-0.2	0	5	6	7	8	13	
143	6	0	-0.31	0	1	2	3	4	14	
144	6	0	-0.42	0	1	2	3	4	14	
145	6	0	-0.53	0	1	2	3	4	14	
146	6	0	-0.75	0	1	2	3	4	14	
147	6	0	-1.5	0	1	2	3	4	14	
148	6	0	-2.0	0	2	2	3	4	14	
149	6	0	-2.5	0	1	2	3	4	14	
150	6	0	-3.0	0	1	2	3	4	14	
151	6	0	-4.0	0	1	2	3	4	14	
152	6	0	-1.0	0	1	2	3	4	14	
153	6	0	+1.0	0	1	2	3	4	14	
154	6	0.2	0.2	0	1	2	3	4	14	
155	6	0.3	0.3	0	1	2	3	4	14	
156	6	0.4	0.4	0	1	2	3	4	14	
157	6	0.7	0.7	0	1	2	3	4	14	
158	6	1.0	1.0	0	1	2	3	4	14	
159	6	1.5	1.5	0	1	2	3	4	14	

Run No.	Reel No.	Spacing (in.)			Channels of Recording					Remark
		ξ_1	ξ_2	ξ_3	$u_{45^\circ F}$	$u_{45^\circ M}$	$u^2_{45^\circ F}$	$u^2_{45^\circ M}$	Voice	
160	7	2.0	2.0	0	5	6	7	8	13	
161	7	2.5	2.5	0	5	6	7	8	13	
162	7	3.0	3.0	0	5	6	7	8	13	
163	7	3.5	3.5	0	5	6	7	8	13	
164	7	-0.2	-0.2	0	5	6	7	8	13	
165	7	-0.3	-0.3	0	5	6	7	8	13	
166	7	-0.4	-0.4	0	5	6	7	8	13	
167	7	-0.7	-0.7	0	5	6	7	8	13	
168	7	-1.0	-1.0	0	5	6	7	8	13	
169	7	-1.5	-1.5	0	5	6	7	8	13	
170	7	-2.0	-2.0	0	5	6	7	8	13	
171	7	-2.5	-2.5	0	5	6	7	8	13	
172	7	-3.0	-3.0	0	5	6	7	8	13	
173	7	-4.0	-4.0	0	5	6	7	8	13	
174	7	0	0	-0.22	5	6	7	8	13	
175	7	0.1	0	-0.22	5	6	7	8	13	
176	7	0.2	0	-0.22	5	6	7	8	13	
177	7	0.4	0	-0.22	1	2	3	4	14	
178	7	0.6	0	-0.22	1	2	3	4	14	
179	7	1.0	0	-0.22	1	2	3	4	14	
180	7	1.5	0	-0.22	1	2	3	4	14	
181	7	2.0	0	-0.22	1	2	3	4	14	
182	7	2.5	0	-0.22	1	2	3	4	14	
183	7	3.0	0	-0.22	1	2	3	4	14	
184	7	4.0	0	-0.22	1	2	3	4	14	
185	7	-0.2	0	-0.22	1	2	3	4	14	
186	7	-0.4	0	-0.22	1	2	3	4	14	
187	7	-0.6	0	-0.22	1	2	3	4	14	

Run No.	Reel No.	Spacing (in.)			Channels of Recording					Remark
		ξ_1	ξ_2	ξ_3	$u_{45°F}$	$u_{45°M}$	$u^2_{45°F}$	$u^2_{45°M}$	Voice	
188	7	-1.0	0	-0.22	1	2	3	4	14	
189	7	-1.5	0	-0.22	1	2	3	4	14	
190	7	-2.0	0	-0.22	1	2	3	4	14	
191	7	-2.5	0	-0.22	1	2	3	4	14	
192	7	-3.0	0	-0.22	1	2	3	4	14	
193	8	-4.0	0	-0.22	1	2	3	4	14	
194	8	0	0	-0.43	1	2	3	4	14	
195	8	0.2	0	-0.43	1	2	3	4	14	
196	8	0.4	0	-0.43	1	2	3	4	14	
197	8	0.6	0	-0.43	1	2	3	4	14	
198	8	1.0	0	-0.43	1	2	3	4	14	
199	8	1.5	0	-0.43	1	2	3	4	14	
200	8	2.0	0	-0.43	1	2	3	4	14	
201	8	2.5	0	-0.43	1	2	3	4	14	
202	8	3.0	0	-0.43	1	2	3	4	14	
203	8	4.0	0	-0.43	1	2	3	4	14	
204	8	0	0	-0.64	1	2	3	4	14	
205	8	0.2	0	-0.64	1	2	3	4	14	
206	8	0.4	0	-0.64	1	2	3	4	14	
207	8	0.6	0	-0.64	1	2	3	4	14	
208	8	1.0	0	-0.64	1	2	3	4	14	
209	8	1.5	0	-0.64	1	2	3	4	14	
210	8	2.0	0	-0.64	1	2	3	4	14	
211	8	2.5	0	-0.64	1	2	3	4	14	
212	8	3.0	0	-0.64	1	2	3	4	14	
213	8	0	0	-0.64	1	2	3	4	14	Repeat Run 204
214	8	4.0	0	-0.64	5	6	7	8	13	
215	8	0	0	-1.06	5	6	7	8	13	

Run No.	Reel No.	Spacing (in.)			Channels of Recording					Remarks
		ξ_1	ξ_2	ξ_3	$u_{45°F}$	$u_{45°M}$	$u^2_{45°F}$	$u^2_{45°M}$	Voice	
216	8	0	0	-1.5	5	6	7	8	13	
217	8	0	0	+2.0	5	6	7	8	13	
218	8	0	0	+2.5	5	6	7	8	13	
219	8	0	0	+3.0	5	6	7	8	13	
220	8	0	0	+4.0	5	6	7	8	13	

FILMED

JUN 24 1970